Title
Quantification of and Controls on Dinitrogen and Nitrous Oxide Fluxes from Terrestrial Ecosystems

Author
Yang, Wendy Hui-I

Publication Date
2010

Peer reviewed|Thesis/dissertation

Quantification of and Controls on Dinitrogen and Nitrous Oxide Fluxes from Terrestrial Ecosystems

by

Wendy Hui-I Yang

A dissertation submitted in partial satisfaction of the

requirements for the degree of

Doctor of Philosophy

in

Environmental Science, Policy, and Management

in the

Graduate Division

of the

University of California, Berkeley

Committee in charge:

Professor Whendee L. Silver
Professor Mary Firestone
Professor Robert C. Rhew

Spring 2010

Quantification of and Controls on Dinitrogen and Nitrous Oxide Fluxes

from Terrestrial Ecosystems

by Wendy Hui-I Yang

Abstract

Quantification of and Controls on Dinitrogen and Nitrous Oxide Fluxes

from Terrestrial Ecosystems

by

Wendy Hui-I Yang

Doctor of Philosophy in Environmental Science, Policy, and Management

University of California, Berkeley

Professor Whendee L. Silver, Chair

The production of dinitrogen (N_2) and emission to the atmosphere returns reactive nitrogen (N) species to the unreactive form, completing the N cycle. Soil N_2 emissions are the most poorly understood portion of the terrestrial N cycle because soil N_2 fluxes are difficult to measure against the high atmospheric background N_2 concentration. For my dissertation, I developed two new methods for quantifying soil N_2 production in soils and described a new pathway for N_2 production in the terrestrial N cycling. I also explored controls on soil N cycling at a regional scale relevant for policymakers. In laboratory experiments, I demonstrated that the N_2/Ar technique can be used to accurately measure surface soil N_2 fluxes when solubility and water vapor fractionation effects on the N_2/Ar ratio are taken into account. Currently the detection limit of the method is 100 mg N m_2 d^{-1}, but proposed modifications to the sampling and analytical protocols can lower the detection limit as well as increase sample throughput. I also developed the ^{15}N-nitrous oxide (N_2O) pool dilution technique in a peatland pasture and showed that it can be used to measure gross N_2O production and consumption rates without changing soil N_2O emissions (i.e., net N_2O production). Vertical diffusion modeling suggested that the $^{15}N_2O$ tracer was able to diffuse through the vadose zone to the water table at 60 cm depth during the sampling period, but additional modeling is necessary to evaluate the impact of lateral tracer movement on vertical tracer penetration into the soil profile. Nitrous oxide emissions ranged from 0.05 to 77.4 mg N m^{-2} d^{-1} across four micro-topographic zones and the proportion of gross N_2O production released to the atmosphere was 0.84 ± 0.03. Mineral N concentrations and denitrifying enzyme activity together best predicted gross N_2O production rates (R^2 = 0.73). When the four landforms were grouped by soil moisture content, soil oxygen concentrations explained over 64% of the variability in N_2O consumption rates. Denitrification is currently thought to be the only N_2 production pathway in terrestrial soils, but I showed that, in a humid tropical forest soil, iron reduction coupled to anaerobic ammonium (NH_4^+) oxidation (Feammox) can lead to N_2 production both directly and indirectly (via denitrification of Feammox-generated nitrite). Anaerobic ammonium oxidation rates were comparable to denitrification rates for this forest, suggesting the potential importance of this pathway. Lastly, I found that a small suite of soil properties could reliably predict internal N cycling processes in soils from deserts, forests,

grasslands, shrublands, and wetlands in California. Microbial biomass N, soil organic carbon (C) concentration, and soil NH_4^+ concentrations together explained 80 % of the variability in gross mineralization rates whereas soil nitrate (NO_3^-) concentration and soil C:N ratios together explained 59 % of the variability in gross nitrification rates. Dissimilatory NO_3^- reduction to NH_4^+ occurred in all soils and rates were best predicted by the combination of gross nitrification rates and soil NH_4^+ concentrations ($R^2 = 0.83$). These results will support modeling efforts at the regional scale that are important for setting land use and N emissions policies. Overall, my dissertation has moved the field closer to understanding soil N_2 emissions and suggests that the controls on soil N cycling can be modeled at a regional scale incorporating many different ecosystem types.

TABLE OF CONTENTS

ACKNOWLEDGMENTS

First and foremost, I would like to thank my advisor, Whendee Silver, who has invested so much in my development as a scientist. She has not only taught me invaluable knowledge and skills in biogeochemistry and the scientific method but has also served as an excellent role model as a woman in science. Mary Firestone and Robert Rhew also provided much guidance over the years as well as put a lot of time and thought into improving my dissertation in a few short months.

I appreciate the many collaborators who helped me make intellectual leaps that I may not have made on my own. Jeffrey Severinghaus generously and bravely allowed me to use his mass spectrometer and patiently taught me laboratory protocols and the theory behind the physical fractionation effects on the N_2/Ar ratios. Members of the Severinghaus lab (Ross Beaudette, Melissa Headly, Vas Petrenko, Anais Orsi, and Takuro Kobashi) helped me troubleshoot and improve the protocols I used. Ralph Keeling also helped me think through applying the N_2/Ar technique to soil N_2 fluxes. Yit Teh suggested using pool dilution to measure nitrous oxide production and consumption as well as taught me how to perform the measurements. Joe von Fischer provided assistance with diffusion modeling.

The assistance and advice of many people made my research possible: Wendy Chou, Daniela Cusack, Steven Hall, Marissa Lafler, Daniel Liptzin, Andrew McDowell, Sarah Placella, Braulio Quintero, Becca Ryals, Bibit Traut, and Tana Wood. In particular, Andy Thompson's endless patience and wealth of knowledge about biogeochemistry and instrumentation got me through my first four years in graduate school. Don Herman suffered through my many (and sometimes idiotic) questions about the mass spectrometer and the lachat but was always willing to help me set-up and troubleshoot. The instrumentation expertise and photographic memory of Paul Brooks were also invaluable.

I could not have completed my dissertation without my husband, Glen Yang, by my side. He had confidence in me when I doubted myself. He spent countless hours helping me in the lab and field on top of his own busy work weeks. And most of all, his love and companionship kept me balanced and grounded when my research overwhelmed my life. I also thank my parents who have always supported me in pursuing my dreams and prayed for my health and happiness.

I received support from the Department of Energy Global Change Environmental Program Fellowship, the National Science Foundation Graduate Research Fellowship, the National Science Foundation Doctoral Dissertation Improvement Grant, and Berkeley Atmospheric Sciences Center Graduate Fellowship. My research was also funded by grants from the National Science Foundation (Atm-0842385, DEB-0543558), Kearney Foundation of Soil Science (2005:213), and AES CA-B*-ECO-7673-MS to W. Silver. Support was also provided by NSF grants DEB-0218039 and DEB-0620910 to the Institute of Tropical Ecosystem Studies, UPR, and USDA-IITF as part of the Long-Term Ecological Research Program in the Luquillo Experimental Forest.

Chapter 1. Introduction

Background

Nitrogen (N) is a macronutrient required for all life. Most N on Earth is stored in the inert form of N_2 in the atmosphere and is metabolically inaccessible to most organisms. Humans have dramatically altered the global N cycle by increasing reactive and bioavailable forms of N through fertilizer production and fossil fuel combustion (Vitousek et al. 1997; Galloway et al. 2003). This in turn has led to a host of direct and indirect environmental consequences including aquatic eutrophication, groundwater pollution, smog production, stratospheric ozone depletion, and global warming (Galloway et al. 2004; Schlesinger 2009). Nitrous oxide (N_2O), a potent greenhouse gas and catalyst for stratospheric ozone depletion, can also be consumed in soil to produce dinitrogen (N_2). This process, known only to occur via denitrification in terrestrial soils, completes the N cycle by returning reactive N to the unreactive form. Despite the importance of soil N_2 emissions in the global N cycle, process rates and controls on N_2 production in upland soils are the most poorly understood portions of the global N cycle (Kulkarni et al. 2008).

Soil N_2 emissions are difficult to detect against the high background N_2 concentration in the atmosphere. Soil N_2 emissions are often omitted from ecosystem N budgets (e.g. Tietema and Verstraten 1991; Hedin et al. 2003) or estimated from mass balance models, which themselves are poorly constrained (e.g., Groffman et al. 2008). These models are based on the assumption that ecosystems are at steady state with respect to N; however, with the increased N inputs from human activity, few if any ecosystems are likely to be in steady state conditions over biological time scales. Almost one third of anthropogenic N cannot be accounted for in a global N budget that includes only a rough estimate of land-based denitrification (Schlesinger 2009).

Unlike soil N_2 emissions, soil N_2O emissions are relatively easy to measure against background atmospheric concentrations. Nitrous oxide is produced via denitrification and nitrification, and is an intermediate compound in denitrification of nitrate (NO_3^-) to N_2. Characterizing the N_2O:N_2 ratio of soil gas emissions as well as determining the controls on the ratio of N_2O:N_2 produced via denitrification could facilitate the modeling and measurement of N_2 fluxes from terrestrial ecosystems. However, the N_2O:N_2 ratio is highly variable and sensitive to a broad suite of environmental conditions, leading to considerable uncertainty in the ratio (Firestone et al. 1980; Weier et al. 1993; Hedin et al. 2003; Dannenman et al. 2008).

Many approaches have been developed to estimate soil N_2 emissions, but each approach has well recognized limitations (Groffman et al. 2006). Acetylene (C_2H_2) inhibits the reduction of N_2O to N_2 via denitrification so that N_2 emissions can be estimated from N_2O production in the presence and absence of C_2H_2. The acetylene inhibition technique can underestimate N_2 emissions by decreasing the supply of NO_3^- substrate via nitrification, through diffusion limitation of C_2H_2 to microsites of denitrification activity, and due to the ineffectiveness of C_2H_2 on some denitrifiers and under low NO_3^- conditions (Knowles 1990; Simarmata et al. 1993). The ^{15}N tracer method requires the addition of ^{15}N-labeled NO_3^-, the substrate for denitrification, and thus can potentially stimulate denitrification rates and change the N_2O:N_2 ratio of denitrification end-products. The use of this method is typically restricted to systems with high soil NO_3^- concentrations, such as agricultural systems (Stevens and Laughlin 1998), because a large amount of $^{15}NO_3^-$ is needed to detect a change in ^{15}N enrichment of the atmospheric N_2 pool. The gas flow soil core method has been used to measure net N_2 fluxes from intact soil cores in the laboratory (Butterbach-Bahl et al. 2002a; Dannenmann et al. 2008). However, the soils are typically incubated under 21 % oxygen (O_2) so that the measured N_2 fluxes may not be

representative of field rates (Butterbach-Bahl et al. 2002b). Each of these methods has specific limitations, but the common limitation among all of the methods is that they typically involve removing soil from the ground so that O_2 availability changes. Denitrification is a redox sensitive process so that this can change process rates as well as the relative proportions of N_2O and N_2 released.

The aim of my dissertation research was to develop new methods for measuring soil N_2 emissions in the field (Chapters 2-3), determine the potential for terrestrial N_2 production via anaerobic ammonium (NH_4^+) oxidation (Chapter 4), and explore cross-ecosystem controls on internal N cycling processes that supply the substrates for N_2 and N_2O production (Chapter 5). The remainder of this chapter briefly introduces each section of my dissertation research.

Dissertation Overview

N_2/Ar Technique

The N_2/Ar technique is used widely to measure net N_2 fluxes in aquatic systems, but the detection limit of the method has been too high to use for terrestrial N_2 fluxes (Groffman et al. 2006). Paleoclimatologists have developed an analytical technique on a dual inlet isotope ratio mass spectrometer that can measure N_2/Ar ratios with very high precision (approximately 0.05 ‰, or 50 per meg; Kobashi et al. 2008). With such high precision measurements, physical fractionation effects on the N_2/Ar ratio confound changes in the ratio due to biological activity. In chapter 2, I present modeling approaches to account for the physical fractionation effects as well as the N_2/Ar technique for measuring surface soil N_2 fluxes.

I tested the N_2/Ar technique under controlled laboratory conditions in a diffusion box filled with sand. I hypothesized that temperature changes during gas sampling would cause thermal fractionation in the N_2/Ar ratio of the surface flux chamber headspace due to changes in temperature gradients that drive thermal diffusion; temperature changes would cause solubility fractionation in the headspace N_2/Ar ratio due to the different temperature-solubility relationships for N_2 and Ar. I also hypothesized that water vapor flux from the soil to the atmosphere would cause a decrease in the headspace N_2/Ar ratio due to faster diffusion of N_2 compared to Ar to replace the water vapor lost from the soil. I used the N_2/Ar technique to measure known N_2 fluxes in dry sand, in which I expected thermal fractionation to be the only physical fractionation factor affecting the N_2/Ar ratio. I also measured N_2 known fluxes in wet sand, in which I expected to observe the thermal, solubility, and water vapor flux fractionation effects. I performed measurements under control conditions (no N_2 flux) and treatment conditions (induced N_2 fluxes). Fick's law describes diffusive transport of gases along concentration gradients, so I hypothesized that N_2 fluxes measured using the N_2/Ar ratio would be similar to those calculated using Fick's law if the N_2/Ar technique accurately measured N_2 fluxes from the soil surface. I expected that the N_2 fluxes calculated from the change in N_2/Ar ratios corrected for the thermal, solubility, and water vapor flux fractionation effects would be similar to the known N_2 fluxes calculated by Fick's law.

$^{15}N_2O$ Pool Dilution Technique

In chapter 3, I present the field-based $^{15}N_2O$ pool dilution technique for measuring gross N_2O production and consumption rates in soils. The pool dilution technique is commonly used to measure gross production and consumption of NH_4^+ and NO_3^- in soils, and the assumptions of the technique have been validated for those applications (Davidson et al. 1991). This technique has also been applied to the field dynamics of trace gases, such methane (von Fischer et al. 2002)

and methyl halides (Rhew and Abel 2007), but has never been used for $^{15}N_2O$ in the field setting. I used a surface flux chamber to test a field-based $^{15}N_2O$ pool dilution technique in a peatland pasture in the San-Joaquin-Sacramento River Delta, California. High soil N_2O emissions had previously been measured at this site (Teh et al, submitted), but the ratio of N_2O:N_2 emissions was unknown.

I first evaluated the $^{15}N_2O$ pool dilution technique against the acetylene inhibition and ^{15}N tracer techniques in closed incubation chambers in the laboratory. Acetylene inhibition can lead to underestimation of N_2 production due to inhibition of nitrification, which supplies the substrate for denitrification. The ^{15}N tracer method can stimulate N_2 production due to the addition of $^{15}NO_3^-$, the substrate for denitrification (Groffman et al. 2006). I hypothesized that gross N_2O consumption rates measured using the $^{15}N_2O$ pool dilution technique represented N_2 production rates. Thus, I expected that gross N_2O consumption rates measured using the $^{15}N_2O$ pool dilution technique would be intermediate to N_2 production rates estimated using the acetylene inhibition and ^{15}N tracer techniques.

In the field, I tested the assumption that small additions of $^{15}N_2O$ to the surface flux chamber headspace would not change N_2O dynamics via stimulation of N_2O consumption or suppress the diffusion of $^{15}N_2O$ out of the soil. In the absence of another method that I could use to measure gross N_2O production or consumption for validation, I expected that if there was no effect of adding $^{15}N_2O$, then net N_2O fluxes would be similar with and without $^{15}N_2O$ addition. I also used a vertical diffusion model to determine if the tracer could travel to the water table during the sampling time period (von Fischer et al. 2009).

I performed measurements on several dates and across a micro-topographical gradient in the pasture to explore controls on N_2O dynamics. Denitrification is a redox sensitive process that uses NO_3^- as an electron acceptor when O_2 is not available. I hypothesized that NO_3^- and O_2 availability were the dominant controls on gross N_2O production via denitrification. Thus, I expected that if denitrification was largely responsible for N_2O production in the peatland pasture, then NO_3^- availability (i.e., substrate) and soil O_2 concentration would be predictors of gross N_2O production. I hypothesized that the ratio of electron donor to electron acceptor determines whether denitrifiers reduce N_2O, which is a less energetically favorable electron acceptor than NO_3^-. Thus, I expected that the ratio of N_2O:N_2 would be predicted by the ratio of NO_3^- to labile carbon (C) (using carbon dioxide emissions as a proxy).

Anaerobic Ammonium Oxidation

Denitrification was once thought to be the only pathway for N_2 production in terrestrial and aquatic systems, but recent studies in marine and freshwater ecosystems have shown that anaerobic NH_4^+ oxidation coupled to nitrite (NO_2^-) reduction (termed anammox) can account for up to 70 % of N_2 production previously attributed to denitrification (Dalsgaard and Thamdrup 2002; Kuypers et al. 2005; Nicholls and Trimmer 2009; Rich et al. 2008; Schubert et al. 2006). Anammox has not been measured in soils, but the organisms capable of anammox have been detected in soil (Penton et al. 2006; Humbert et al. 2010). Anaerobic NH_4^+ oxidation coupled to iron (Fe) reduction (termed Feammox) is also thermodynamically favorable, but its occurrence in nature has only been suggested (Anschutz et al. 2000; Clement et al. 2005; Hulth et al. 1999; Luther et al. 1997; Shrestha et al. 2009). Highly weathered terrestrial soils, such as those found in humid tropical forests, are rich in poorly crystalline iron, and thus could support Feammox. In chapter 4, I investigate the occurrence of anammox and Feammox in a humid tropical forest soil from the Luquillo Experimental Forest, Puerto Rico.

Based on thermodynamic calculations, I hypothesized that Feammox was likely to occur under anoxic conditions in a highly weathered humid tropical forest soil rich in poorly crystalline iron. I used the ^{15}N isotope pairing technique to detect Feammox and anammox in soil slurries incubated in an anoxic glove box. With the addition of $^{15}NH_4^+$, anammox in the absence of Feammox could only lead to $^{29}N_2$ production whereas Feammox to NO_2^- or to N_2 could lead to $^{29}N_2$ and $^{30}N_2$ production. I expected that, if Feammox occurred, the addition of Fe(III) would stimulate $^{30}N_2$ production relative to a $^{15}NH_4^+$ control. Acetylene inhibits N_2O reduction to N_2 via denitrification as well as N_2 production from anammox (Jetten et al. 1998; Jensen et al. 2007). Thus, if Feammox to NO_2^- occurred, then I expected that the addition of C_2H_2 would reduce $^{30}N_2$ production. If anammox occurred, then C_2H_2 would inhibit $^{29}N_2$ production more than $^{30}N_2$ production.

Regional Assessment of Soil N Cycling

Recent studies have demonstrated strikingly similar controls on N release during litter decomposition (Parton et al 2007; Manzoni et al. 2008), microbial biomass and community composition (Fierer et al. 2006; Cleveland and Liptzin 2007; Fierer et al. 2009), and soil microbial mineralization of amino acids (Jones et al. 2009) from a wide range of ecosystems and environmental conditions. A meta-analysis of gross N cycling studies showed similar controls on internal N cycling processes across grasslands, woodlands, and agricultural lands (Booth et al. 2005). Identifying and quantifying these relationships can help direct policy aimed at controlling N pollution and limiting greenhouse gas emissions. In chapter 5, I examine the controls on N cycling across a broad range of ecsoystems at a regional scale. I explore the controls on rates of gross mineralization, gross nitrification, and dissimilatory NO_3^- reduction to NH_4^+ (DNRA) in soils from deserts, forests, grasslands, shrublands, and wetlands across California.

Significance

The production of N_2 in terrestrial soils is the most poorly understood portion of the global N cycle because of the difficulty in measuring soil N_2 emissions against the high background N_2 concentration in the atmosphere. My dissertation research directly addresses the need for *in situ* measurements of soil N_2 emissions through the development of two new field-based methods, the N_2/Ar and $^{15}N_2O$ pool dilution techniques. The ability to measure N_2 production in the field will allow us to better constrain ecosystem N budgets and investigate controls on denitrification. The current assumption is that denitrification is the only pathway for N_2 production in terrestrial soils, but my research investigates the potential for N_2 production via anammox and Feammox. The occurrence of anaerobic NH_4^+ oxidation would transform our current understanding of terrestrial N cycle. Feammox to N_2 represents a short circuit of the N cycle so that reactive N can be converted to N_2 without the potential for the release of N_2O. Finally, I explored key controls in internal N cycling rates across broad ecosystem types that will help guide science and policy at a regional scale.

References

Anschutz P, Sundby B, Lefrancois L, Luther GW, Mucci A (2000) Interactions between metal oxides and species of nitrogen and iodine in bioturbated marine sediments. Geochimica Et Cosmochimica Acta 64:2751-2763

Booth MS, Stark JM, Rastetter E (2005) Controls on nitrogen cycling in terrestrial ecosystems: A synthetic analysis of literature data. Ecological Monographs 75:139-157

Butterbach-Bahl K, Gasche R, Willibald G, Papen H (2002a) Exchange of N-gases at the Hoglwald Forest - A summary. Plant and Soil 240:117-123

Butterbach-Bahl K, Willibald G, Papen H (2002b) Soil core method for direct simultaneous determination of N_2 and N_2O emissions from forest soils. Plant and Soil 240:105-116

Clement JC, Shrestha J, Ehrenfeld JG, Jaffe PR (2005) Ammonium oxidation coupled to dissimilatory reduction of iron under anaerobic conditions in wetland soils. Soil Biology & Biochemistry 37:2323-2328

Cleveland CC, Liptzin D (2007) C:N:P stoichiometry in soil: Is there a "Redfield ratio" for the microbial biomass? Biogeochemistry 85:235-252

Dalsgaard T, Thamdrup B (2002) Factors controlling anaerobic ammonium oxidation with nitrite in marine sediments. Applied and Environmental Microbiology 68:3802-3808

Dannenmann M, Butterbach-Bahl K, Gasche R, Willibald G, Papen H (2008) Dinitrogen emissions and the N_2:N_2O emission ratio of a Rendzic Leptosol as influenced by pH and forest thinning. Soil Biology & Biochemistry 40:2317-2323

Davidson EA, Hart SC, Shanks CA, Firestone MK (1991) Measuring gross nitrogen mineralization, immobilization, and nitrification by ^{15}N isotope pool dilution in intact cores. Journal of Soil Science 42:335-349

Fierer N, Jackson RB (2006) The diversity and biogeography of soil bacterial communities. Proceedings of the National Academy of Sciences of the United States of America 103:626-631

Fierer N, Strickland MS, Liptzin D, Bradford MA, Cleveland CC (2009) Global patterns in belowground communities. Ecology Letters 12:1238-1249

Firestone MK, Firestone RB, Tiedje JM (1980) Nitrous oxide from soil denitrification: factors controlling its biological production. Science 208:749-751

Galloway JN et al. (2003) The nitrogen cascade. Bioscience 53:341-356

Galloway J et al. (2004) Nitrogen cycles: past, present, and future. Biogeochemistry 70:153-226

Groffman PM, Altabet MA, Bohlke JK, Butterbach-Bahl K, David MB, Firestone MK, Giblin AE, Kana TM, Nielsen LP, Voytek MA (2006) Methods for measuring denitrification: diverse approaches to a difficult problem. Ecological Applications 16:2091-2122

Groffman PM (2008) Nitrogen balances at ecosystem, landscape, regional and global scales. In: Schepers J, Raun W (eds) Nitrogen in Agricultural Soils. Soil Science Society of America, Madison, WI

Hedin LO, Vitousek PM, Matson PA (2003) Nutrient losses over four million years of tropical forest development. Ecology 84:2231-2255

Hulth S, Aller RC, Gilbert F (1999) Coupled anoxic nitrification manganese reduction in marine sediments. Geochimica Et Cosmochimica Acta 63:49-66

Humbert S, Tarnawksi S, Fromin N, Mallet M, Aragno M, Zopfi J (2010) Molecular detection of anammox bacteria in terrestrial ecosystems: distribution and diversity. The ISME Journal 4:450-454

Jensen M, Thamdrup B, Dalsgaard T (2007) Effects of specific inhibitors on anammox and denitrification in marine sediments. Applied and Environmental Microbiology 73:3151-3158
Jetten MSM et al. (1998) The anaerobic oxidation of ammonium. FEMS Microbiology Reviews 22:421-437
Jones DL et al. (2009) Soil organic nitrogen mineralization across a global latitudinal gradient. Global Biogeochemical Cycles 23:GB1016, doi:10.1029/2008GB003250
Knowles R (1990) Acetylene inhibition technique: development, advantages, and potential problems. In: Denitrification in Soil and Sediment (eds N.P. Revsbech and J. Sorensen) pp 151-166. Plenum Press, New York.
Kobashi T, Severinghaus JP, Kawamura K (2008) Argon and nitrogen isotopes of trapped air in the GISP2 ice core during the Holocene epoch (0-11,500 B.P.): Methodology and implications for gas loss processes. Geochimica Et Cosmochimica Acta 72:4675-4686
Kulkarni MV, Groffman PM, Yavitt JB (2008) Solving the global nitrogen problem: it's a gas! Frontiers in Ecology and the Environment 6:199-206
Kuypers M, et al. (2005) Massive nitrogen loss from the Benguela upwelling system through anaerobic ammonium oxidation. Proceedings of the National Academy of Sciences 102:6478-6483
Luther GW, Sundby B, Lewis BL, Brendel PJ, Silverberg N (1997) Interactions of manganese with the nitrogen cycle: Alternative pathways to dinitrogen. Geochimica Et Cosmochimica Acta 61:4043-4052
Manzoni S, Jackson RB, Trofymow JA, Porporato A (2008) The global stoichiometry of litter nitrogen mineralization. Science 321:684-686
Nicholls J, Trimmer M (2009) Widespread occurrence of the anammox reaction in estuarine sediments. Aquatic Microbial Ecology 55:105-113
Parton W et al. (2007) Global-scale similarities in nitrogen release patterns during long-term decomposition. Science 315:361-364
Penton C, Devol A, Tiedje J (2006) Molecular evidence for the broad distribution of anaerobic ammonium-oxidizing bacteria in freshwater and marine sediments. Applied and Environmental Microbiology 72:6829-6832
Rhew RC and T Abel (2007) Measuring simultaneous production and consumption fluxes of methyl chloride and methyl bromide in annual temperate grasslands. Environmental Science and Technology 41:7837-7843
Rich J, Dale O, Song B, Ward B (2008) Anaerobic ammonium oxidation (Anammox) in Chesapeake Bay sediments. Microbial Ecology 55:311-320
Schlesinger WH (2009) On the fate of anthropogenic nitrogen. Proceedings of the National Academy of Sciences 106:203-208
Shrestha J, Rich J, Ehrenfeld J, Jaffe P (2009) Oxidation of ammonium to nitrite under iron-reducing conditions in wetland soils: Laboratory, field demonstrations, and push-pull rate determination. Soil Science 174:156-164
Schubert CJ, Durisch-Kaiser E, Wehrli B, Thamdrup B, Lam P, Kuypers MMM (2006) Anaerobic ammonium oxidation in a tropical freshwater system (Lake Tanganyika). Environmental Microbiology 8:1857-1863
Simarmata T, Benckiser G, Ottow JCG (1993) Effect of an increasing carbon-nitrate-N ratio on the reliability of acetylene in blocking the N_2O-reductase activity of denitrifying bacteria in soil. Biology and Fertility of Soils 15:107-112

Stevens RJ, Laughlin RJ (1998) Measurement of nitrous oxide and di-nitrogen emissions from agricultural soils. Nutrient Cycling in Agroecosystems 52:131-139

Tietema A, Verstraten JM (1991) Nitrogen cycling in an acid forest ecosystem in the Netherlands under increased atmospheric nitrogen input - the nitrogen budget and the effect of nitrogen transformations on the proton budget. Biogeochemistry 15:21-46

Vitousek PM et al. (1997) Human alteration of the global nitrogen cycle: Sources and consequences. Ecological Applications 7:737-750

von Fischer JC, Butters G, Duchateau PC, Thelwell RJ, Siller R (2009) In situ measures of methanotroph activity in upland soils: a reaction-diffusion model and field observation of water stress. Journal of Geophysical Research 114:G01015, doi:10.1029/2008JG000731

Weier KL, Doran JW, Power JF, Walters DT (1993) Denitrification and the dinitrogen nitrous-oxide ratio as affected by soil-water, available carbon, and nitrate. Soil Science Society of America Journal 57:66-72

Chapter 2. Applying the N_2/Ar technique to soil surface N_2 fluxes

Abstract

The emission of dinitrogen (N_2) gas from soil is the most poorly constrained flux in terrestrial nitrogen (N) budgets because the high background atmospheric N_2 concentration makes soil N_2 emissions difficult to measure. The existing methods for measuring soil N_2 emissions have well-recognized limitations and cannot be applied to unmanipulated soils in the field setting. Here we report on a new approach using the N_2/Ar technique to measure soil surface N_2 fluxes. Our goal was to determine the theoretical and analytical feasibility of the approach, and provide the first test of the N_2/Ar technique for soil. Physical fractionation effects on the N_2/Ar ratio—solubility, thermal, and water vapor flux fractionations—were modeled allowing us to determine the actual N_2 flux from soil. In laboratory experiments using dry sand in a diffusion box, we measured a simulated biological (i.e., induced) N_2 flux of 108 mg N m^{-2} d^{-1} as 111 ± 19 mg N m^{-2} d^{-1} (± SE). In wet sand at 10 % gravimetric soil moisture, we measured an induced N_2 flux of 160 mg N m^{-2} d^{-1} as 146 ± 23 mg N m^{-2} d^{-1} when solubility and water vapor flux fractionation were taken into account. The correction for thermal fractionation was omitted because it caused measured N_2 fluxes to diverge from the expected values as well as increased variability in the measurements. For control measurements (i.e., zero N_2 added), we measured an N_2 flux of 43 ± 27 mg N m^{-2} d^{-1} in dry sand and 86 ± 47 mg N m^{-2} d^{-1} in wet sand. These data suggest that our application of the N_2/Ar method to soil surface fluxes is valid only above a detection limit of approximately 100 mg N m^{-2} d^{-1}, calculated from the external precision in $\delta Ar/N_2$ analysis. We conclude that the N_2/Ar method is currently best used as a validation tool for other methods in ecosystems with high soil N_2 emissions, but with future technological advances, it holds promise to provide high resolution measurements in low soil N_2 emission systems.

1. Introduction

Soil dinitrogen (N_2) emissions represent the loss of nitrogen (N) from the biosphere to the atmospheric pool, thus completing the N cycle. Despite the importance of this flux, terrestrial ecosystem N budgets often do not include it because it is difficult to measure against the high background atmospheric N_2 concentration (Hedin et al. 2003; Tietema and Verstraten 1991). In terrestrial ecosystems, N_2 is primarily produced via denitrification, a process by which nitrate (NO_3^-) is reduced to nitrous oxide (N_2O) and then subsequently to N_2. Nitrous oxide is a potent greenhouse gas and catalyst for stratospheric ozone depletion so that the relative amounts of N_2O and N_2 released to the atmosphere via denitrification can have major implications for atmospheric chemistry. Humans have drastically increased the amount of reactive N in the environment which has stimulated soil N_2O emissions (Schlesinger 2009). However, the effect of anthropogenic N loading on soil N_2 emissions is largely unknown (Galloway et al. 2003; Vitousek et al. 1997). In human impacted ecosystems, N inputs greatly exceed measured outputs, suggesting that a large amount of anthropogenic N is either stored in the ecosystem or released as N_2 (Groffman 2008). Accurate measurements of soil N_2 emissions are needed to better constrain ecosystem N budgets, elucidate controls on denitrification, and provide the data necessary to validate and improve models that predict ecosystem N losses as N_2O and N_2 emissions (Boyer et al. 2006).

A wide range in approaches has been used to estimate soil N_2 emissions, but each approach has well recognized limitations (Groffman et al. 2006). Acetylene (C_2H_2) inhibits the reduction of N_2O to N_2 via denitrification so that N_2 emissions can be estimated from N_2O

production in the presence and absence of C_2H_2. The acetylene inhibition technique can underestimate N_2 emissions by decreasing the supply of NO_3^- substrate via nitrification, through diffusion limitation of C_2H_2 to microsites of denitrification activity, and due to the ineffectiveness of C_2H_2 on some denitrifiers and under low NO_3^- conditions (Knowles 1990; Simarmata et al. 1993). The ^{15}N tracer method requires the addition of ^{15}N-labeled NO_3^-, the substrate for denitrification, and thus can potentially stimulate denitrification rates and change the relative amounts of N_2O and N_2 produced. The use of this method is typically restricted to systems with high soil NO_3^- concentrations, such as agricultural systems (Stevens and Laughlin 1998), because a large amount of $^{15}NO_3^-$ is needed to detect a change in ^{15}N enrichment of the atmospheric N_2 pool. The gas flow soil core method has been used to estimate ecosystem-level soil N_2 emissions from intact soil cores in the laboratory (Butterbach-Bahl et al. 2002a; Dannenmann et al. 2008). However, the soils are typically incubated under 21 % oxygen so that the N_2 flux estimates may not be representative of field rates (Butterbach-Bahl et al. 2002b). Attempts have been made to the characterize the N_2:N_2O ratio of denitrification end-products for specific study sites so that soil N_2 emissions can be estimated from soil N_2O emissions alone, which are relatively easy to measure with high resolution (Chestnut et al. 1999; Scheer et al. 2009). However, the N_2:N_2O ratios are often very variable (Dannenmann et al. 2008) and also dependent on environmental conditions (Firestone et al. 1980; Weier et al. 1993) so that there is large uncertainty in estimates of soil N_2 emissions derived by this method (Hedin et al. 2003).

Several recent advances have contributed to our understanding of soil N_2 emissions. First, ^{15}N isotope budgets can be used to constrain gaseous N losses based on mass balance models, and with measurements of NO_x losses, soil N_2 emissions can be estimated at the ecosystem scale (Houlton et al. 2006) and at the global scale (Houlton and Bai 2009). This method integrates over time and space to avoid the need for high resolution measurements of soil N_2 emissions, but as a result, it cannot provide insight into smaller scale patterns in emissions within ecosystems or with changing environmental conditions. Second, the $^{15}N_2O$ pool dilution method provides field measurements of gross N_2O production and consumption that can be related to soil characteristics, such as soil O_2 and mineral N concentrations (Yang et al., submitted a). Because this method measures N_2O consumption from the loss $^{15}N_2O$ tracer, it may not capture complete denitrification that occurs intracellularly. Thus, measured N_2O consumption rates may only be an index of soil N_2 emissions. These methods can be powerful tools for answering specific questions about N budgets or denitrification and, if used in conjunction with complementary methods that compensate for their limitations, can be used to answer a broader set of questions about denitrification to N_2 and the controls on the N_2O:N_2 ratio.

All of the methods presented thus far, except for the gas flow soil core technique, specifically measure N_2 production via denitrification, but recent studies suggest that there may be other important terrestrial N_2 production pathways. In marine and freshwater ecosystems, anaerobic ammonium (NH_4^+) oxidation using nitrite (NO_2^-) as an electron acceptor (termed anammox) accounts for up to 67 % of N_2 production (Dalsgaard and Thamdrup 2002; Rich et al. 2008; Schubert et al. 2006). Anammox has not been demonstrated to occur in soils (Jetten et al. 2009), but the Planctomycetes responsible for anammox have been detected in soils (Penton et al. 2006). Recently, iron (Fe) reduction coupled to anaerobic NH_4^+ oxidation was demonstrated in humid tropical forest soils (Yang et al., submitted b). This process, termed Feammox, may be important in highly weathered soils rich in poorly crystalline Fe. Thus, methods that specifically measure N_2 production via denitrification could underestimate gross N_2 production, but they would remain useful for studying rates of and controls on denitrification.

The N_2/Ar technique is used widely in aquatic systems to measure net N_2 production, but is more challenging to apply in terrestrial ecosystems. This method uses argon (Ar), an inert gas, as a conservative tracer. Thus, measured changes in measured N_2/Ar ratios can be attributed to changes in the abundance of N_2. Membrane inlet mass spectrometry (MIMS) can be used to measure N_2/Ar ratios with high throughput (20-30 samples per hour) and with 0.05 % precision (in terms of coefficient of variation) so that N_2 fluxes as low as 0.7 mg N m^{-2} d^{-1} can be measured (Kana et al. 1994). The N_2/Ar technique is more challenging to apply in terrestrial ecosystems because higher precision is necessary to detect changes in the N_2/Ar ratio in air. The concentration of N_2 in air is approximately 50 times more than that at saturation in fresh water at 20 °C. In addition, soils on average exhibit 10 times lower denitrification rates than aquatic sediments (Seitzinger et al. 2006). These factors together suggest that soil N_2 fluxes are approximately 500 times more difficult to measure than sediment N_2 fluxes so that MIMS does not have the precision to detect changes in N_2/Ar ratios due to soil N_2 fluxes. Paleoclimatologists have developed an analytical approach to measure N_2/Ar ratios with per meg level precision (i.e., 10^{-3} per mil) on isotope ratio mass spectrometers (IRMS) to reconstruct past climate from ice core bubbles (Kobashi et al. 2008). Such high precision measurements introduce the additional challenge of accounting for physical fractionation effects on the N_2/Ar ratio that can confound estimates of soil N_2 emissions due to biological processes. In terrestrial ecosystems, these effects include thermal fractionation, solubility fractionation, and water vapor flux fractionation. Because these fractionation effects on the N_2/Ar ratio are governed by physics, they can be modeled to remove their confounding effect on measured shifts in N_2/Ar ratios.

In this paper, we present the theoretical considerations of the N_2/Ar approach for terrestrial N_2 fluxes and provide a preliminary test of the validity and accuracy of the N_2/Ar technique for measuring surface soil N_2 fluxes under controlled laboratory conditions. Our goal was to explore the theoretical and analytical feasibility of this approach. This is a necessary first step to determine if the approach holds promise prior to the significant effort involved in optimizing the method for deployment under real-world conditions. The objectives of this study were to determine a preliminary detection limit of the N_2/Ar method for soil fluxes and also to determine if observed changes in the N_2/Ar ratio can be corrected for physical fractionation effects. While we refer to this method as the "N_2/Ar method" because N_2 is the gas of interest, when presenting methods and data, we will refer to $\delta Ar/N_2$ according to the tradition of expressing isotope ratios (or in this case, elemental ratios) with the heavier isotope in the numerator.

2. Theory and Calculations

2.1. Thermal Fractionation

In the presence of a temperature gradient, a mixture of N_2 and Ar will become fractionated because the heavier molecule, Ar, tends to reside on the colder end of the gradient while the lighter molecule, N_2, tends to reside on the warmer end of the gradient (Kincaid et al. 1987). This phenomenon is known as thermal diffusion (Chapman and Dootson 1917; Grew and Ibbs 1952). Temperature changes during a surface flux measurement can affect the N_2/Ar ratio via thermal diffusion by disturbing the temperature gradient from the soil to the atmosphere. We assume that the soil column and air are at thermal steady state initially and that they reach a new steady state by the final gas sampling. Thus, the thermal fractionation effect (expressed as $\delta Ar/N_2$ in units of per meg) can be calculated as the difference in the thermal diffusion effect at the initial and final sampling time points.

At each time point, the thermal diffusion effect (in per meg units), δ_d, can be calculated using the following equation (Chapman and Cowling 1970), where T_o is the soil temperature at bottom of soil (K), T is the chamber air temperature (K), and α is the thermal diffusion factor for N_2-Ar (Equation 1):

$$\delta_d = [(T_o/T)^{\propto} - 1] \times 10^6 \qquad \text{(Equation 1)}$$

We used a α-value of 0.078 for a mixture of N_2-Ar in atmospheric proportions at 293 K based on empirically determined values for different N_2-Ar mixtures and at different temperatures reported in the literature (see Supplementary Material). This α-value translates to a thermal diffusion effect of 286 per meg per K.

2.2. Solubility Fractionation

Temperature changes during surface flux measurements can also affect the N_2/Ar ratio because of the differing temperature-solubility curves for different gases dissolved in water (Figure 1). We call this the solubility fractionation effect. The magnitude of the solubility fractionation effect depends on soil moisture and the change from a given initial temperature (Figure 2). For example, at 10 % gravimetric soil moisture, up to 0.5 °C changes in temperature from 20 °C result in < 50 per meg shifts in the N_2/Ar ratio. However, at 40 % gravimetric soil moisture, the solubility fractionation effect is 100 per meg for every 0.1 °C change in temperature.

To estimate the solubility fractionation effect, we first calculated the proportion of soil that is particles (f_p) , water (f_w), and air (f_a) from the gravimetric soil water content (θ, kg water kg soil^{-1}), bulk density (ρ_b, g cm^{-3}), and total soil porosity (P_T, m^3 voids m^{-3} soil) using equations 2-4. The sum of f_p, f_w, and f_a must equal one. Thus, in 1 m^3 of soil at standard temperature and pressure (STP), the amount of soil particles (n_p), water (n_w), and air (n_a) is equivalent to f_p, f_w, and f_a, respectively, in units of m^3 STP.

$$f_w = \theta * \rho_b \qquad \text{(Equation 2)}$$

$$f_a = P_T - f_w \qquad \text{(Equation 3)}$$

$$f_p = 1 - P_T \qquad \text{(Equation 4)}$$

Total porosity was calculated from ρ_b, 1.42 g cm^{-3}, and particle density (ρ_p, 2.55 g cm^{-3}) determined for the diffusion box sand (Blake and Hartge 1986) (Equation 5).

$$P_T = 1 - \frac{\rho_b}{\rho_p} \qquad \text{(Equation 5)}$$

Hamme and Emerson (2004) recently made high precision measurements of N_2 and Ar solubility in distilled water from 0 to 30 °C. We used their equations to calculate N_2 and Ar Bunsen coefficients (β, L of gas dissolved per L of water) at the temperatures measured when the initial and final gas samples were taken. We calculated the change in N_2 contained in soil water, $\Delta n_{N2,w}$, using Equation 6 where X_{N2} is the dry air mole fraction of N_2 (0.78084 m^3 STP N_2 m^{-3} STP) from Glueckauf (1951):

$$\Delta n_{N2,w} = \left(X_{N2} * \beta_{N2,final} * n_w\right) - \left(X_{N2} * \beta_{N2,initial} * n_w\right) \qquad \text{(Equation 6)}$$

We calculated the change in N_2 contained in soil air, $\Delta n_{N2,a}$, using Equation 7 where T_{STP} is the temperature at STP, 273.15 K; and $T_{initial}$ (K) is the initial average soil temperature from the five thermocouples weighted by soil depth:

$$\Delta n_{N2,a} = \left(\frac{X_{N2} * n_a * T_{STP}}{T_{initial}}\right) - \Delta n_{N2,w} \qquad \text{(Equation 7)}$$

We scaled $\Delta n_{N2,a}$ to the volume of soil beneath the chamber, $\Delta n_{N2,a*}$, using Equation 8 where A is the basal area of the chamber in m^2 and z is the soil depth in m:

$$\Delta n_{N2,a*} = \Delta n_{N2,a} * A * z \qquad \text{(Equation 8)}$$

We calculated the initial amount of N_2 in the chamber headspace, $n_{N2,\,c,\,initial}$ in m^3 STP, using equation 9 where V is the chamber volume in m^3:

$$n_{N2,c,initial} = \left(\frac{V * T_{STP}}{T_{initial}}\right) * X_{N2} \qquad \text{(Equation 9)}$$

We then determined the final amount of N_2 in the chamber headspace, $n_{N2,\,c,\,final}$ in m^3 STP, using equation 10:

$$n_{N2,c,final} = n_{N2,c,initial} + \Delta n_{N2,a*} \qquad \text{(Equation 10)}$$

We performed the same calculations for Ar to determine $n_{Ar,\,c,\,initial}$ and $n_{Ar,\,c,\,final}$ in m^3 STP. The dry air mole fraction of Ar was 0.009340 m^3 STP N_2 m^{-3} STP (Glueckauf 1951).

We estimated the initial Ar/N_2 ratio, in per meg, using Equation 11:

$$\left(\delta\frac{Ar}{N_2}\right)_{initial} = \left\{\left[\left(\frac{n_{Ar,c,initial}}{n_{N2,c,initial}}\right)\Big/\left(\frac{X_{Ar}}{X_{N2}}\right)\right] - 1\right\} * 10^6 \qquad \text{(Equation 11)}$$

We performed the same calculation for the final Ar/N_2 ratio and determined the solubility fractionation effect as the difference between the final and initial Ar/N_2 ratios in units of per meg.

2.3. Water Vapor Flux Fractionation

Water vapor flux fractionation occurs when evaporation causes air to diffuse into the soil to replace the water vapor lost; N_2 is a smaller and lighter molecular than Ar so that the N_2/Ar ratio decreases in response to evaporation (Severinghaus et al. 1996). This effect is smaller in environments with low soil evaporation rates, such as those with high atmospheric humidity or low soil moisture. The water vapor flux fractionation effect can be limited to less than 100 per meg if the relative humidity changes from initial value of 95 % to a final value of 100 % with no accompanying changes in temperature (Figure 3). Even if the relative humidity begins and ends at 100 %, up to a 0.5 °C change in temperature can result in up to a 48 per meg shift in the N_2/Ar ratio because saturation vapor pressure is a function of temperature (Figure 3).

The water vapor flux fractionation effect (per meg), δ_w, can be estimated from the binary diffusion coefficients of gases i and j with water vapor ($D_{i\text{-}H2O}$ and $D_{j\text{-}H2O}$, respectively) and the initial and final water vapor mole fractions (X_{H2O_o} and X_{H2O}, respectively) according to Severinghaus et al.(1996) (Equation 12). Gas j is the lighter molecule of the pair, so in this case, j is N_2 and i is Ar. This equation gives the water vapor fractionation effect in terms of Ar/N_2 in per meg.

$$\delta_w = \left[\frac{(1 - X_{H2O})}{(1 - X_{H2O_0})}^{(D_{j-H2O}/D_{i-H2O}) - 1} - 1\right] \times 10^6 \qquad \text{(Equation 12)}$$

The ratio of the binary diffusion coefficients of N_2 and Ar in water vapor was estimated to be 1.0644 according to Equation 13 where m_i, m_j, and m_{H2O} are the respective molecular weights of gases i, j, and water vapor (Severinghaus et al. 1996).

$$\frac{D_{j-H2O}}{D_{i-H2O}} = \left[\frac{\frac{m_j + m_{H2O}}{m_j \times m_{H2O}}}{\frac{m_i + m_{H2O}}{m_i \times m_{H2O}}}\right]^{1/2} \qquad \text{(Equation 13)}$$

The water vapor mole fraction was calculated from water vapor pressure (p_{H2O}, atm) and atmospheric pressure (P, mbar) using Equation 14:

$$X_{H2O} = pH_2O \times \frac{1013.25}{P} \qquad \text{(Equation 14)}$$

The saturation vapor pressure (p_s, atm) was calculated from measured air temperature (T_{air}, °C) using Equation 15 (Severinghaus et al. 1996):

$$pH_2O_s = [1.69803084 + (0.7568078 \times T_{air}) - (0.0109724 \times T_{air}^2) + (0.00063967 \times T_{air}^3)]/760 \quad \text{(Equation 15)}$$

The water vapor pressure was then determined from measured relative humidity (RH, %) and p_s (Equation 16):

$$pH_2O = \frac{RH}{100} \times p_s \quad \text{(Equation 16)}$$

2.4. Soil Surface N_2 Flux Calculation

Soil surface N_2 fluxes can be calculated from the change in $\delta Ar/N_2$ of gas sampled from a surface flux chamber headspace over time. The fundamental assumption of the N_2/Ar technique is that the headspace Ar concentration remains constant so that changes in $\delta Ar/N_2$ are due solely to changes in the headspace N_2 concentration. For soil surface N_2 fluxes, the physical fractionation effects discussed earlier also cause changes in $\delta Ar/N_2$ so these effects must be removed from the measured change in $\delta Ar/N_2$ to obtain the biological change in $\delta Ar/N_2$. The thermal and solubility fractionation effects enhance measured changes in $\delta Ar/N_2$ when temperatures increase and lower measured fluxes in $\delta Ar/N_2$ when temperatures decrease. Thus, these effects are subtracted from the measured $\delta Ar/N_2$ for the final headspace sample. The water vapor flux fractionation effect causes an apparent N_2 flux into the soil, so this effect was added to the measured $\delta Ar/N_2$ for the final headspace sample. We used the resulting biological $\delta Ar/N_2$ value for the final headspace sample in the following calculations to estimate the actual N_2 flux over the one hour sampling period.

We determined the N_2 concentration in each sample (mole fraction), c_{sample}, using the following equation where c_{atm} is the atmospheric N_2 concentration (assumed to be 0.78084 mole fraction in air, Glueckauf 1951), $\delta Ar/N_2$ is the measured sample value (per meg), and $\delta Ar/N_2$ is the reference standard value (per meg) (Equation 21). The reference standard is La Jolla air sampled from Scripps pier at UCSD. The reference standard and samples were analyzed against a working standard consisting of UHP N_2 and Ar in near atmospheric proportions.

$$c_{sample} = \left\{\left[\frac{(\delta Ar/N_2)_{sample}}{1000} + 1\right]/\left[\frac{(\delta Ar/N_2)_{ref}}{1000} + 1\right]\right\} \times c_{atm} \quad \text{(Equation 21)}$$

The soil surface N_2 flux (mg N m^{-2} d^{-1}), F, was calculated as the linear change in N_2 concentration in the chamber headspace between the two time points using the following equation where m_{N2} is the molecular weight of N_2 (g mol^{-1}), t is the time elapsed (d), and R is the ideal gas constant (8.2057 * 10^{-5} m^3 atm K^{-1} mol^{-1}) (Equation 22).

$$F = \left[\left(c_{final} - c_{initial}\right) \times V \times m_{N2} \times 10^3\right]/\left(a \times t \times \frac{P}{R \times T_{air}}\right) \quad \text{(Equation 22)}$$

3. Laboratory Test

3.1. Experimental Design

We tested the N_2/Ar method by inducing known N_2 fluxes in a diffusion box located in a climate-controlled laboratory at the University of California, San Diego (UCSD). The box consisted of 61 cm x 61 cm mirror-finished aluminum sheets welded together to leave an open top. A 10.2 cm tall perforated aluminum platform was placed in the diffusion box to create a void space in the bottom. The platform was lined with window screening to minimize sand

falling through into the void space. Two 50 mm x 50 mm fans were mounted on opposite sides of the diffusion box and offset from the center to promote air circulation within the void space. A septum port was installed in the center of a third side to allow injection of N_2 into the void space. The box was filled with air dried Felton sand (American Soil and Stone, Richmond, California) to 30 cm depth.

We performed ten consecutive control measurements of N_2 fluxes in dry sand (no N_2 injected) as well as ten consecutive measurements with 2 mL ultra-high purity (UHP) N_2 injected. We also performed ten consecutive measurements of N_2 fluxes in wet sand with no N_2 injected and five consecutive measurements with 10 mL UHP N_2 injected. After each measurement with N_2 injections, we opened the septum port and waited at least 20 hours before performing the next measurement. To wet the sand, we added 20 L deionized water to the diffusion box to bring the soil moisture to 10 % gravimetric water content. Lysimeters containing 400 g wet sand were used to monitor changes in soil moisture daily. Typically, 1 L deionized water was added every other day to maintain the soil moisture. The sand was mixed to create homogeneous soil moisture throughout the diffusion box, and then the sand was allowed to equilibrate for at least 12 hours before the next measurement. After each flux measurement, triplicate 30 g samples of sand were removed from the diffusion box to determine the gravimetric water content.

The expected N_2 flux induced by the injection of N_2 into the bottom void space of the diffusion box was calculated using Fick's law (Equation 23), where D_s is the soil diffusivity of N_2 ($m^2\ s^{-1}$), dc is the difference in N_2 concentration between the top and bottom of the soil column (mole m^{-3}), and dz is the height of the soil column (m):

$$F = D_s \frac{dc}{dz} \qquad \text{(Equation 23)}$$

Unit conversions are required to obtain F in units of mg N $m^{-2}\ d^{-1}$. The soil diffusivity of N_2 was estimated as the product of the free air diffusivity of N_2 and soil tortuosity. The free air diffusivity of N_2 at 20 °C, the ambient air temperature in the laboratory, was $1.92 * 10^{-5}\ m^2\ s^{-1}$ according to the Fuller equation (Reid et al. 1977). Soil tortuosity, τ (unitless), was described using the Millington and Quirk (1961) model where f_a is air-filled porosity (m^3 air-filled voids m^{-3} soil) and $P_{T\ is}$ is total soil porosity (m^3 voids m^{-3} soil) (Equation 24):

$$\tau = \frac{{f_a}^{10/3}}{{P_T}^2} \qquad \text{(Equation 24)}$$

3.2. Sample Collection

Gas samples were collected from a custom-made two piece 18 L aluminum chamber covered with two layers of reflective bubble wrap. Two internal mixing fans (50 mm x 50 mm) were attached to the chamber lid. The lid also had inlet and outlet ports consisting of stainless steel Swagelok bulkhead tube fittings sealed on viton. The lip of the chamber lid sealed against a viton strip lining the 1.5" wide lip of the chamber base when clamped together using either six spring clamps or four C-clamps. The chamber was deployed over water and leak checked with SF_6; the measured leak rate over three hours was 0.3 % per hour.

Gas samples were stored in custom-made 2 L cylindrical glass flasks with two parallel 9 mm (OD) high vacuum valves (Louwers, Hapert, The Netherlands) on one end. The outlet valve was centered on the end of the flask with a glass tube protruding inside almost to the bottom of the flask; the inlet valve was off-centered and connected to a third valve to create a pipette of approximately 1.5 mL volume (Figure 4). The viton o-rings on the valves were regularly cleaned

of lint and other particles, and greased sparingly with high vacuum lubrication (TorrLube, Santa Barbara, CA). The valves were leak checked on the vacuum line after maintenance. To leak check, a bellows-sealed valve in-between the turbo pump and the vacuum line was closed for one minute, and the vacuum line pressure was monitored using a high vacuum pressure gauge. A change in pressure of $< 10^{-4}$ torr was not considered to be a significant leak.

The chamber, flasks, and a pumping module were connected using 1/4" Dekabon tubing attached with stainless steel Swagelok and Ultra-torr fittings. A stainless steel bellows-sealed valve (SS-4H-TH3, Swagelok, Solon, OH) was placed in-between the inlet and outlet valves for the first flask. Thus, when the bellows-sealed valve was closed, all of the sample flask valves were opened to allow flow through both flasks. When the bellows-sealed valve was opened, only the second sample flask valves were open so that the first flask was bypassed. To sample, the flask valves were opened wide to not restrict flow. The pump and chamber fans were then turned on for 10 minutes. A flow meter was used to ensure the flow rate was at least 4 L/min. The flasks valves were also closed in-between samplings. The chamber was first sampled with gas circulating between both flasks and the chamber. After one hour, the chamber headspace was circulated with only the second flask.

Fractionation during sampling can introduce large biases into N_2/Ar measurements, so a number of precautions were taken. The pump was placed downstream of the flasks so that gas fractionated by the pump would not be directly sampled. Long lengths (2-4 m) of Dekabon tubing were coiled in a horizontal orientation so that any fractionation caused by the pump was separated from the flask. This also helped to minimize gravitational fractionation. Furthermore, the flask valves were closed five seconds after the pump was turned off so that fractionation due to turbulence would be minimized. Lastly, the flask valves were closed very quickly by rolling them with the palm of the hand instead of finger-turning them. This minimizes the fractionation that occurs when a small orifice is left before the valve is completely closed.

For each measurement, we inserted the chamber base 3 cm into the sand in the center of the box and then inserted T-type thermocouples to five depths (0, 5, 10, 15, 26 cm) next to the chamber. The thermocouples were connected to a CR10X datalogger (Campbell Scientific, Logan, UT) that recorded temperature every thirty seconds. We turned on the void fans just before injecting the desired amount of UHP N_2 through the septum port using a polypropylene syringe equipped with a zero-volume stopcock. We allowed the void air to continue circulating for five minutes while placing the lid on the chamber base and sealing the chamber. We then turned off the void fans, turned on the chamber fans, and started sampling using the pumping module. We measured the initial relative humidity by placing a thermohygrometer probe (Oakton, Vernon Hills, IL) on the sand surface next to the chamber while the initial gas sample was taken, and we measured the final relative humidity by quickly placing the probe inside the chamber after the final gas sample was taken.

3.3. Sample Preparation

Gas samples were prepared for mass spectrometer analysis on a vacuum line using a method developed for Ar/N_2 analysis of gas bubbles trapped in ice core samples (Kobashi et al. 2008). The stainless steel vacuum line included a series of traps: (1) a glass U-trap in ethanol-liquid N_2 mix to -90° C to remove water vapor, (2) a glass U-trap in liquid N_2 to remove N_2O, carbon dioxide, and hydrocarbons, (3) copper (Cu) mesh in a 5 cm long quartz tube heated to 500° C to remove O_2, and (4) a glass U-trap in liquid N_2 to remove any hydrocarbons produced

in the Cu oven. The Cu was regenerated after every 4-8 samples by passing hydrogen through the heated Cu oven at greater than 5 torr pressure for 5-10 minutes.

The sample flask was placed horizontally in the center of an isothermal box with a small opening to allow a ¼" stainless steel tube to protrude to the exterior of the box. This tube connected the flask side port to the end of the vacuum line via Ultra-torr fittings. The flask pipette was pumped down until enough water vapor was removed to leak check the vacuum line. If no leaks were detected, then a sample aliquot was transferred from the sample flask to the pipette by closing the vertical valve and then opening the horizontal valve to the flask side port. The gas was allowed to equilibrate for 30 minutes before the horizontal valve was closed to seal off the bulk sample in the flask.

Sample aliquots were quantitatively transferred from the sample flask pipette to an evacuated dip tube cooled in a liquid helium dewar. To transfer the aliquot, the vertical valve was opened very slowly to keep the pressure in the vacuum line below 1 torr; this ensured that all of the O_2 in the sample was removed in the Cu oven. The leak check procedure was also used to determine that the entire sample had been transferred into the dip tube and that no leaks had occurred during the transfer. Samples were then allowed to homogenize in the dip tubes for 2-18 hours before analysis on the mass spectrometer. As a precaution against variability in measured N_2/Ar ratios caused by differences in homogenization times, all samples for a given flux measurement were homogenized for a similar amount of time (i.e., no greater than 4 hours difference in homogenization time).

3.4. Sample Analysis

Samples were analyzed on a dual inlet Finnegan DeltaPlus XP IRMS with multiple collectors for N, Ar, and O isotopes. Samples containing O_2 are normally analyzed on this instrument, but during this study, no O_2 was introduced into the IRMS. Samples were analyzed for 6 blocks of 16 cycles using a 12 second integration window. At the beginning of each block, the bellows are compressed to achieve a 4.2 V *m/z* 36 signal to minimize potential errors due to non-linearity. The IRMS output was corrected for pressure imbalance between the two bellows using a linear regression equation based on the 6 block averaged data. For the flux calculations, we used the average Ar/N_2 ratio of 2-3 analytical replicates from each flask.

A working standard gas consisting of high purity N_2 and Ar in near atmospheric proportions was standardized against La Jolla air collected from the Scripps pier (Blaine et al. 2006; Severinghaus et al. 2003). An aliquot of gas was transferred from the standard can to a stainless steel pipette (bracketed by 4H bellows valves) that had been pumped down online. The gas was allowed to equilibrate between the standard can and the pipette for 20 minutes before the inner valve was closed; the outer valve was then opened to fill the evacuated standard bellows. Meanwhile, the closed dip tube containing the prepared sample was pumped down online for at least one hour, and then the dip tube was opened to fill the evacuated sample bellows. The sample and standard are allowed to equilibrate in the completely expanded bellows for 10 minutes. The standard can, dip tube, and bellows were contained in an isothermal box to minimize N_2/Ar fractionation due to thermal diffusion (Grachev and Severinghaus 2003) as well as variability in measured N_2/Ar due to temperature changes during bellows equilibration and/or sample analysis.

We evaluated the external precision of the δAr/N_2 measurements by calculating the pooled standard deviation for all analytical replicates within each treatment (e.g., N_2 injected in dry sand). The flux measurements in dry sand with an induced N_2 flux were performed with

samples analyzed in triplicates whereas the samples for the other treatments were analyzed in duplicates. The use of duplicates rather than triplicates allowed us to analyze samples for two flux measurements each day rather than only one per day.

4. Results and Discussion

4.1. Precision and Detection Limit

We consistently measured N_2/Ar ratios with very high precision. For the flux measurements in dry sand with an induced N_2 flux, the precision was 5 per meg for triplicate sample analysis. For the other treatments, the precision ranged from 12-13 per meg for duplicate sample analysis. The poorest reproducibility among analytical replicates for all samples was a standard deviation of 42 per meg for a duplicate set. There were no indications of leaks or other reasons for the poor reproducibility of some replicates, so none of the data were rejected. Despite the higher precision yielded by analyzing triplicates, time constraints forced us to analyze duplicates for most of the flux measurements performed. This allowed us to approximately double our throughput, analyzing samples for two flux measurements per 14 hour work day versus one flux measurement per 12 hour work day. Using our sampling equipment and procedure, a 1 per meg change in $\delta Ar/N_2$ was equivalent to an N_2 flux of approximately 3 mg N m^{-2} d^{-1}. If the detection limit of the method is calculated as three times the precision in $\delta Ar/N_2$ analysis, then the detection limit is 45 mg N m^{-2} d^{-1} using triplicates whereas it is 108 mg N m^{-2} d^{-1} using duplicates.

The correction for the physical fractionation effects on N_2/Ar ratios can create additional errors in the flux measurements if temperature and relative humidity are not accurately measured. These errors would likely overwhelm the errors associated with the models used to estimate the physical fractionation effects. For example, if the chamber temperature was initially 0.1° C warmer than measured, then the thermal fractionation effect would be 28.6 per meg greater and the water vapor flux fractionation effect would be 9 per meg less than measured for a total underestimate of 19.6 per meg for these fractionation effects. This would translate to a 78 mg N m^{-2} d^{-1} error in the corrected N_2 flux.

4.2. Measurements in Dry Sand

The control measurements in dry sand demonstrate that the measurements of fluxes below the calculated detection limit of 108 mg N m^{-2} d^{-1} are highly variable and can be inaccurate. For three out of the ten measurements, we observed a 1 per meg change in $\delta Ar/N_2$, which is consistent with no induced N_2 flux. However, overall we measured changes in $\delta Ar/N_2$ ranging from -71 to 18 per meg corresponding to an average N_2 flux of 43 ± 27 mg N m^{-2} d^{-1} (n = 10). When corrected for thermal fractionation, which ranged in magnitude from 19 to 96 per meg, the N_2 flux was 46 ± 45 mg N m^{-2} d^{-1}. This could suggest that the sampling protocol causes an artifact of approximately 45 mg N m^{-2} d^{-1}. However, the addition of 2 mL UHP N_2 into the diffusion box void space induced an N_2 flux of 108 mg N m^{-2} d^{-1}, which was very similar to the average measured N_2 flux of 111 ± 19 mg N m^{-2} d^{-1} (± SE, n = 10). Therefore, the control measurements likely do not represent a sampling artifact but simply reflect our inability to accurately measure N_2 fluxes below the detection limit.

The induced N_2 flux measurements in dry sand suggest that thermal fractionation may not be manifested within the one hour sampling period we used. In dry soil, solubility and water vapor flux fractionation do not occur, so we were able to test for thermal fractionation alone. The measured changes in $\delta Ar/N_2$ ranging from 2 to -59 per meg while the thermal fractionation effect

ranged from -34 to 34 per meg. When thermal fractionation was taken into account, the average corrected N_2 flux was 91 ± 36 mg N m^{-2} d^{-1}. The correction for thermal fractionation not only caused the measured N_2 flux to diverge from the expected N_2 flux, but it also increased the variability in the measured N_2 fluxes. The coefficient of variation (CV) for the uncorrected N_2 fluxes was 53 % whereas the CV for the corrected N_2 fluxes was 124 %. This suggests that the correction for thermal fractionation does not improve the N_2 flux estimation and does not accurately represent the effects of thermal diffusion on the N_2/Ar ratio. For these reasons we do not recommend the use of a thermal fractionation correction.

There are several reasons why the correction for thermal fractionation may not be valid or necessary for our N_2 flux measurements. First, thermal fractionation has been observed in sand dunes, polar firn, and ice cores where the gases have reached steady state equilibria (Severinghaus et al. 1996, Severinghaus et al. 1998, Severinghaus et al. 2003). In the diffusion box, the temperature changed throughout the sampling period so that the gases were not in steady state with respect to thermal diffusion. This violates a fundamental assumption of thermal diffusion so that thermal fractionation may not have been manifested despite changes in temperature. Second, the temperature profiles show that the temperature change was often non-linear with depth so that a shift in the $\delta Ar/N_2$ of the chamber headspace due to thermal fractionation is difficult to model. Here we simply used a change in an assumed linear temperature gradient between the chamber headspace and the bottom of the diffusion box to calculate the thermal fractionation effect. This simplified approach may not have been valid. Last, in our flux measurements, changes in the temperature gradient were $\leq 0.3°$ C. Though thermal fractionation causes a 286 per meg shift in $\delta Ar/N_2$ per degree of temperature change, it is possible that small changes in the temperature gradient within one hour do not cause a detectable shift in the $\delta Ar/N_2$ of the chamber headspace.

4.3. Measurements in Wet Sand

When we wet the diffusion box sand to 10 % gravimetric soil water content, we observed evidence of the water vapor flux fractionation effect, which causes a decrease in the N_2/Ar ratio to create an apparent net uptake of N_2 by the soil. For the control measurements, we observed N_2 fluxes of -44 ± 19 mg N m^{-2} d^{-1} (n = 5) when the water vapor flux fractionation effect was not taken into account. We also performed these flux measurements after allowing for an initial ten minute period with the chamber lid set but not sealed on the chamber base before the sampling procedure began. This additional time would be needed for the added N_2 to move through the wet sand for the induced N_2 flux measurements. This change in procedure did not significantly change the measured N_2 fluxes, with a measured N_2 flux of -48 ± 77 mg N m^{-2} d^{-1} (n = 5). We used this modified sampling protocol for flux measurements with a known N_2 flux of 160 mg N m^{-2} d^{-1} (from the injection of 10 mL UHP N_2) in wet sand; the measured N_2 flux was 61 ± 25 mg N m^{-2} d^{-1}. As expected, the measured N_2 fluxes were lower than the expected N_2 fluxes for all treatments when the water vapor flux fractionation effect was not considered.

The water vapor flux fractionation effect was difficult to quantify because the thermohygrometer readout took approximately 5 minutes to stabilize, and during this time, the relative humidity inside the chamber was changing in response to ongoing evaporation. The measurement was also complicated by the fact that we could not place the thermohygrometer probe inside the chamber during the flux measurement due to the design of the chamber. Measurements of changes in relative humidity inside the chamber taken when gas was not being sampled show that the relative humidity reached 98.8 % in ten minutes and 99.4% in 20 minutes

after the chamber lid was placed on the deployed chamber base. Assuming that the initial air inside connecting tubing was at ambient relative humidity (50%), the initial air inside the flasks was at 90% relative humidity, and that the chamber headspace was at 99.9% relative humidity, we calculate a relative humidity of 97.0% at the initial time point, and an assumed relative humidity of 99.9% at the final time point. A 1% error in relative humidity translates into a 15 per meg error in the water vapor flux fractionation effect.

Solubility fractionation had a relatively small effect on $\delta Ar/N_2$ compared to the other fractionation effects. With the assumed relative humidity and measured air temperature, we estimated that the water vapor flux fractionation effect ranged from 15-60 per meg for all of the measurements in wet sand, the solubility fractionation effect ranged from -17 to 15 per meg, and thermal fractionation effect ranged from -64 to 32 per meg. We calculated solubility fractionation based on the average soil temperature. If the solubility fractionation effect was calculated for each depth increment and then summed, then it only produced a 1 per meg difference compared to the approach we used. With the relatively low soil moisture in the diffusion box and the small temperature changes during our flux measurements, the solubility fractionation effect was only -17 to 15 per meg, with the direction of the effect dependent on whether the bulk soil cooled or warmed during the measurement. This effect could be larger when soil moisture is higher or when temperature changes are greater. For example, Figure 2 shows that at 40 % gravimetric soil water content, the solubility fractionation effect is greater than 100 per meg per 0.1 °C change in temperature. This underscores the importance of limiting temperature changes during N_2/Ar measurements, which can be accomplished by shading the chamber and avoiding the times of day with large changes in soil temperature (e.g., just after sunrise).

The flux measurements in wet sand support the implications from the flux measurements in dry sand. For the control measurements, the average measured N_2 flux corrected for all physical fractionation factors was 75 ± 44 mg N m^{-2} d^{-1} whereas the average N_2 flux was 86 ± 47 mg N m^{-2} d^{-1} when only corrected for solubility and water vapor flux fractionation. These measurements demonstrate that we cannot measure N_2 fluxes below the calculated detection limit. For the induced N_2 flux measurements, the average N_2 flux was 134 ± 39 mg N m^{-2} d^{-1} when all physical fractionation effects were accounted for and 146 ± 23 mg N m^{-2} d^{-1} when only solubility and water vapor flux fractionation were considered. Without correcting for thermal fractionation, the average measured N_2 flux was more similar to the expected N_2 flux of 160 mg N m^{-2} d^{-1} and also less variable. Thus, this provides additional evidence that the correction for thermal fractionation is not necessary.

Water vapor flux fractionation was the least well constrained physical fractionation effect, but we were able to effectively account for its effect on the N_2/Ar ratio. Our approximation of the initial relative humidity in the chamber headspace appears to be valid because the measured N_2 fluxes corrected for the water vapor flux and solubility fractionation effects agreed well with the expected values for the induced N_2 fluxes. However, it is ideal for water vapor pressure to be measured in the chamber headspace in real time with an instrument that stabilizes more quickly.

4.5. Future Improvements to the Method

The detection limit for this method at present is very high but it can easily be lowered by increasing the ratio of chamber basal area to volume as well as increasing the sampling time period. Chambers with large basal areas can be unwieldy and difficult to deploy in ecosystems

with dense vegetation. However, the ratio of chamber basal area to volume can also be increased by decreasing the chamber height from the 12 cm we used. Short chambers (< 10 cm tall) can suppress soil surface trace gas fluxes by approximately 16 % because of gas storage in the soil surface. A longer sampling time period can also lower the detection limit, but like short chambers, it can cause changes in the concentration gradients of trace gases in the soil and suppress the surface flux. While N_2 is not a trace gas, changes in the diffusion of trace gases could cause corresponding non-trivial changes in N_2 diffusion. Thus, these measures for lowering the detection limit should be employed with caution.

The N_2/Ar technique can be applied to soil depth profiles which may exhibit greater differences in N_2/Ar that can be measured accurately using the gas analysis approach described here. This approach creates the challenge of sampling soil gas without causing fractionation at the per meg level. We have attempted passive sampling in laboratory tests with no induced change in N_2, but we have measured approximately 500 per meg fractionation in $\delta Ar/N_2$ (data not shown). The sampling procedure we used involved pumping air through large volume flasks and resulted from many years of testing to minimize sampling artifacts. For example, Blaine et al. (2006) found that temperature gradients within the sampling equipment can cause N_2/Ar fractionation. Another factor in using the soil profile approach is the sample volume of soil gas that can be collected. A large sample volume is required for running analytical replicates without fractionating the remaining sample in the flask. If analytical replicates are not desired, then entire small samples could be analyzed to avoid fractionation. Beyond these practical considerations, the physical fractionation effects will also need to be constrained along the soil profile.

Theoretically, the observed fractionation of inert gas ratios or isotope ratios of inert gases can be used to constrain the physical fractionation effects on N_2/Ar. For example, $\delta^{40}Ar$ and $\delta^{15}N$ are often used together in paleoclimate work to separate different physical fractionation effects (Severinghaus et al. 1998). Argon is the most abundant naturally occurring inert gas, so that the isotopic composition of Ar can be measured with higher precision than for other inert gases. However, the precision for Ar isotopes is worse than that for $\delta Ar/N_2$ so that it cannot be used to accurately constrain physical fractionation effects on N_2/Ar. Future improvements in $\delta^{40}Ar$ analysis could allow this approach to be used as validation of the modeling approach we employed to estimate the physical fractionation effects.

Gas analysis using a dual inlet IRM with offline sample preparation had very low throughput that precludes its use for high resolution measurements of soil N_2 emissions. This analytical approach was chosen for this study because the instrumentation and protocols were already set up and tested for our analyses. Keeling et al. (2004) presented a higher throughput method on a continuous flow IRMS with online removal of water vapor and carbon dioxide that provides $\delta Ar/N_2$ analysis with per meg level precision similar to that presented here. The addition of online O_2 removal would permit their method to be applied to our approach. Gas handling likely introduces a large proportion of the variability between analytical replicates so that online gas preparation would likely improve external precision. Thus, a continuous flow IRMS approach could not only increase throughput but also lower the detection limit of the method.

5. Conclusions

We demonstrated that the N_2/Ar technique can be used to measure soil N_2 emissions without manipulating soil conditions. Given the current high detection limit and throughput limitations of the method, it is currently best suited as a verification tool for other methods in

ecosystems with high soil N_2 emissions rather than a technique for high resolution field measurements. Physical fractionation effects on the N_2/Ar ratio can be constrained, but accurate measurements of temperature and relative humidity are necessary. Moreover, temperature changes and evaporation during the sampling period should be minimized to limit the physical fractionation effects. With technological and methodological advances we can lower the detection limit, better constrain the physical fractionation effects, and increase sample throughput so that the N_2/Ar technique can be used in a wider range of ecosystems for high resolution field measurements of soil N_2 emissions.

References

Batabyal AK, Ghosh AK, Barua AK (1967) Improved design for Trennschaukel - Measurement of thermal diffusion factors in gas mixtures. Journal of Chemical Physics 47:448-451

Blaine TW, Keeling RF, Paplawsky WJ (2006) An improved inlet for precisely measuring the atmospheric Ar/N-2 ratio. Atmospheric Chemistry and Physics 6:1181-1184

Blake G, Hartge K (1986) Particle Density. In: Klute A (ed) Methods of Soil Analysis. Part 1. Physical and Mineralogical Methods. Soil Science Society of America, Madison, WI

Boyer EW et al. (2006) Modeling denitrification in terrestrial and aquatic ecosystems at regional scales. Ecological Applications 16:2123-2142

Butterbach-Bahl K, Gasche R, Willibald G, Papen H (2002a) Exchange of N-gases at the Hoglwald Forest - A summary. Plant and Soil 240:117-123

Butterbach-Bahl K, Willibald G, Papen H (2002b) Soil core method for direct simultaneous determination of N_2 and N_2O emissions from forest soils. Plant and Soil 240:105-116

Chapman S, Cowling T (1970) The Mathematical Theory of Non-Uniform Gases. Cambridge University Press, Cambridge

Chapman S, Dootson F (1917) Thermal diffusion. Philosophical Magazine 33:248-253

Chestnut TJ, Zarin DJ, McDowell WH, Keller M (1999) A nitrogen budget for late-successional hillslope tabonuco forest, Puerto Rico. Biogeochemistry 46:85-108

Dalsgaard T, Thamdrup B (2002) Factors controlling anaerobic ammonium oxidation with nitrite in marine sediments. Applied and Environmental Microbiology 68:3802-3808

Dannenmann M, Butterbach-Bahl K, Gasche R, Willibald G, Papen H (2008) Dinitrogen emissions and the N_2:N_2O emission ratio of a Rendzic Leptosol as influenced by pH and forest thinning. Soil Biology & Biochemistry 40:2317-2323

Firestone MK, Firestone RB, Tiedje JM (1980) Nitrous oxide from soil denitrification: Factors controlling its biological production. Science 208:749-751

Galloway JN et al. (2003) The nitrogen cascade. Bioscience 53:341-356

Glueckauf E (1951) The composition of atmospheric air. In: Compendium of Meterology. American Meteorological Society, Boston, pp 3-11

Grachev AM, Severinghaus JP (2003) Laboratory determination of thermal diffusion constants for N-29(2)/N-28(2) in air at temperatures from-60 to 0 degrees C for reconstruction of magnitudes of abrupt climate changes using the ice core fossil-air paleothermometer. Geochimica Et Cosmochimica Acta 67:345-360

Grew K, Ibbs T (1952) Thermal Diffusion in Gases. Cambridge University Press, Cambridge

Groffman PM (2008) Nitrogen balances at ecosystem, landscape, regional and global scales. In: Schepers J, Raun W (eds) Nitrogen in Agricultural Soils. Soil Science Society of America, Madison, WI

Hamme RC, Emerson SR (2004) The solubility of neon, nitrogen and argon in distilled water and seawater. Deep-Sea Research Part I-Oceanographic Research Papers 51:1517-1528

Hedin LO, Vitousek PM, Matson PA (2003) Nutrient losses over four million years of tropical forest development. Ecology 84:2231-2255

Houlton BZ, Bai E (2009) Imprint of denitrifying bacteria on the global terrestrial biosphere. Proceedings of the National Academy of Sciences of the United States of America 106:21713-21716

Houlton BZ, Sigman DM, Hedin LO (2006) Isotopic evidence for large gaseous nitrogen losses from tropical rainforests. Proceedings of the National Academy of Sciences of the United States of America 103:8745-8750
Jetten MSM, van Niftrik L, Strous M, Kartal B, Keltjens JT, Op den Camp HJM (2009) Biochemistry and molecular biology of anammox bacteria. Critical Reviews in Biochemistry and Molecular Biology 44:65-84
Kana TM, Darkangelo C, Hunt MD, Oldham JB, Bennett GE, Cornwell JC (1994) Membrane inlet mass spectrometer for rapid high precision determination of N_2, O_2, and Ar in environmental water samples. Analytical Chemistry 66:4166-4170
Keeling RF, Blaine T, Paplawsky B, Katz L, Atwood C, Brockwell T (2004) Measurement of changes in atmospheric Ar/N-2 ratio using a rapid-switching, single-capillary mass spectrometer system. Tellus Series B-Chemical and Physical Meteorology 56:322-338
Kincaid J, Cohen E, Lopez de Haro M (1987) The Enskog theory for multicomponent mixtures. IV. Thermal diffusion. Journal of Chemical Physics 86:963-975
Knowles R (1990) Acetylene inhibition technique: development, advantages, and potential problems. In: Revsbech N, Sørensen J (eds) Denitrification in Soil and Sediment. Plenum Press, New York, pp 151–166
Kobashi T, Severinghaus JP, Kawamura K (2008) Argon and nitrogen isotopes of trapped air in the GISP2 ice core during the Holocene epoch (0-11,500 B.P.): Methodology and implications for gas loss processes. Geochimica Et Cosmochimica Acta 72:4675-4686
McCourt FRW (2003) Thermal diffusion in binary mixtures containing molecular gases II: mixtures of N_2 with He, Ne, Ar, and Kr and of CO_2 with He and Ar. Molecular Physics 101:2409-2426
Millington R, Quirk JP (1961) Permeability of porous solids. Transactions of the Faraday Society 57:1200-1207
Penton CR, Devol AH, Tiedje JM (2006) Molecular evidence for the broad distribution of anaerobic ammonium-oxidizing bacteria in freshwater and marine sediments. Applied and Environmental Microbiology 72:6829-6832
Reid R, Prausnitz J, Sherwood T (1977) The Properties of Gases and Liquids. McGraw-Hill
Rich JJ, Dale OR, Song B, Ward BB (2008) Anaerobic ammonium oxidation (Anammox) in Chesapeake Bay sediments. Microbial Ecology 55:311-320
Scheer C, Wassmann R, Butterbach-Bahl K, Lamers J, Martius C (2009) The relationship between N_2O, NO, and N_2 fluxes from fertilized and irrigated dryland soils of the Aral Sea Basin, Uzbekistan. Plant and Soil 314:273-283
Schlesinger WH (2009) On the fate of anthropogenic nitrogen. Proceedings of the National Academy of Sciences of the United States of America 106:203-208
Schubert CJ, Durisch-Kaiser E, Wehrli B, Thamdrup B, Lam P, Kuypers MMM (2006) Anaerobic ammonium oxidation in a tropical freshwater system (Lake Tanganyika). Environmental Microbiology 8:1857-1863
Seitzinger S et al. (2006) Denitrification across landscapes and waterscapes: A synthesis. Ecological Applications 16:2064-2090
Severinghaus JP, Bender ML, Keeling RF, Broecker WS (1996) Fractionation of soil gases by diffusion of water vapor, gravitational settling, and thermal diffusion. Geochimica Et Cosmochimica Acta 60:1005-1018
Severinghaus JP, Grachev A, Luz B, Caillon N (2003) A method for precise measurement of argon 40/36 and krypton/argon ratios in trapped air in polar ice with applications to past

firn thickness and abrupt climate change in Greenland and at Siple Dome, Antarctica. Geochimica Et Cosmochimica Acta 67:325-343
Severinghaus JP, Sowers T, Brook EJ, Alley RB, Bender ML (1998) Timing of abrupt climate change at the end of the Younger Dryas interval from thermally fractionated gases in polar ice. Nature 391:141-146
Shashkov AG, Zolotukhina AF, Abramenko TN, Mathur BP, Saxena SC (1979) Thermal-Diffusion Factors for Binary Gas Systems - Ar-N_2, Ar-CO_2, He-H_2, He-N_2O, Kr-N_2O and He-NH_3. Journal of Physics B-Atomic Molecular and Optical Physics 12:3619-3630
Simarmata T, Benckiser G, Ottow JCG (1993) Effect of an increasing carbon:nitrate-N ratio on the reliability of acetylene in blocking the N_2O-reductase activity of denitrifying bacteria in soil. Biology and Fertility of Soils 15:107-112
Stevens RJ, Laughlin RJ (1998) Measurement of nitrous oxide and di-nitrogen emissions from agricultural soils. Nutrient Cycling in Agroecosystems 52:131-139
Tietema A, Verstraten JM (1991) Nitrogen cycling in an acid forest ecosystem in the Netherlands under increased atmospheric nitrogen input - the nitrogen budget and the effect of nitrogen transformations on the proton budget. Biogeochemistry 15:21-46
Trengove RD, Dunlop PJ (1982) Diffusion coefficients and thermal diffusion factors for 5 binary systems of nitrogen and a noble gas. Physica A 115:339-352
Vitousek PM et al. (1997) Human alteration of the global nitrogen cycle: Sources and consequences. Ecological Applications 7:737-750
Weier KL, Doran JW, Power JF, Walters DT (1993) Denitrification and the dinitrogen nitrous-oxide ratio as affected by soil-water, available carbon, and nitrate. Soil Science Society of America Journal 57:66-72

Figure Legends

Figure 1. Temperature-solubility curves for N_2 (solid line) and Ar (dashed line). Bunsen coefficients were calculated from the fitting curves reported by Hamme and Emerson (2004).

Figure 2. Isolines and shading represent the solubility fractionation effect (in per meg units of $\delta Ar/N_2$) as a function of soil moisture (g H_2O g^{-1} soil) and a change in soil temperature (°C) from an initial value of 20.0 °C.

Figure 3. Isolines and shading represent the water vapor flux fractionation effect (in per meg units of $\delta Ar/N_2$) as a function of change in initial relative humidity (%) to a final value of 100% and a change in chamber air temperature (°C) from an initial value of 20.0 °C.

Figure 4. Photograph of sample flask valves.

Figures

Figure 1

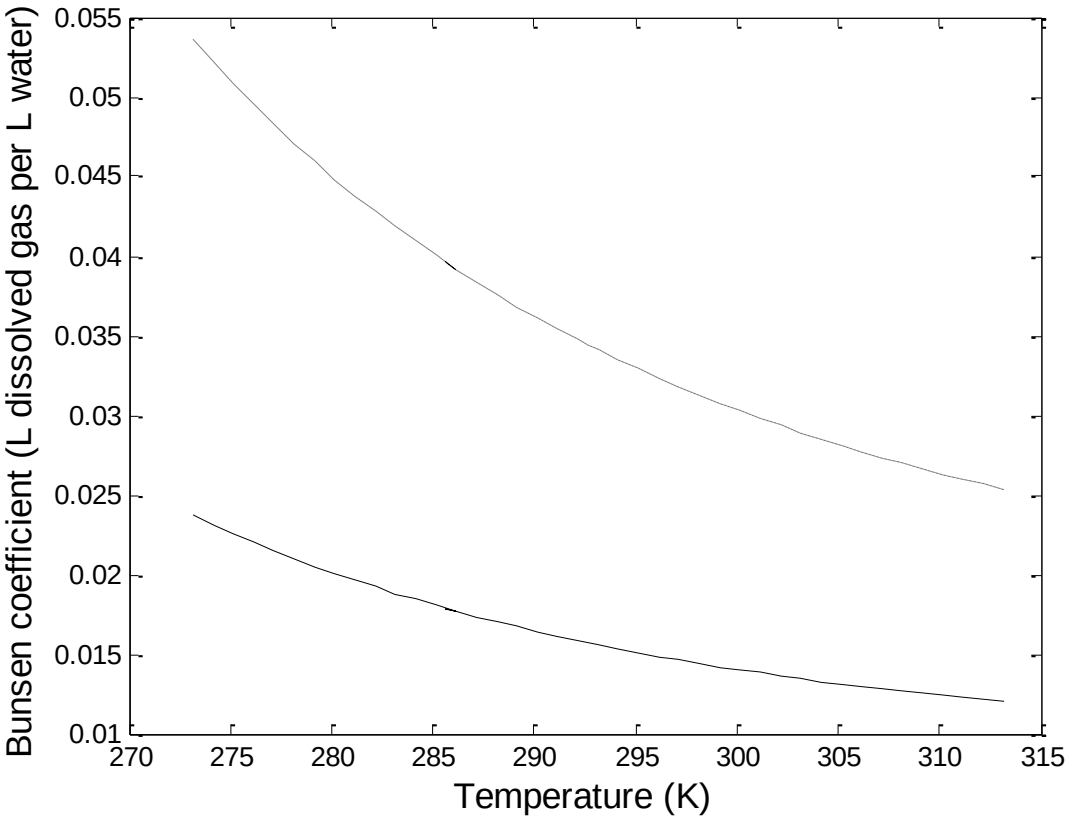

Figure 2.

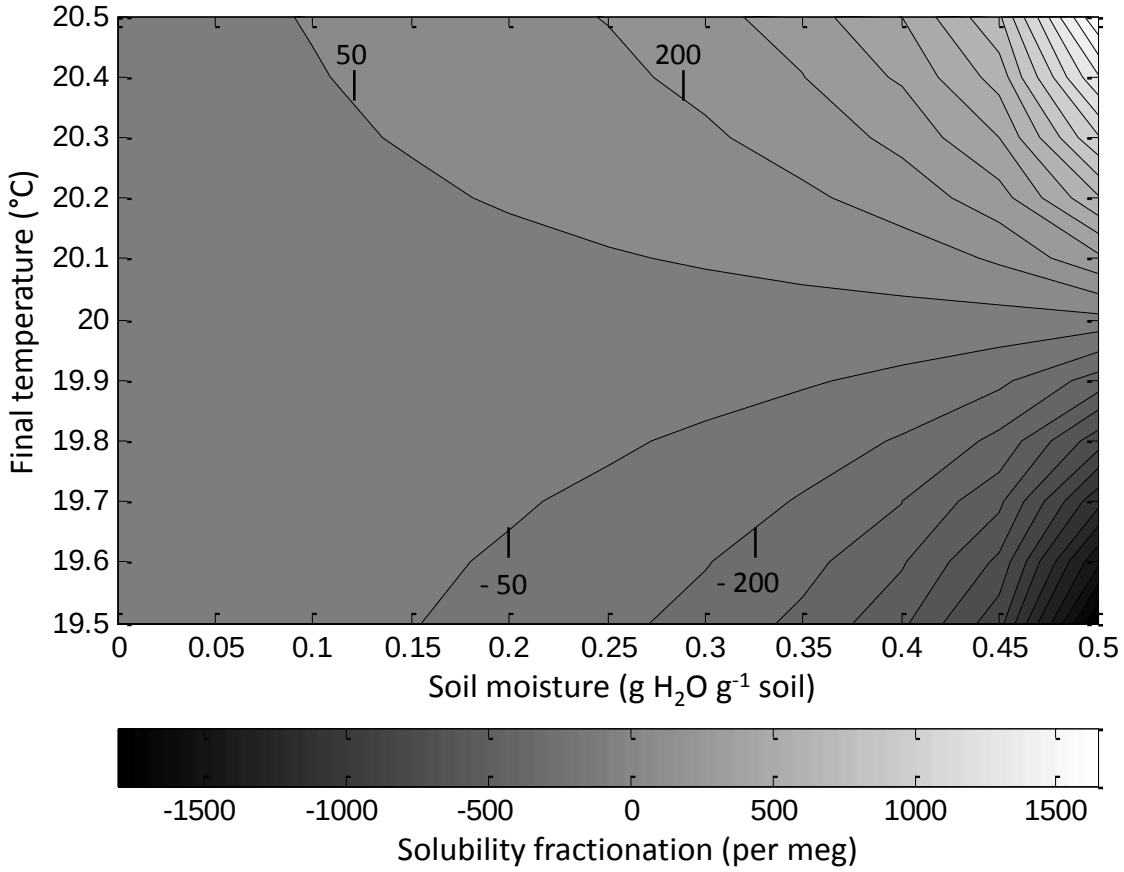
Final temperature (°C)
20.5
20.4
20.3
20.2
20.1
20
19.9
19.8
19.7
19.6
19.5
50
200
- 50
- 200
0
0.05
0.1
0.15
0.2
0.25
0.3
0.35
0.4
0.45
0.5
Soil moisture (g H2O g-1 soil)
-1500
-1000
-500
0
500
1000
1500
Solubility fractionation (per meg)

Figure 3.

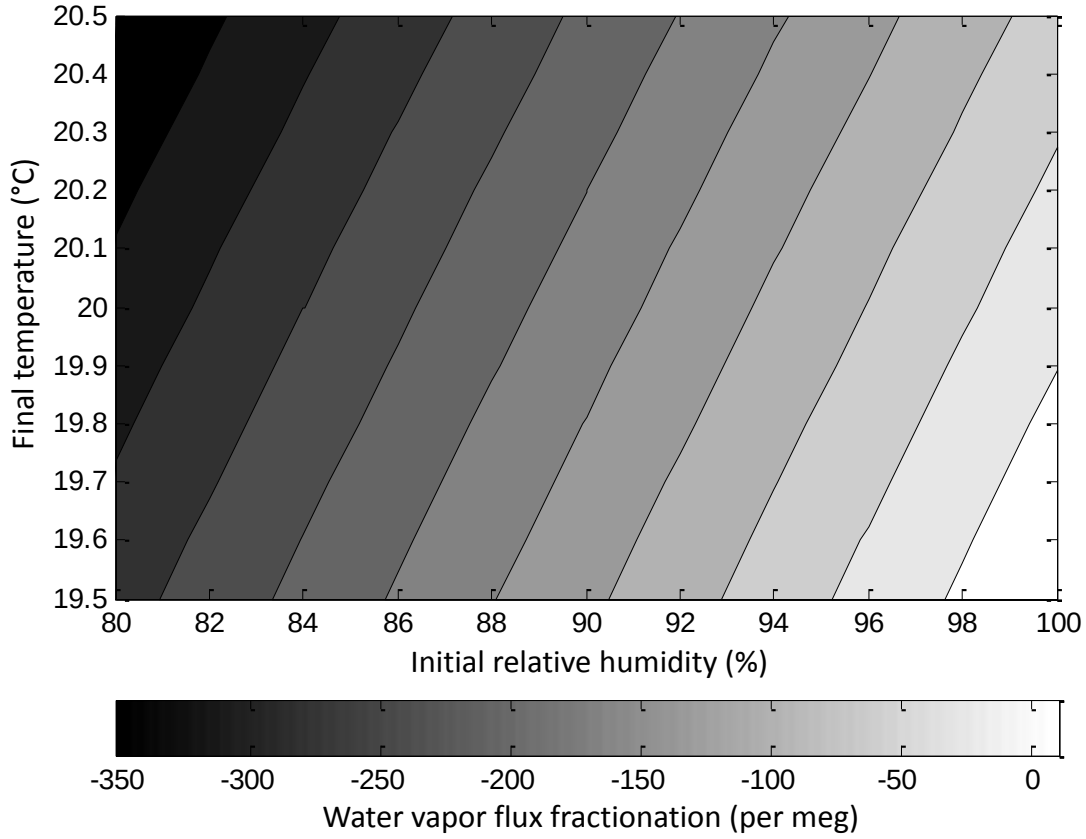

Figure 4.

Appendix

Determination of Thermal Diffusion Factor

The thermal diffusion factor is dependent on temperature and gas composition. Empirical measurements of the thermal diffusion factor across wide ranges in temperature and mixtures of N_2-Ar are generally in agreement and have been used to create predictive equations (Batabyal et al. 1967; McCourt 2003; Shashkov et al. 1979; Trengove and Dunlop 1982). However, these studies only examine the effect of a single variable, either temperature or gas composition, on the thermal diffusion factor. Over a wide range of temperatures (290-310 K), the thermal diffusion factor increases 0.001 per Kelvin in an equimolar mix of N_2-Ar (Batabyal et al. 1967; Shashkov et al. 1979). In a wide range of N_2-Ar mixtures (N_2 mole fraction of 0.8-1) at 300 K, the thermal diffusion factor increases 0.0005 per 0.1 N_2 mole fraction (McCourt 2003). Using these relationships, we corrected published values of the N_2-Ar thermal diffusion factor to a temperature 293.15 K and N_2 mole fraction of 0.988, considering atmospheric air as a binary mixture of N_2 and Ar. The range in corrected values is 0.0716 – 0.0788 with a median of 0.078. This translates to a median thermal diffusion effect of 286 (range 244 – 288) per meg per Kelvin, which is consistent with value measured by Nezmez and Severinghaus (in prep.).

Chapter 3. Nitrous oxide production and consumption in a drained peatland pasture: a test of a field-based ^{15}N-nitrous oxide pool dilution technique

Abstract

Soil dinitrogen (N_2) emissions are one of the most poorly understood aspects of the terrestrial nitrogen (N) cycle because they are difficult to measure. In soils, N_2 is produced from the consumption of N_2O via denitrification, so the quantification of soil N_2 emissions is critical to improving our understanding of the effects of global change on ecosystem N budgets and N_2O dynamics. We report on a new approach, the $^{15}N_2O$ pool dilution technique, to measure field rates of gross N_2O production and consumption as well as explore potential controls on N_2O dynamics in a N-rich peatland pasture in the Sacramento-San Joaquin River Delta in California. Nitrous oxide emissions ranged from 0.05 to 77.4 mg N m^{-2} d^{-1} across four micro-topographic zones, with the proportion of gross N_2O production released to the atmosphere (termed the N_2O mole fraction) averaging 0.84 ± 0.03. High soil mineral N concentrations, averaging 27 ± 8 µg N g^{-1} (± SE), supported very high gross N_2O production rates, averaging 8.4 ± 3.2 mg N m^{-2} d^{-1}. Mineral N concentrations and denitrifying enzyme activity together best predicted gross N_2O production rates (R^2 = 0.73). When the four landforms were grouped by soil moisture content, soil O_2 concentrations explained over 64% of the variability in N_2O consumption rates. Our data suggest that the high N_2O emissions observed at the peatland pasture result from high mineral N concentrations that drive high rates of incomplete denitrification in surface soils. We discuss the potential of the $^{15}N_2O$ pool dilution technique in ecosystems with low N_2O emissions or even net N_2O uptake, and suggest broader applications of the approach for improving our understanding of N cycling in terrestrial ecosystems.

Introduction

Nitrous oxide (N_2O) is a potent greenhouse gas and catalyst for stratospheric ozone depletion, and has been accumulating in the atmosphere since the Industrial Revolution (Prather *et al.* 1995). Nitrous oxide emissions from natural and agricultural soils represent over half of global N_2O emissions (Stein and Yung 2003). Nitrification and denitrification, both microbial processes, are responsible for N_2O production in soil. However, denitrifiers can also consume N_2O to dinitrogen (N_2), an inert gas that constitutes 78 % of Earth's atmosphere. Soil N_2 emissions are very difficult to measure against the high background atmospheric N_2 concentration and cannot be predicted from N_2O emissions, which represent net N_2O production rates (Groffman et al. 2006). Without the ability to quantify soil N_2 emissions, the amount of nitrogen (N) denitrified in terrestrial ecosystems is uncertain, leaving ecosystem N budgets poorly constrained (Kulkarni et al. 2008). This limits how well we can predict how global change and human activities will affect future ecosystem N balance and soil N_2O emissions (Boyer et al. 2006).

The magnitude of N_2O emissions produced via denitrification results from both total denitrification rates and the relative importance of N_2O to N_2 as denitrification end-products (Firestone and Davidson 1989). For example, theory suggests that denitrification rates increase while the ratio of N_2O:N_2 emissions decreases with decreasing soil oxygen (O_2) concentrations (Firestone et al. 1980). Thus, high N_2O emissions may reflect high denitrification rates or a high ratio of N_2O:N_2 emissions. The ratio of N_2O:N_2 emissions is likely to vary both spatially and

temporally within ecosystems because of its sensitivity to redox, pH, nitrate (NO_3^-) availability, and labile carbon (C) availability (Firestone et al. 1980; Weier et al. 1993; Del Grosso et al. 2000).

Our current knowledge about denitrification in upland soils is derived from methods that are not ideal for determining N_2 emissions in undisturbed field soil (Groffman et al. 2006). The most common techniques for measuring soil N_2 emissions are the use of ^{15}N tracers, the use of acetylene (C_2H_2) to inhibit N_2O reduction, and the use of N_2-free gas flowed through closed systems containing soil cores. The ^{15}N tracer methods involve adding $^{15}NO_3^-$ to soil and tracing it into the N_2 pool. The high detection limit of isotope ratio mass spectrometers (IRMS) for measuring changes in $^{15}N_2$ necessitates large $^{15}NO_3^-$ additions, potentially stimulating denitrification in soils with low background NO_3^- concentrations. The C_2H_2 inhibition method has a variety of problems that may cause N_2 production to be underestimated (Knowles 1990). The gas flow soil core technique is regarded as the most accurate of existing methods but still requires removing soil from the field and incubating it in the laboratory (Butterbach-Bahl et al. 2002; Groffman et al. 2006). While these methods have yielded valuable information about denitrification, they cannot provide field measurements of N_2 emissions from unmanipulated soils.

The isotope pool dilution technique, used to measure gross rates of N mineralization and nitrification (Kirkham and Bartholomew 1954), can also be applied to measuring simultaneous production and consumption of gases. Gas consumption is characterized by the loss of a heavy stable isotope tracer added to the product pool in the headspace of a closed chamber containing soil or of a surface flux chamber inserted into the soil surface. Isotope tracer loss is due only to biological consumption and physical losses (i.e., diffusion and advection), of which the latter are accounted for using a conservative tracer such as sulfurhexafluoride (SF_6). A mixing model is used to solve for gross gas production from the dilution of the heavy isotope pool by the light isotope gas produced. This technique has been used successfully for measuring simultaneous soil production and consumption of methane (von Fisher and Hedin 2002) and methyl halides (Rhew et al. 2003, Rhew and Abel 2007) in the field and laboratory. Other techniques utilizing ^{15}N-labelled N_2O have been used to estimate laboratory rates of N_2O production and consumption in seawater samples (Punshon and Moore 2004) and a soil column (Clough et al. 2006). To the best of our knowledge, the $^{15}N_2O$ pool dilution technique has been used in laboratory incubations of salt marsh sediments (Anderson et al. 1997) but has never been applied in upland soils or in the field setting.

In this study we used the $^{15}N_2O$ pool dilution technique to measure field rates of gross N_2O production and consumption from a drained peatland currently used as a pasture in the Sacramento-San Joaquin River Delta in California. Agricultural peatlands can be large N_2O sources when drained or impacted by runoff from upslope fertilized cropping (Martikainen et al. 1993; Flessa et al. 1998; Regina et al. 2004). The proportion of produced N_2O that is released to the atmosphere (hereafter referred to as N_2O fractional release) is poorly characterized, and N loss via denitrification is uncertain for these ecosystems. The objectives of this study were to: (1) test the accuracy of the $^{15}N_2O$ pool dilution technique, (2) characterize the N_2O fractional release for a N-rich peatland pasture, and (3) examine the controls on gross N_2O production and consumption rates and the N_2O mole fraction.

Methods

Site Description

The study site is an upland pasture on Sherman Island (38.04 N, 121.75 W) in the Sacramento – San Joaquin River Delta region of northern California. The soils consist of mucky clay over buried peat and are classified as fine, mixed, superactive, thermic Cumulic Endoaquolls (USDA Web Soil Survey 2008). The climate is Mediterranean with a winter wet season. The mean annual temperature is 20.5 ^{o}C, and the mean annual precipitation is 375-625 mm (Atwater 1980). A micro-topographical gradient across the pasture creates a range of soil conditions while controlling for soil type, climate, and land use. We divided the gradient into four landforms, from high to low elevation: crown, slope, hollow/hummock, and irrigation ditch. High N_2O emissions (average 6.4 ± 0.4 mg N m^{-2} d^{-1}) have previously been measured from all landforms (Teh et al. submitted).

Method Testing

We performed eight pairs of field measurements in the crown and slope landforms in February 2009 to determine if N_2O dynamics were affected by raising the N_2O concentration in the surface flux chamber headspace for the $^{15}N_2O$ pool dilution technique. For each pair, we measured N_2O emissions (i.e., net N_2O production) with and without the injection of spiking gas ($^{15}N_2O$ and SF_6 in N_2), allowing the soil to re-equilibrate with the atmosphere for one hour between the two measurements. We reversed the order of the measurements for half of the pairs to avoid systematic bias in the measurements. We injected 10 mL of spiking gas at 100 ppm 98 atom % ^{15}N-N_2O and 10 ppm SF_6. This increased the headspace concentrations of the surface flux chamber (described below) by approximately 60 ppb N_2O and 6 ppb SF_6 and increased the headspace N_2O ^{15}N-enrichment by approximately 14 atom %. The spiking gases were made volumetrically in gas bags using certified 99.8% of 98 atom % ^{15}N-N_2O (Isotech), 99.8% SF_6 (Scotty Specialty Gases), and ultra high purity N_2. We compared the net N_2O production rates with and without the spiking gas injection using regression analysis; a slope for the regression line deviating from unity would suggest a significant effect of spiking gas injection on N_2O dynamics. We also evaluated the accuracy of the $^{15}N_2O$ pool dilution technique using regression analysis to compare the observed and predicted net N_2O production rates for the spiked measurements. Predicted net N_2O production was calculated as the difference between gross N_2O production and consumption determined by the $^{15}N_2O$ pool dilution technique described later.

In the laboratory, we compared the $^{15}N_2O$ pool dilution technique against two existing methods for measuring N_2 production, C_2H_2 inhibition and ^{15}N tracer. For the C_2H_2 inhibition technique, we used three headspace treatments: 0 Pa C_2H_2 (control), 10 Pa C_2H_2 (nitrification inhibited), and 10 kPa C_2H_2 (nitrification + N_2O reduction inhibited). The C_2H_2 was produced by adding deionized water to calcium carbide in a gas bag. For the ^{15}N tracer technique, 2 mL of 99.7 atom % ^{15}N-NO_3^- solution was added; this increased the soil NO_3^- concentration by 5 µg N/g. The soil was lightly mixed to distribute the ^{15}N label. For the $^{15}N_2O$ pool dilution technique, 5 mL of a 98 atom % $^{15}N_2O$ spiking gas was added to increase the headspace N_2O concentration by 1 ppm.

Soil was collected from 0-10 cm depth (crown topographic zone) and stored in a gas permeable bag at ambient conditions for five days before the experiment. The soil was gently homogenized, preserving aggregates up to 1 cm diameter, and then 100 g was weighed into each sample jar (490 mL). The jars were sealed on viton gaskets with aluminum lids equipped with

Swagelok o-seal fittings containing septa for gas sampling. The jars were flushed with N_2 for three minutes to create an anoxic headspace and then the appropriate gas treatment was added.

For the C_2H_2 inhibition and $^{15}N_2O$ pool dilution treatments, the jars were sampled at 0.25, 1, 2, and 3 hours. For ^{15}N tracer treatment, the jars were only sampled at 0.25 and 3 hours because detectable changes in ^{15}N-N_2 atom % were not expected before three hours. For all treatments, 60 mL headspace gas was removed and stored in a pre-evacuated glass Wheaton vial sealed with an aluminum crimp and a Teflon septum (National Scientific); 60 mL ultra high purity helium (He) was injected into the jar to keep the headspace at atmospheric pressure without changing the isotopic composition of the headspace N_2 or N_2O. For the C_2H_2 treatments, C_2H_2 was also added back to maintain the desired C_2H_2 concentration. We corrected for the dilution of headspace gases caused by adding He.

Field Sampling

Twelve $^{15}N_2O$ pool dilution measurements were performed across all landforms (n = 3 per landform) in March 2009 and again in April 2009. We used a two-piece aluminum static flux chamber with a square basal area of 0.14 m^2 and approximate volume of 17 L. The chamber lid was equipped with two fans, a 60 cm long 1/8" stainless steel pigtail vent, and two septum ports (one for sampling and one for spiking gas injection). The chamber was covered in two layers of reflective bubble wrap to minimize heating of the chamber headspace under sunny field conditions. The chamber sealed on a 1/8" thick viton gasket using spring clamps or C-clamps. The leak rate from the chamber was determined to be 0.3 % per hour by placing the sealed chamber over a tray of water, injecting SF_6, and determining the change in SF_6 concentration over three hours.

The chamber base was inserted approximately 3 cm into the soil and allowed to equilibrate for 30-45 minutes before sampling. The chamber lid was then sealed to the base and the fans turned on to mix the chamber headspace. The spiking gas was injected through a septum port in the chamber lid using a syringe. The chamber headspace was sampled from a different septum port in the chamber lid at 3, 8, 15, 30, and 45 minutes after spiking gas injection. The vent was sealed when the chamber was not being sampled so that loss of $^{15}N_2O$ and SF_6 through the vent could be minimized. The samples were stored in pre-evacuated glass vials sealed with aluminum crimps and Teflon septa: a 90 mL aliquot in a 70 mL vial for isotope analysis and a 20 mL aliquot in a 10 mL vial for GC analysis. The vial septa were immediately coated in silicone sealant to minimize the potential for leakage, and the samples were stored for up to five days before analysis.

After the last sampling time point, we measured the temperature of the ambient air, chamber headspace, and soil (0-10 cm depth). The chamber height was measured at three points along each side of the chamber and then averaged to calculate the chamber volume. Four 5 cm diameter soils cores (0-10 cm depth) were taken, one from each quadrant of the chamber footprint. The intact cores were transported to UC Berkeley (UCB) in gas permeable bags at ambient temperature and processed on the same day as detailed below.

Laboratory assays

In the laboratory, each soil core was homogenized, and approximately 15 g soil (oven dry equivalent) was extracted in 75 mL of 2M KCl. The 2M KCl extracts were analyzed colorimetrically for NO_3^- and NH_4^+ (Lachat Quik Chem flow injection analyzer, Lachat Instruments, Milwaukee, WI). A 10 g subsample was oven-dried at 105 ^oC for determination of

gravimetric soil water content. We calculated water-filled pore space (WFPS) from gravimetric soil water content measured in this study and average soil bulk densities for each landform measured previously (Teh et al. submitted).

Denitrifying enzyme activity was also measured according to a modified protocol based on those described in Tiedje (1994) and Silver et al. (2000): 100 mL of de-gassed 1 mM glucose, 1 mM potassium nitrate, and 1 g/L chloramphenicol in DI water to 20 g soil (5 g from each of four soil cores taken from a given chamber footprint) in a 250 mL Mason jar. The jar was sealed with a lid equipped with a rubber septum port, and then it was flushed with N_2 for three minutes to create an anoxic headspace. Acetylene was added to achieve a concentration of 10 kPa. The jar was shaken to slurry the soil and then placed on an orbital shaker at 100 rpm. The jar headspace was sampled at 10, 20, 30, and 40 minutes after vigorously shaking the jar each time, and the gas samples were immediately analyzed on the GC. Denitrifying enzyme activity was calculated from the linear increase in N_2O concentration over time. The remaining soil was air-dried, and pH in 1M KCl was measured using 10 g soil in a 4:1 ratio of KCl to air-dried soil.

Soil oxygen (O_2) concentrations were measured in April 2009 after we deployed twelve cow-proof soil O_2 chambers based on the design described by Silver et al. (1999). The chambers consisted of a polypropylene centrifuge tube (3 cm diameter and 15 cm length) with a 1/8" Swagelok union inserted through a hole drilled into the round end. The union was sealed to the tube with marine goop, and a septum was inserted into the fitting on the exposed side of the union. The chambers were inserted into 10 cm deep holes slightly wider than the chamber so that the bottom 5 cm of the chamber was filled with soil and the Swagelok end barely protruded from the soil surface. The removed soil was packed back in around the chambers to create a seal against atmospheric air. The chambers were allowed to equilibrate for one week before sampling. A 30 mL sample was drawn from the chamber and immediately analyzed using a dissolved O_2 meter (Model 52, Yellow Springs Instruments, Yellow Springs, OH) and Clark-type electrode calibrated in the field using atmospheric air (Silver et al. 1999). Each of the surface flux measurements in April 2009 were taken at 0.5 m distance from a soil O_2 chamber.

Gas Analyses

In February 2009 when we performed method testing in the field, samples were analyzed for N_2O isotopic composition on a PDZ Europa 20-20 IRMS and a SerCon Cryoprep trace gas concentration system at the University of California, Davis (UCD) Stable Isotope Facility. For rest of the samples, isotope analyses were performed at UCB on an PDZ Europa IRMS with a manually operated custom-built trace gas concentration system. Precision for $^{15}N_2O$ analysis was 0.004 atom %. $^{15}N_2$ analyses were performed on the UCB IRMS by directly injecting 100 µL sample into the He carrier stream upstream of a heated copper reduction tube to remove O_2; samples were injected using a glass gas-tight syringe with a zero-volume stopcock. Samples were analyzed for N_2O, SF_6, and CO_2 concentrations on a Shimadzu GC-14A equipped with an electron capture detector (ECD) and thermal conductivity detector at UCB. A 4m x 1 mm Hayesep Q column was used to allow adequate peak separation between N_2O and SF_6 on the ECD. We used a 10.1 ppb SF_6 in N_2 standard gas as well as a 998 ppm CO_2, 10.4 N_2O ppm in N_2 standard gas for one-point calibrations because previous work showed that the detector responses were linear in the concentration range of our samples and standards. The precision (i.e., standard deviation of 5 replicates of the standard gas) for SF_6 and N_2O analyses were 0.05 ppb and 0.03 ppm, respectively.

Pool Dilution Model

We used an adaptation of the stable isotope pool dilution technique (Kirkham and Bartholomew 1954) to measure simultaneous N_2O production and consumption in surface soils. Nitrous oxide consumption is determined empirically from the losses of $^{15}N_2O$ and SF_6 from the chamber headspace over time. First-order kinetics for N_2O production and consumption can be assumed based on other studies of soil N_2O dynamics (Vieten et al. 2007; Vieten et al. 2009). The use of SF_6 as a tracer for physical loss of N_2O is reasonable based on observations of similar loss rates for SF_6 and CFC-113 despite different molecular properties (Rhew et al. 2003). In the field, the tracer loss can be approximated as a first-order process based on observed loss rates (Rhew and Abel 2007). Thus, the first-order exponential decay constant for $^{15}N_2O$ concentration represents biological and physical loss whereas the first-order exponential decay constant for SF_6 should represent only physical loss (i.e., diffusion or advection). The difference in the *k*-values is deduced to be the biological loss of $^{15}N_2O$ due to N_2O consumption to N_2 through denitrification. The observed gross N_2O consumption rate is calculated as the product of the biological N_2O loss rate and the N_2O concentration of background air (e.g., field air). The gross N_2O consumption rate can also be calculated as the difference between the predicted gross N_2O production rate and observed net N_2O production rate. Observed net N_2O production, or N_2O emissions from the soil to the atmosphere, is calculated from the increase in N_2O concentration in the chamber headspace over time. Net N_2O consumption by soil has been observed in some studies (Chapuis-Lardy et al. 2007), but in this study, only net N_2O emissions were observed so that we do not consider net N_2O consumption.

Gross N_2O production was determined using the modeling approach described by von Fisher and Hedin (2002) for methane production. The model uses the following two equations (Eq. 1-2), where $[^{14}N_2O]_t$ and $[^{15}N_2O]_t$ are the concentrations of $^{14}N_2O$ and $^{15}N_2O$ at time *t*; F_{14} and F_{15} are the $^{14}N_2O$ and $^{15}N_2O$ mole fractions of produced N_2O; k_{14} and k_{15} are the first order rate constants for $^{14}N_2O$ and $^{15}N_2O$ reduction to N_2; k_L is the first order rate constant for loss of the conservative tracer, SF_6. These are the input variables for the model.

$$[^{14}N_2O] = \frac{F_{14} \times P}{k_{14}} - \left(\frac{F_{14} \times P}{k_{14}} - [^{14}N_2O]_0\right) \times \exp\{-k_{14} \times (t - t_0)\} \quad (1)$$

$$[^{15}N_2O] = \frac{F_{15} \times P}{k_{15} - k_L} - \left(\frac{F_{15} \times P}{k_{15} - k_L} - [^{15}N_2O]_0\right) \times \exp\{-(k_{15} + k_L) \times (t - t_0)\} \quad (2)$$

$[^{15}N_2O]_t$ is calculated as the product of N_2O concentration and ^{15}N-N_2O atom % excess assuming the isotopic composition of background N_2O is the average tropospheric value of 6.72 per mil or 0.3688 atom % (Kaiser *et al.* 2003). $[^{14}N_2O]_t$ is calculated as the product of N_2O concentration and ^{14}N-N_2O atom % (i.e., 100 minus ^{15}N-N_2O atom %). F_{14} and F_{15} were calculated assuming that the initial substrates were at natural abundance ^{15}N (0.3663 atom%) and that nitrification and denitrification contributed equally to N_2O production. The fractionation factors associated with N_2O production were assumed to be the average literature values: 0.9203 ± 0.0120 for nitrification (Table A1) and 0.9715 ± 0.0028 for denitrification (Table A2). Thus, the N_2O produced was assumed to be 0.3465 atom % ^{15}N. We performed sensitivity analyses to determine the effect of F_{14} and F_{15} values on predicted gross N_2O production and consumption rates. We assumed relative contributions of nitrification and denitrification to N_2O production ranging from all nitrification and no denitrification to all denitrification and no nitrification; the model output changed by less than 1% in response to the range of F_{14} and F_{15} values. k_{14} is calculated

from the fractionation factor, α, for N_2O reduction to N_2 and the observed k_{15} for each measurement using the definition, $\alpha = k_{14}/k_{15}$. The fractionation factor was assumed to be 0.9930 ± 0.0009, the average literature value (Table A3). Sensitivity analysis using the range of literature values (0.9871-0.9984) showed that the model output was not sensitive to the fractionation factor value, changing by less than 1 % over the entire range.

The model is solved iteratively for gross N_2O production rate, *P*, and the initial concentrations of $^{14}N_2O$ and $^{15}N_2O$, $[^{14}N_2O]_0$ and $[^{15}N_2O]_0$. The model seeks to minimize the error estimated by the following equation (Equation 3), where $[^{14}N_2O]_{pred}$ and $[^{15}N_2O]_{pred}$ are the predicted $^{14}N_2O$ and $^{15}N_2O$ concentrations; $[^{14}N_2O]_{obs}$ and $[^{15}N_2O]_{obs}$ are the observed $^{14}N_2O$ and $^{15}N_2O$ concentrations; SD_{14} and *p* is the instrument precision. The instrument precision (expressed as standard deviation) is calculated by Gaussian error propagation from the standard deviation of all standards analyzed on the IRMS and GC on the days the relevant samples were analyzed. The model goodness of fit was evaluated by regressing $[^{14}N_2O]_{pred}$ against $[^{14}N_2O]_{obs}$; a slope of 1 for the regression line represents a good fit.

$$E = \sum\left\{\left([^{14}N_2O]_{pred}(t) - [^{14}N_2O]_{obs}(t)\right)^2\right\} \times p + \sum\left\{\left([^{15}N_2O]_{pred}(t) - {}^{15}N_2O obst2 \times p \right. \right. \quad (3)$$

We also ran the model using k_{15} as a floating variable that is solved for in the model with the observed k_{15} used as the initial value.

Diffusion Modeling

We modeled vertical transport of the $^{15}N_2O$ tracer via diffusion through the soil profile using Fick's law. We used the analytical solution for the Fick's law equation presented by von Fischer et al. 2009. Soil tortuosity was described for each landform on each sampling date using the Millington and Quick (1961) model. Nitrous oxide diffusivity in air at STP is 0.1436 $cm^2\ s^{-1}$ and changes with temperature according to the scaling factor, $(T/T_0)^{1.81}$ (Massman 1998). We used the free-air N_2O diffusion coefficient at 15° C, 0.1582 $cm^2\ s^{-1}$. Because we are interested in the potential for the tracer to diffuse through the soil and then back into the chamber headspace, we modeled diffusion over a 20 minute time period. Thus, during the 45 minute sampling period, the tracer diffuses to a certain depth in the first 20 minutes and then diffuses back to the soil surface in the next 20 minutes. We used the diffusion model to determine the maximum soil depth that the tracer reaches in 20 minutes.

Statistical Analysis

We used SYSTAT Version 10 (SPSS Inc., Evanston, IL) to perform statistical analyses and the Microsoft Excel 2007 (Microsoft Corporation, Redmond, WA) to run the iterative pool dilution model. We log-transformed variables with non-normal distributions (all except soil moisture, soil oxygen, and pH) to meet the normality assumptions of ANOVA and linear regressions. We used ANOVA and Tukey tests to compare N_2O dynamics and soil variables among the four landforms. We used linear regressions to explore patterns in N_2O and N_2 dynamics. Mean values are reported in the text followed by standard errors (± SE). Statistical significance was determined at $P < 0.05$.

Results

Method Evaluation

We used laboratory and field experiments to evaluate the $^{15}N_2O$ pool dilution method and identify potential artifacts. In the laboratory we compared net N_2O production and gross N_2O consumption among the $^{15}N_2O$ pool dilution approach, the $^{15}N_2$ tracer method, and the acetylene inhibition technique using controlled incubations. Net N_2O production did not differ significantly among the three methods tested. However, gross N_2O consumption rates estimated by the ^{15}N tracer method were significantly higher those measured using the other two methods ($p < 0.001$, Figure 1). The background soil NO_3^- concentration was 1.98 ± 0.97 μg N g^{-1} so the addition of 5 μg ^{15}N-NO_3^- g^{-1} for the ^{15}N tracer method increased the soil NO_3^- by a factor of 2.5. Gross N_2O consumption rates estimated by $^{15}N_2O$ pool dilution and acetylene inhibition did not differ significantly. In the field, we tested whether increasing the headspace N_2O concentrations altered net N_2O production. Increasing the N_2O concentration of the chamber headspace by up to 100 ppb decreased net N_2O fluxes by only 1 % (Figure 2a). We also found that predicted net N_2O fluxes, calculated as the difference between gross N_2O production and consumption rates, were 11 % greater than observed net N_2O fluxes (Figure 2b). In all of the analyses, we used gross N_2O production and consumption rates estimated from the model employing k_{15} as a floating variable that was solved for by the model using the observed k_{15} as the initial value. With high gross N_2O production rates, non-trivial amounts of produced $^{15}N_2O$ can accumulate in the chamber headspace. High gross N_2O consumption rates can also cause $^{15}N_2O$ accumulation in the chamber because of discrimination against $^{15}N_2O$ during N_2O reduction via denitrification. Thus, with the high gross N_2O production and consumption rates, such as at our study site, the observed k_{15} is underestimated and would cause underestimates of N_2O production and consumption rates. We found that gross N_2O production rates were 27 % higher and N_2O consumption rates were 427 % higher using floating values of k_{15} compared to using the observed k_{15} as a fixed value.

We used diffusion modeling to determine the maximum soil depth that the tracers could reach and then diffuse back to the soil surface within the 45 minute sampling period. We calculated that, within 20 minutes, $^{15}N_2O$ and SF_6 concentrations in the soil would reach 1 % of the headspace concentrations at depths of 41 cm and greater. The range in tracer penetration into the soil profile was primarily due to differences in soil bulk density and soil moisture that affect soil diffusivity, which ranged from 2.5 to 6.6 cm^2 min^{-1}. In all cases, some amount of tracer calculated to reach 80 cm depth within 20 minutes.

Soil Characteristics

Soil characteristics varied significantly among landforms (Table 1). Gravimetric soil moisture content was lower in the crown and slope compared to the hollow/hummock and irrigation ditch, with landform means ranging from 0.29 - 0.48 g-H_2O g^{-1}- dry soil ($p < 0.001$). Soil mineral N concentrations averaged 27 ± 8 μg N g^{-1} overall. Soil NH_4^+ concentrations were highly variable, and thus did not differ significantly among landforms; soil NO_3^- concentrations were higher in the crown compared to the other landforms ($p < 0.001$). Soil pH varied among landforms, with higher pH in the crown than in the slope ($p = 0.03$). Soil O_2 concentrations were spatially heterogeneous within and across landforms (1.1 - 20.1 %), except for the slope where soil O_2 concentrations were all relatively aerobic, averaging 17.3 ± 0.7 % ($n = 3$). Denitrifying enzyme activity was lower in the slope compared to the irrigation ditch ($p = 0.04$) and was most

strongly correlated to pH (R^2 = 0.72, Figure 3). The combination pH and soil O_2 concentration explained 91% of the variability in DEA (Table 2).

Gross N_2O Production and Consumption

The pasture exhibited high N_2O emissions across all landforms and sampling dates, ranging from 0.05 – 77.4 mg N m^{-2} d^{-1}. Nitrous oxide consumption rates averaged 1.2 ± 0.4 mg N m^{-2} d^{-1} while gross N_2O production rates averaged 8.4 ± 3.2 mg N m^{-2} d^{-1}. Thus, N_2O consumption was a small proportion of gross N_2O production (Figure 4). The N_2O mole fraction (i.e., the proportion of gross N_2O production released to the atmosphere) averaged 0.84 ± 0.03 and was greater than 0.5 for all but one of the measurements.

Nitrous oxide dynamics varied among the landforms. Nitrous oxide emissions were lower in the slope compared to the crown and irrigation ditch ($p < 0.001$). Gross N_2O production rates were higher in the crown compared to all of the other landforms, though the difference was not statistically significant due to high variability in the crown ($p = 0.10$). Nitrous oxide consumption rates and the N_2O:N_2 ratio did not differ significantly among landforms.

Across landforms, mineral N concentration was the strongest predictor of gross N_2O production (R^2 = 0.57, Figure 5a). Mineral N concentration together with DEA explained 73% of the variability in gross N_2O production (Table 2). As a single variable, DEA had a strong positive relationship with gross N_2O production, (R^2 = 0.47, Figure 5b) but only a weak positive relationship with N_2O consumption (R^2 = 0.25). Nitrous oxide consumption was most strongly correlated to gross N_2O production (R^2 = 0.66). There were no significant relationships between the measured soil characteristics and N_2O:N_2 ratios.

Grouping the landforms by high soil moisture (hollow/hummock and irrigation ditch) and low soil moisture (crown and slope) revealed additional relationships among soil characteristics and N_2O dynamics. In the drier landforms, gross N_2O production was best predicted by DEA (R^2 = 0.75) and NO_3^- concentrations (R^2 = 0.71), which together explained 87% of the variability in gross N_2O production rates (Table 2). Gross N_2O production also had a positive relationship with pH (R^2 = 0.49) and a negative relationship with soil diffusivity (R^2 = 0.40). In contrast, in the wetter landforms, NH_4^+ concentration was the only variable that was strongly correlated to gross N_2O production (R^2 = 0.66, Table 2). While soil O_2 concentration and N_2O consumption rates did not have a significant relationship when all landforms were considered together, they were strongly correlated when the landforms were grouped by soil moisture (R^2 = 0.64 for drier landforms and R^2 = 0.76 for wetter landforms, Table 2 and Figure 6).

Discussion

Method Evaluation

This $^{15}N_2O$ pool dilution method provides measurements of simultaneous soil N_2O production and consumption rates in both the laboratory and the field. In the laboratory, gross N_2O production and consumption rates measured by the $^{15}N_2O$ pool dilution and acetylene inhibition methods were similar. Not surprisingly, for the ^{15}N tracer method, the large amount of added $^{15}NO_3$ necessary to detect changes in $^{15}N_2$ greatly stimulated N_2O production and consumption. In the field, we showed that the increase in chamber headspace N_2O concentration (up to 100 ppb) as a result of $^{15}N_2O$ addition did not impact net N_2O emissions. Predicted net N_2O fluxes did not deviate substantially from observed net N_2O fluxes, consistent with accurate model predictions of gross N_2O production and consumption rates.

In situations where gross N_2O production and consumption rates are very high, such as at our study site, non-trivial amounts of $^{15}N_2O$ can accumulate in the chamber headspace. High gross N_2O production rates cause underestimates of N_2O consumption rates because produced natural abundance $^{15}N_2O$ accumulating in the chamber headspace causes a smaller observed loss of the $^{15}N_2O$ tracer. High N_2O consumption rates cause underestimates of gross N_2O production rates because the discrimination against reduction of $^{15}N_2O$ causes a lesser observed dilution of the $^{15}N_2O$ pool. Theoretically, this problem can be avoided by increasing the ^{15}N enrichment of the chamber headspace N_2O pool to a level where accumulation of $^{15}N_2O$ becomes trivial against the initial $^{15}N_2O$ pool and atom% ^{15}N enrichment. However, to further enrich the $^{15}N_2O$ pool, we would also further increase the chamber headspace N_2O concentration and risk stimulating N_2O consumption. Thus, we addressed this problem by using k_{15} as a floating variable rather than a fixed variable in the model so that k_{15} was predicted by the model using the observed k_{15} as an initial value. The model includes terms for $^{14}N_2O$ and $^{15}N_2O$ mole fractions of produced N_2O and fractionation that occurs during N_2O consumption, but these effects are not transmitted to k_{15} if it is fixed at the observed value. Given that N_2O production was far greater than N_2O consumption at our study site, we expected fixed k_{15} values to yield greatly underestimated N_2O consumption rates and moderately underestimated gross N_2O production rates. Indeed, using floating k_{15} values increased estimates of N_2O consumption rates by 427% and gross N_2O production rates by only 27%, on average. We recommend comparing gross N_2O production and consumption rates estimated using fixed and floating values of k_{15} as a check that the model provides reasonable estimates of both rates.

A general concern when using the $^{15}N_2O$ pool dilution method is that N_2O consumption rates can be underestimated if the $^{15}N_2O$ tracer does not diffuse down to soil depths where N_2O consumption could occur. Gross N_2O production rates are integrated over the entire soil profile because, at steady state, the N_2O emitted at the soil surface represents N_2O that was produced at any depth that was not consumed while traveling towards the soil surface. However, N_2O consumption rates predicted from $^{15}N_2O$ tracer loss represent consumption only at the soil depths penetrated by the tracer during the sampling period. In systems with lower N_2O emissions, the sampling time period could be lengthened to allow greater tracer penetration into the soil profile. In systems with high N_2O emissions such as our study site, rapid $^{14}N_2O$ accumulation in the chamber headspace can quickly dilute the $^{15}N_2O$ pool to natural abundance levels and also suppress N_2O emissions to preclude longer sampling time periods.

We used diffusion modeling to show that the $^{15}N_2O$ tracer diffused adequately through the soil profile to provide reasonable estimates of N_2O consumption rates in our study. After 20 minutes, $^{15}N_2O$ tracer concentrations in the soil reached 1 % of the chamber headspace concentration at depths of at least 41 cm and that some amount of tracer could reach depths of 80 cm in all cases. The water table at Sherman Island varies between 30 cm and 70 cm depth (Deverel et al. 2007), so the tracer was likely able to diffuse to the bottom of the unsaturated zone and back to the soil surface during the 45 minute sampling period. Heterogeneous distribution of ^{15}N label does not substantially affect gross N transformation rates estimated using pool dilution whereas biased distribution of ^{15}N label can have a greater impact on estimated rates (Davidson et al. 1991). This impact is limited when ^{15}N enrichment decreases with depth and gross production also decreases with depth or is uniform throughout the soil profile (Davidson et al. 1991). Laboratory incubations of drained peat soil from different depths have shown that the majority of N_2O and N_2 was produced in the top 20 cm, and denitrification potential was greatest in the top 20 cm (Koops et al. 1996; Koops et al. 1997; van Beek et al.

2004). The strong relationships between surface soil characteristics and N_2O dynamics that we observed suggest that N_2O production and consumption is also greatest near the soil surface at our study site.

Patterns in Gross N_2O Production and Consumption

We observed consistently high N_2O emissions across all landforms that were comparable to those measured previously at this site (Teh et al. submitted) and reported for other managed peatlands (Koops *et* al. 1997; Flessa et al. 1998). We also documented high N_2O:N_2 ratios across all landforms. To the best of our knowledge, N_2O:N_2 ratios have not been reported for drained peatlands under agriculture. Agricultural soils span the entire range of possible N_2O fractional losses (typically referred to as N_2O mole fractions which can be confused with terminology referring to molar concentrations) from 0 to 1 (reviewed by Schlesinger 2009). However, the reported N_2O fractional losses are generally much lower than 1, averaging 0.375. It is important to note that many other studies have used C_2H_2 inhibition to measure N_2 production; C_2H_2 inhibits N_2O production via nitrification so that many of the reported N_2O mole fractions represent denitrification only. In addition, disturbing soil structure for measurements of N_2 emissions has been shown to affect the N_2O:N_2 ratio (Del Grosso et al. 2000). Most likely, the high N_2O mole fractions observed in our study, 0.84 ± 0.03, are a result of high soil mineral N concentrations that would inhibit N_2O consumption.

Mineral N concentrations in surface soils (0-10 cm depth) were very high across the pasture and were the strongest predictor of gross N_2O production rates. Across all landforms, mineral N concentration together with DEA explained 73% of the variability in gross N_2O production rates. In the drier landforms, NO_3^- concentration together with DEA explained 87% of the variability in gross N_2O production rates. While the $^{15}N_2O$ pool dilution approach does not distinguish between nitrification and denitrification as N_2O sources, these relationships imply that denitrification was likely the dominant N_2O source. Moreover, the strength of the relationships suggests that the N_2O was produced in surface soils rather than diffusing upward from groundwater below the vadose zone.

The crown landform exhibited the highest N_2O emissions and the highest mineral N concentrations. This is the only landform on which the invasive pepperweed, *Lepidium latifolium*, is currently found. Pepperweed can stimulate microbial enzyme activity to increase soil N mineralization, and thus mineral N concentrations (Blank 2002; Blank and Young 2004). If pepperweed is associated with the higher N_2O emissions via elevated mineral N concentrations, then overall N_2O emissions from the pasture may increase if pepperweed advances to the other landforms.

Nitrous oxide consumption rates were most strongly correlated to soil O_2 concentrations, but this relationship was apparent only when the landforms were grouped by soil moisture. The slopes of the regression lines were similar between the drier and wetter landforms, but the intercepts differed. This suggests that the control of soil O_2 concentrations on N_2O consumption is similar across the pasture, but that the N_2O consumption rates at any given soil O_2 concentration is greater in the drier landforms compared to the wetter landforms. Soil moisture or WFPS are often used as proxies for soil O_2 concentrations, but here, they were not related to N_2O consumption rates.

Broader Application of the Method

We have presented the $^{15}N_2O$ pool dilution method in a form optimized for sites with high N_2O emissions and high soil diffusivity, but the method can also be applied to ecosystems with low N_2O emissions and low soil diffusivity. Using a lower ^{15}N enrichment of the chamber headspace N_2O pool and a longer sampling time period will lower the detection limit of the method and allow the $^{15}N_2O$ tracer to diffuse deeper into the soil profile. A longer sampling time period would have to be accompanied with a deeper insertion of the chamber into the soil to reduce lateral diffusion of the tracer which increases with time (von Fischer et al. 2009). Pilot data from a high marsh site that exhibits net N_2O uptake (data not shown) suggest that this technique may even be able to provide insight into the growing evidence of soils acting as atmospheric N_2O sinks (Chapuis-Lardy et al. 2007).

We conservatively do not equate soil N_2 production rates with N_2O consumption rates measured by the $^{15}N_2O$ pool dilution method for several reasons. First, it is possible that complete denitrification of NO_3^- to N_2 can occur intra-cellularly so that N_2O is not exchanged between the microbial cell and the soil atmosphere. In this situation, N_2O consumption to N_2 would not be captured by the $^{15}N_2O$ pool dilution method. Second, there is recent evidence of soil N_2 production pathways other than denitrification (Yang et al., in prep). Currently, the importance of these pathways relative to denitrification is unknown. We could use the $^{15}N_2O$ pool dilution method simultaneously with the gas flow core method to determine how well N_2O consumption rates represent N_2 production rates. Regardless, the $^{15}N_2O$ pool dilution method is a valuable tool for understanding the dynamics of N_2O that can be exchanged between the soil and the atmosphere, and thus the N_2O that can potentially contribute to climate change.

Conclusions

We conclude that the high N_2O emissions observed at the peatland pasture are a result of high mineral N concentrations that drive high rates of incomplete denitrification in the surface soils. The N_2O mole fractions observed at our study site were generally higher than those reported for other agricultural soils (Schlesinger 2009), but they may not be directly comparable because of differences between laboratory and field measurements as well as between the methods used. Nitrous oxide emissions at the pasture could increase in the future, as the pepperweed invasion spreads downslope (M. Detto, personal communication), if the presence of pepperweed in the crown landform is responsible for the higher mineral N concentrations and higher N_2O emissions found there.

We demonstrated that the $^{15}N_2O$ pool dilution technique can provide accurate laboratory and field measurements of gross N_2O production and consumption in an ecosystem with high N_2O emissions. It is critical to understand N_2O dynamics in ecosystems with high N_2O emissions because they are likely to have substantial impacts on future atmospheric N_2O concentrations. With some modifications, this method can also be applied to ecosystems with low N_2O emissions and potentially even provide insight into observations of net N_2O uptake. Additional investigation is required to determine if N_2O consumption rates measured by the $^{15}N_2O$ pool dilution method represent soil N_2 production rates. If so, then this method will provide an approach for estimating soil N_2 production rates in the field and thus improve estimates of ecosystem N budgets.

References

Anderson IC, Tobias CR, Neikirk BB, Wetzel RL (1997) Development of a process-based nitrogen mass balance model for a Virginia (USA) *Spartina alterniflora* salt marsh: implications for net DIN flux. Marine Ecology Progress Series 159:13-27

Atwater BF (1980) Attempts to correlate late Quartenary climatic records between San Francisco Bay, the Sacramento-San Joaquin Delta, and the Mokelumne River, California. Ph.D. Dissertation. University of Delaware, Newark, DE, USA

Blank RR (2002) Amidohydrolase activity, soil N status, and the invasive crucifer *Lepidium latifolium*. Plant and Soil 239:155-163

Blank RR, Young JA (2004) Influence of three weed species on soil nutrient dynamics. Soil Science 169:385-397

Butterbach-Bahl K, Willibald G, Papen H (2002) Soil core method for direct simultaneous determination of N_2 and N_2O emissions from forest soils. Plant and Soil 240: 105-116.

Chapuis-Lardy L, Wrage N, Metay A, Chotte JL, Bernoux M (2007) Soils, a sink for N_2O? A review. Global Change Biology 13:1-17

Clough TJ, Kelliher FM, Wang YP, Sherlock RR (2006) Diffusion of ^{15}N-labelled N_2O into soil columns: a promising method to examine the fate of N_2O in subsoils. Soil Biology and Biochemistry 38:1462-1468

Davidson EA, Hart SC, Shanks CA, Firestone MK (1991) Measuring gross nitrogen mineralization, immobilization, and nitrification by ^{15}N isotope pool dilution in intact cores. Journal of Soil Science 42:335-349

Del Grosso SJ, Parton WJ, Mosier AR, Ojima DS, Kulmala AE, Phongpan S (2000) General model for N_2O and N_2 gas emissions from soils due to denitrification. Global Biogeochemical Cycles 14:1045-1060

Deverel SJ, Leighton DA, Finlay MR (2007) Processes affecting agricultural drainwater quality and organic carbon loads in California's Sacramento – San Joaquin Delta. San Francisco Estuary and Watershed Science 5:25

Drexler JZ, De Fontaine CS, Deverel SJ (2009) The legacy of wetland drainage on the remaining peat in the Sacramento – San Joaquin Delta, California, USA. Wetlands 29:372-286

Firestone MK, Davidson EA (1989) N_2O production and consumption in soil. In: Exchange of Trace Gases between Terrestrial Ecosystems and the Atmosphere (eds Andreae MO, Schimel DS), pp 7-21. John Wiley and Sons, New York

Firestone MK, Firestone RB, Tiedje JM (1980) Nitrous oxide from soil denitrification: factors controlling its biological production. Science 208:749-751

Firestone MK, Smith MS, Firestone RB, Tiedje JM (1979) The influence of nitrate, nitrite, and oxygen on the composition of the gaseous products of denitrification in soil. Soil Science Society of America Journal 43:1140-1144

Flessa H, Wild U, Klemisch M, Pfadenhauer J (1998) Nitrous oxide and methane fluxes from organic soils under agriculture. European Journal of Soil Science 49:327-335

Groffman PM, Altabet MA, Bohlke JK, Butterbach-Bahl K, David MB, Firestone MK, Giblin AE, Kana TM, Nielsen LP, Voytek MA (2006) Methods for measuring denitrification: diverse approaches to a difficult problem. Ecological Applications 16:2091-2122

Kaiser J, Rockmann T, Brenninkmeijer CAM (2003) Complete and accurate mass spectrometric isotope analysis of tropospheric nitrous oxide. Journal of Geophysical Research 108:4476, doi:10.1029/2003JD003613

Kirkham D, Bartholomew WV (1954) Equations for following nutrient transformations in soil, utilizing tracer data. Soil Science Society of America Proceedings 18:33-34
Knowles R (1990) Acetylene inhibition technique: development, advantages, and potential problems. In: Denitrification in Soil and Sediment (eds N.P. Revsbech and J. Sorensen) pp 151-166. Plenum Press, New York
Koops JG, Oenema O, van Beusichem ML (1996) Denitrification in the top and sub soil of grassland on peat soils. Plant and Soil 184:1-10
Koops JG, van Beusichem ML, Oenema O (1997) Nitrogen loss from grassland on peat soils through nitrous oxide production. Plant and Soil 188:119-130
Kulkarni MV, Groffman PM, Yavitt JB (2008) Solving the global nitrogen problem: it's a gas! Frontiers in Ecology and the Environment 6:199-206
Martikainen PJ, Nykanen H, Crill P, Silvola J (1993) Effect of a lowered water-table on nitrous oxide fluxes from northern peatlands. Nature 366:51-53
Massman WJ (1998) A review of the molecular diffusivities of H_2O, CO_2, CH_4, CO, O_3, SO_2, NH_3, N_2O, NO, and NO_2 in air, O_2, and N_2 near STP. Atmospheric Environment 32:1111-1127
Millington RJ, Quirk JP (1961) Permeabiliy of porous solids. Transactions of the Faraday Society 57:1200-1207
Prather M J, Derwent R, Ehhalt D, Fraser P, Sanhueza E, Zhou X (1995) Other trace gases and atmospheric chemistry. In: Climate Change 1994 (eds Houghton JT, et al.) pp 73-126. Cambridge University Press, Cambridge
Pushon S and Moore RM (2004) Nitrous oxide production and consumption in a eutrophic coastal embayment. Marine Chemistry 91:37-51
Regina K, Silvola J, Martikainen PJ (1998) Mechanisms of N_2O and NO production in the soil profile of a drained and forested peatland, as studied with acetylene, nitrapyrin, and dimethyl ether. Biology and Fertility of Soils 27:205-210
Rhew RC, Aydin M, Saltzman ES (2003) Measuring terrestrial fluxes of methyl chloride and methyl bromide using a stable isotope tracer technique. Geophysical Research Letters 30:2103, doi:10.1029/2003GL018160
Rhew RC and T Abel (2007) Measuring simultaneous production and consumption fluxes of methyl chloride and methyl bromide in annual temperate grasslands. Environmental Science and Technology 41:7837-7843
Schlesinger WH (2009) On the fate of anthropogenic nitrogen. Proceedings of the National Academy of Sciences 106:203-208
Silver WL, Lugo AE, Keller M (1999) Soil oxygen availability and biogeochemical cycling along elevation and topographical gradients in Puerto Rico. Biogeochemistry 44:301-328
Silver WL, Neff J, Veldkamp E, McGroddy M, Keller M, Cosme R (2000) The effects of soil texture on below ground carbon and nutrient storage in a lowland Amazonian forest ecosystem. Ecosystems 3:193-209
Simek M, Cooper JE (2002) The influence of soil pH on denitrification: progress towards the understanding of this interaction over the last 50 years. European Journal of Soil Science 53:345-354
Stein LY, Yung YL (2003) Production, isotopic composition, and atmospheric fate of biologically produced nitrous oxide. Annual Review in Earth and Planetary Sciences 31:329-356
Stevens RJ, Laughlin RJ, Malone JP (1998) Soil pH affects the processes reducing nitrate to

nitrous oxide and dinitrogen. Soil Biology and Biochemistry 30:1119-1126
Tiedje JM (1994) Denitrifiers. In: Methods of soil analysis, Part 2. Microbiological and biochemical properties (eds Weaver RW, Angle JS, Bottomly PJ) pp 256-267. Soil Science Society of America, Madison
van Beek CL, Hummelink EWJ, Veltoh GL, Oenema O (2004) Denitrification rates in relation to groundwater level in a peat soil under grassland. Biology and Fertility of Soils 39:329-336
Vieten B, Blunier T, Neftel A, Alewell C, Conen F (2007) Fractionation factors for stable isotopes of N and O during N_2O reduction in soil depend on reaction rate constant. Rapid Communications in Mass Spectrometry 21:846-850
Vieten B, Conen F, Neftel A, Alewell C (2009) Respiration of nitrous oxide in suboxic soil. European Journal of Soil Science 60:332-337
von Fisher JC, Hedin LO (2002) Separating methane production and consumption with a field-based isotope pool dilution technique. Global Biogeochemical Cycles 16: 1034, doi:10.1029/2001GB001448
von Fischer JC, Butters G, Duchateau PC, Thelwell RJ, Siller R (2009) In situ measures of methanotroph activity in upland soils: a reaction-diffusion model and field observation of water stress. Journal of Geophysical Research 114:G01015, doi:10.1029/2008JG000731
Weier KL, Doran JW, Power JF, Walters DT (1993) Denitrification and the dinitrogen nitrous-oxide ratio as affected by soil-water, available carbon, and nitrate. Soil Science Society of America Journal 57:66-72

Tables

Table 1. Soil variables by landform (± SE; letters indicate significant differences, $P < 0.05$).

Landform	n	Soil moisture ($g\text{-}H_2O\ g^{-1}$)	Soil pH	Soil NO_3^- concentration ($ug\ N\ g^{-1}$)	Soil NH_4^+ concentration ($ug\ N\ g^{-1}$)	Gross N_2O production ($mgN\ m^{-2}\ d^{-1}$)	N_2O:N_2 ratio	Denitrifying enzyme activity ($ugN\ g^{-1}\ h^{-1}$)
Crown	10	0.29 ± 0.02 a	5.46 ± 0.12 a	14.65 ± 4.36 a	44.73 ± 20.05 a	20.09 ± 9.43 a	16.1 ± 6.4 a	1.23 ± 0.53 ab
Hollow/hummock	6	0.46 ± 0.04 b	5.19 ± 0.12 ab	0.69 ± 0.18 b	9.56 ± 5.46 a	3.31 ± 1.70 ab	18.3 ± 10.2 ab	0.53 ± 0.13 ab
Irrigation ditch	6	0.48 ± 0.02 b	5.36 ± 0.05 ab	0.88 ± 0.39 b	19.19 ± 7.03 a	6.40 ± 2.86 ab	22.7 ± 14.9 ab	0.71 ± 0.11 a
Slope	10	0.35 ± 0.02 a	5.08 ± 0.05 b	1.25 ± 0.34 b	5.92 ± 1.50 a	1.02 ± 0.27 b	5.9 ± 2.0 b	0.19 ± 0.02 b

Table 2. Linear regressions describing N_2O dynamics.

Landforms included	Dependent variable	Independent variable	Regression coefficient (± SE)	P-value	n	R^2
All	Log(Gross N_2O Production, μg N m^{-2} d^{-1})	Constant	2.881 ± 0.236	< 0.01	24	0.73
		Log(Mineral N concentration, μg N g^{-1})	0.729 ± 0.163	< 0.01		
		Log(DEA, μg N g^{-1} h^{-1})	0.574 ± 0.223	< 0.01		
Crown, Slope	Log(Gross N_2O Production)	Constant	3.412 ± 0.257	< 0.01	12	0.87
		Log(NO_3^- concentration, μg N g^{-1})	0.651 ± 0.230	0.02		
		Log(DEA)	0.819 ± 0.240	< 0.01		
Irrigation ditch, Hollow/hummock	Log(Gross N_2O Production)	Constant	2.593 ± 0.211	< 0.01	12	0.66
		Log(NH_4^+ concentration, μg N g^{-1})	0.903 ± 0.205	< 0.01		
All	Log(N_2O Consumption, μg N m^{-2} d^{-1})	Constant	-0.657 ± 0.422	0.13	32	0.66
		Log(Gross N_2O production)	0.921 ± 0.121	< 0.01		
Crown, Slope	Log(N_2O Consumption)	Constant	3.919 ± 0.355	< 0.01	6	0.64
		Log(Soil O_2 concentration, %)	-0.062 ± 0.023	0.06		
Irrigation ditch, Hollow/hummock	Log(N_2O Consumption)	Constant	3.194 ± 0.277	< 0.01	6	0.76
		Log(Soil O_2 concentration)	-0.103 ± 0.029	0.02		
All	Log(DEA)	Constant	- 3.394 ± 0.791	< 0.01	12	0.91
		pH	0.649 ± 0.139	< 0.01		
		Log(Soil O_2 concentration)	- 0.027 ± 0.007	< 0.01		

Figure Legends

Figure 1. Mean N_2O consumption, gross N_2O production, and net N_2O production rates measured by the ^{15}N tracer (black bars), $^{15}N_2O$ pool dilution (gray bars), and acetylene inhibition (hatched bars) methods. Error bars represent standard errors.

Figure 2. (a) Net N_2O flux without $^{15}N_2O$ spiking gas addition versus net N_2O flux with $^{15}N_2O$ spiking gas addition. (b) Observed net N_2O flux (from change in chamber headspace N_2O concentration over time) versus predicted net N_2O flux (from difference between predicted gross N_2O production and consumption rates). Regression lines are shown in each panel.

Figure 3. Denitrifying enzyme activity versus pH. The regression line is shown.

Figure 4. Mean gross N_2O production rates across sampling dates by landform are shown by the whole bars with the grey portion representing N_2O consumption and the black portion representing net N_2O production. Error bars represent standard errors for gross N_2O production rates.

Figure 5. (a) Gross N_2O production versus mineral N concentration. (b) Gross N_2O production versus denitrifying enzyme activity. Regression lines are shown in each panel.

Figure 6. Nitrous oxide consumption versus soil O_2 concentration. The solid line represents the regression line for the drier landforms (i.e. crown and slope), and the hatched line represents the regression line for the wetter landforms (i.e., irrigation ditch and hollow/hummock).

Figures

Figure 1.

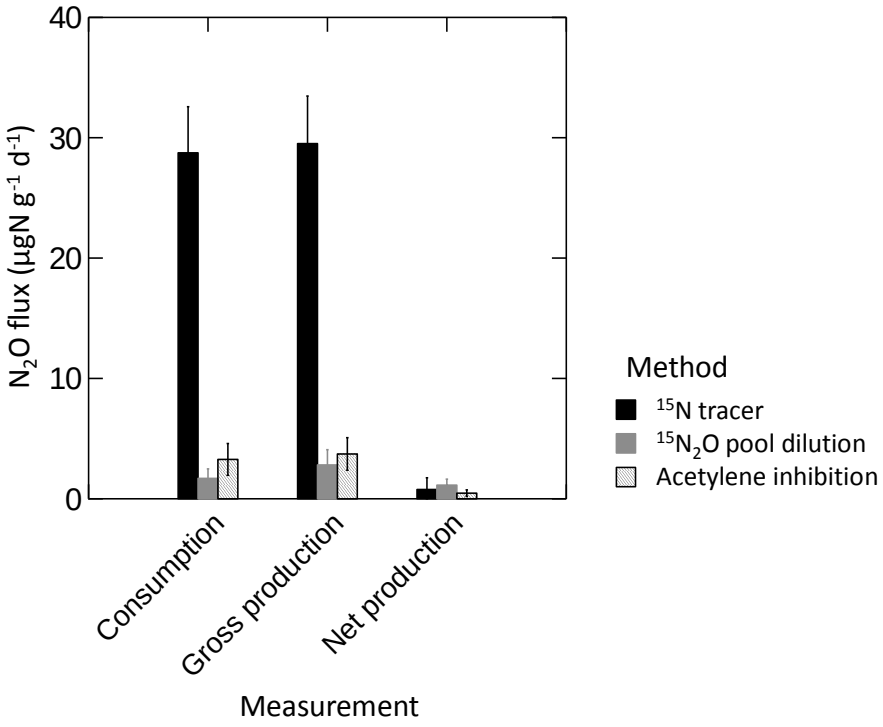

Figure 2.

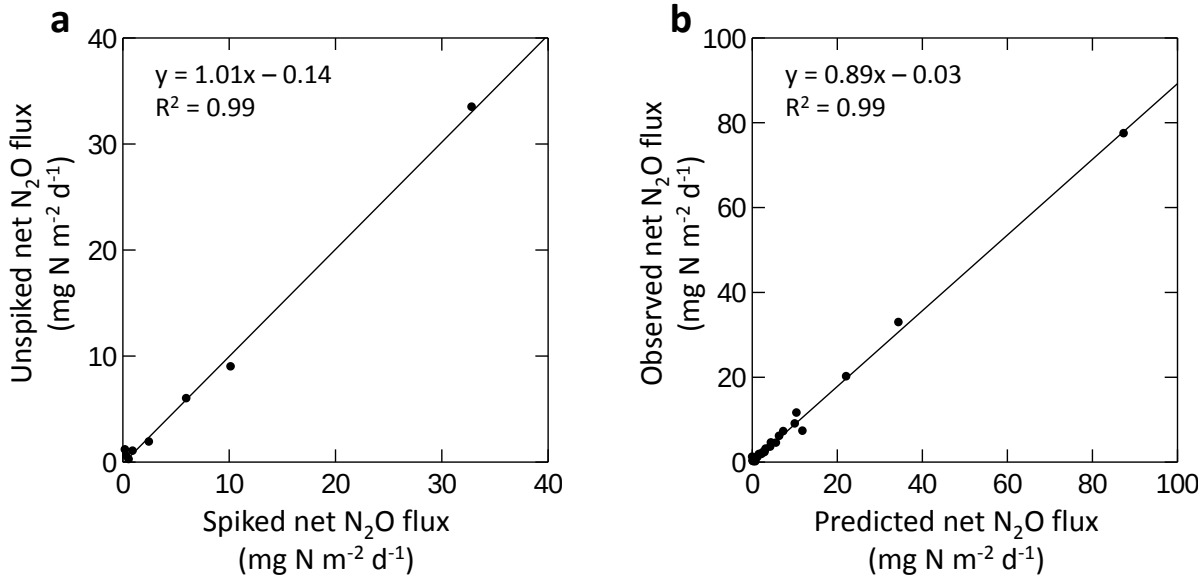

Figure 3.

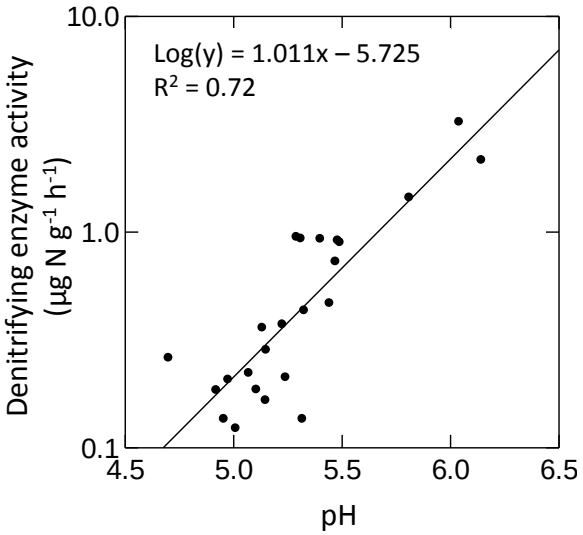

Figure 4.

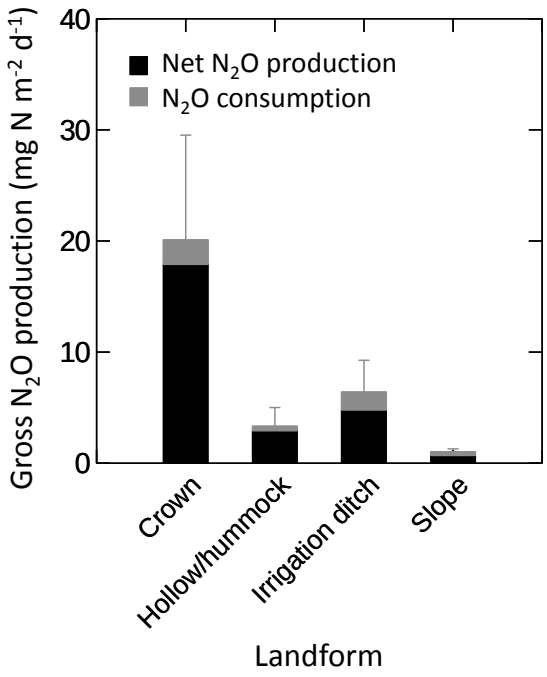

Figure 5.

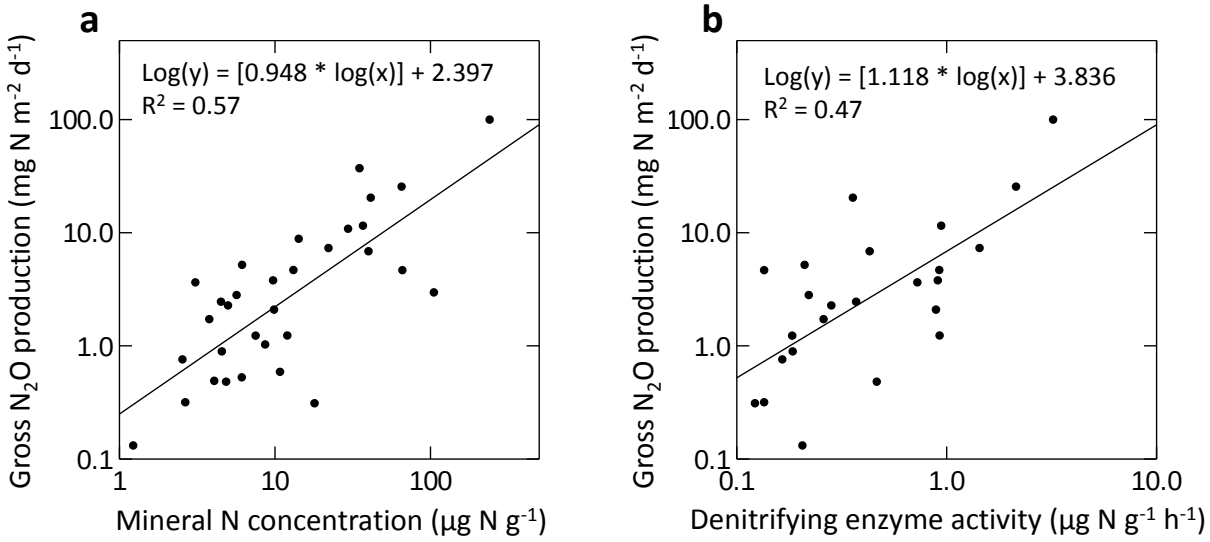

Figure 6.

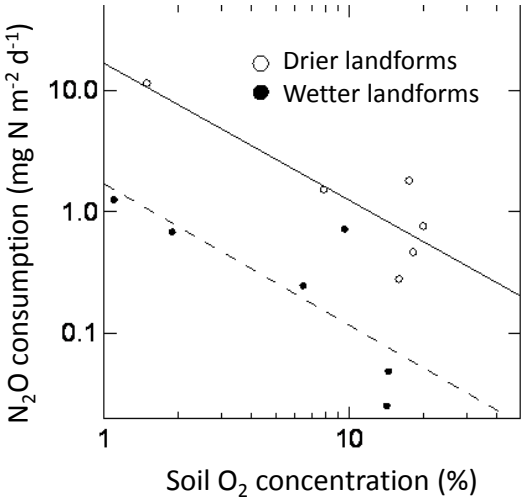

Appendix

Table A1. Published fractionation factors associated with N_2O production via nitrification (NH_4^+ → N_2O).

System	Sample details	Reported enrichment factor, ε (‰)	Fractionation factor used, α [a]	Reference
soil	clay	-112 ± 12	0.8880	Perez et al. 2006
	sandy loam	-102 ± 5	0.8980	
pure culture	*Nitrosomonas europaea*	-68 to -60	0.9360	Wada and Ueda 1996
pure culture	*Nitrosomonas europaea*	-46.9	0.9531	Sutka et al. 2006
pure culture	*Nitrosomonas europaea*	-73.4 ± 0.1	0.9266	Yoshida 1988

[a] $\alpha = 1 - (\varepsilon / 1000)$

Table A2. Published fractionation factors associated with N_2O production via denitrification.

System	Sample details	Reported enrichment factor, ε (‰)	Fractionation factor used, α [a]	Reference
soil		-31 to -11	0.9790	Mariotti et al. 1982
soil	20 °C	-29.4 ± 2.4	0.9706	Mariotti et al. 1981
	30 °C	-24.6 ± 0.9	0.9754	
soil	birch	-29 to -24	0.9735	Menyailo and
	larch	-25 to -24	0.9755	Hungate 2006
soil	clay	-31 ± 11	0.9690	Perez et al. 2006
	sandy loam	-45 ± 5	0.9550	
	sand	-10.4 ± 3.5	0.9896	
soil	silt loam	-52.37 ± 0.92	0.9476	Well and Flessa
	sand	-47.85 ± 3.18	0.9521	2009
soil		-27	0.9730	Wada and Ueda 1996
soil		-16	0.9840	Wada and Ueda 1996
pure culture	*Pseudomonas fluoroscens*	-37 to -33	0.9650	Wada and Ueda 1996
pure culture	*Paracoccus denitrificans*	-28.6 ± 1.9	0.9714	Barford et al. 1999
pure culture	*Pseudomonas fluoroscens*	-39 to -17	0.9720	Toyoda et al 2005
	Paracoccus denitrificans	-22 to -10	0.9840	
pure culture	*Pseudomonas aureofaciens*	-36.7	0.9633	Sutka et al. 2006a
	Pseudomonas chlororaphis	-12.7	0.9873	

[a] $\alpha = 1 - (\varepsilon / 100)$

Table A3. Published fractionation factors associated with N_2O reduction to N_2 ($N_2O \rightarrow N_2$).

System	Sample details	Reported enrichment factor, ε (‰)	Fractionation factor used, α [a]	Reference
soil	birch	-6.3 to -8.3[b]	0.9937	Menyailo and
	larch	-6.3 to -9.8[b]	0.9902	Hungate 2006
soil		-5.8	0.9942	Ostrom et al. 2007
soil		-9.3 ± 1.3	0.9907	Vieten et al. 2007
soil	60 % WFPS	-7.8 ± 0.7	0.9922	Jinuntuya-
	80 % WFPS	-6.0 ± 0.3	0.9940	Nortman et al.
	100% WFPS	-4.2 ± 1.5	0.9958	2008
soil	silt loam	-5.7 ± 0.7	0.9943	Well and Flessa
	sand	-7.5 ± 1.8	0.9925	2009b
soil		-4	0.9960	Wada and Ueda 1996
ocean		-11.6 ± 1.0	0.9884	Yamagishi et al. 2007
pure culture	*Pseudomonas denitrificans*	-27 to -1	0.9860	Wada and Ueda 1996
pure culture	*Paracoccus denitrificans*	-12.9 ± 2.6	0.9871	Barford et al. 1999
pure culture	*Pseudomonas stutzeri*	-4.1	0.9959	Ostrom et al. 2007
	Pseudomonas denitrificans	-6.6	0.9934	

[a] $\alpha = 1 - (\varepsilon / 1000)$

[b] Used fractionation factor calculated from the median of this range

Appendix References

Barford CC, Montoya JP, Altabet MA, Mitchell R (1999) Steady-state nitrogen isotope effects of N_2 and N_2O production in *Paracoccus denitrificans*. Applied and Environmental Microbiology 65:989-994

Jinuntuya-Nortman M, Sutka RL, Ostrom PH, Gandhi H, Ostrom NE (2008) Isotopologue fractionation during microbial reduction of N_2O within soil mesocosms as a function of water-filled pore space. Soil Biology and Biochemistry 40:2273-2280

Mariotti A, Germon JC, Hubert P, Kaiser P, Letolle R, Tardieux A, Tardieux P (1981) Experimental determination of nitrogen kinetic isotope fractionation: some principles; illustration for the denitrification and nitrification processes. Plant and Soil 62:413-430

Mariotti A, Germon JC, and Leclerc A (1982) Nitrogen isotope fractionation associated with the $NO_2^- \rightarrow N_2O$ step of denitrification in soils. Canadian Journal of Soil Science 62:227-241

Menyailo OV, Hungate BA (2006) Stable isotope discrimination during soil denitrification: production and consumption of nitrous oxide. Global Biogeochemical Cycles 20: GB3025, doi:10.1029/2005GB002527

Opdyke MR, Ostrom, NE, Ostrom PH (2009) Evidence for the predominance of denitrification as a source of N_2O in temperate agricultural soils based on isotopologue measurements. Global Biogeochemical Cycles 23:GB4018, doi:10.1029/2009GB003523

Ostrom NE, Pitt A, Sutka R, Ostrom PH, Grandy AS, Huizinga KM, Robertson GP (2007) Isotopologue effects during N_2O reduction in soil and in pure cultures of denitrifiers. Journal of Geophysical Research-Biogeosciences 112:GO2005, doi:10.1029/2006JG000287

Perez T, Garcia-Montiel D, Trumbore S, Tyler S, de Camargo P, Moreira M, Piccolo M, Cerri C (2006) Nitrous oxide nitrification and denitrification ^{15}N enrichment factors from Amazon forest soils. Ecological Applications 16:2153-2167

Snider DM, Schiff SL, Spoelestra J (2009) $^{15}N/^{14}N$ and $^{18}O/^{16}O$ stable isotope ratios of nitrous oxide produced during denitrification in temperate forest soils. Geochimica et Cosmochimica Acta 73:877-888

Sutka RL, Ostrom RE, Ostrom PH, Breznak JA, Gandhi H, Pitt AJ, Li F (2006) Distinguishing nitrous oxide production from nitrification and denitrification on the basis of isotopomer abundances. Applied and Environmental Microbiology 72:638-644

Toyoda S, Mutobe H, Yamagishi H, Yoshida N, Tanji Y (2005) Fractionation of N_2O isotopomers during production by denitrifier. Soil Biology and Biochemistry 37:1535-1545

Vieten B, Blunier T, Neftel A, Alewell C, Conen F (2007) Fractionation factors for stable isotopes of N and O during N_2O reduction in soil depend on reaction rate constant. Rapid Communications in Mass Spectrometry 21:846-850

Wada E and Ueda S (1996) Carbon, nitrogen, and oxygen isotope ratios of CH_4 and N_2O in soil ecosystems. In: Boutton TW, Tamasaki S-I (eds) Mass spectrometry of soils. Dekker, New York, pp 177-204

Well R and Flessa H (2009a) Isotopologue signatures of N_2O produced by denitrification in soils. Journal of Geophysical Research-Biogeosciences 114: G02020, doi:10.1029/2008JG000804

Well R, Flessa H (2009b) Isotopologue enrichment factors of N_2O reduction in soils. Rapid Communications in Mass Spectrometry 23:2996-3002

Yamagishi H, Westley MB, Popp BN, Toyoda S, Yoshida N, Watanabe S, Koba K, Yamanaka Y (2007) Role of nitrification and denitrification on the nitrous oxide cycle in the eastern tropical North Pacific and Gulf of California. Journal of Geophysical Research-Biogeosciences 112:G02015, doi:10.1029/2006JG000227

Yoshida N (1988) ^{15}N-depleted N_2O as a product of nitrification. Nature 335:528-529

Chapter 4. Nitrogen loss from soil via anaerobic ammonium oxidation coupled to iron reduction

Abstract

The oxidation of ammonium to nitrate is a key conduit in the terrestrial nitrogen cycle, regulating nitrate leaching into groundwater, the production of the potent greenhouse gas, nitrous oxide, and the completion of the nitrogen cycle to dinitrogen gas. We report on a short circuit in the nitrogen cycle: anaerobic ammonium oxidation couple to iron(III) reduction (Feammox) producing dinitrogen or nitrite. In stable isotope pairing experiments, Feammox produced $^{30}N_2$ as well as $^{29}N_2$ that was previously attributed only to anammox. Maximum potential rates of Feammox ranged from 0.3-1.2 μg NH_4-N oxidized g^{-1} soil d^{-1}, similar to aerobic nitrification rates. Terrestrial ecosystems that have large pools of reactive iron minerals and experience periodic reducing events are likely to fuel globally important nitrogen losses via this newly identified pathway.

Introduction

Terrestrial net primary productivity is often limited by the availability of fixed nitrogen (N) due in large part to the mobility of N across ecosystem boundaries, particularly via denitrification (Vitousek and Howarth 1991). Denitrification is dominantly a microbial process that converts nitrate (NO_3^-) to nitrous oxide (N_2O) and dinitrogen (N_2) gases. In terrestrial ecosystems, denitrification is thought to be the only process by which fixed N is converted to N_2, thereby completing the nitrogen cycle. However, in marine and freshwater ecosystems, up to 67 % of N_2 production can be attributed to anaerobic ammonium (NH_4^+) oxidation (termed anammox), which directly produces N_2 from nitrite (NO_2^-) and NH_4^+ and thus bypasses the potential for N_2O production (Dalsgaard and Thamdrup 2002; Kuypers et al. 2005; Nicholls and Trimmer 2009; Rich et al. 2008; Schubert et al. 2006). Bacteria capable of anammox have been detected in soil (Penton et al. 2006; Humbert et al. 2010), but the occurrence of anammox has not been demonstrated in terrestrial ecosystems (Jetten et al. 2009).

Theoretically the reduction of ferric iron (Fe(III)), which is abundant in many terrestrial soils, can be coupled to anaerobic NH_4^+ oxidation to produce N_2, NO_2^-, or NO_3^- (Anschutz et al. 2000; Clement et al. 2005; Hulth et al. 1999; Luther et al. 1997; Shrestha et al. 2009). This process is termed Feammox (Sawayama 2006). In environments rich in poorly crystalline Fe minerals, Feammox to N_2 is energetically more favorable than Feammox to NO_2^- or NO_3^-, and favorable over a wider range of conditions. Thus Feammox to N_2 is more likely to occur. Under typical upland soil conditions, Feammox to N_2 utilizing ferrihydrite, a common poorly crystalline Fe oxide, yields -212 kJ $mole^{-1}$ reaction via the following process:

$$3\ Fe(OH)_3 + 5\ H^+ + NH_4^+ \rightarrow 3\ Fe^{2+} + 9\ H_2O + 0.5\ N_2 \qquad \text{(Equation 1)}$$

This reaction remains energetically favorable over a wide pH range. Feammox to NO_2^- occurs only below pH 6.5, stoichiometrically requires more Fe(III) and yields less energy than Feammox to N_2 (-99 kJ $mole^{-1}$ reaction) under the same conditions (Equation 2).

$$6\ Fe(OH)_3 + 10\ H^+ + NH_4^+ \rightarrow 6\ Fe^{2+} + 16\ H_2O + NO_2^- \qquad \text{(Equation 2)}$$

Feammox to NO_3^- is also thermodynamically feasible under these conditions (-119 kJ $mole^{-1}$ reaction).

Results and Discussion

Using the isotope pairing technique, we measured Feammox in replicate surface soils (0-10 cm depth) of an upland humid tropical forest in the Luquillo Mountains, Puerto Rico, USA. Slurried soils were pre-incubated in an anaerobic glovebox to remove oxygen (O_2), inhibit aerobic nitrification, and deplete background NO_2^- and NO_3^-. We calculated $^{29}N_2$ and $^{30}N_2$ production from the difference in $^{29}N_2$ and $^{30}N_2$ mole fractions in soil slurry treatments relative to $^{29}N_2$ and $^{30}N_2$ mole fractions in soil-free blank jars. We observed $^{30}N_2$ production with the addition of $^{15}NH_4^+$ alone ($p<0.001$). The addition of hydrous ferric oxide (HFO) stimulated $^{30}N_2$ production ($p<0.001$) (Figure 1a). Feammox directly to N_2 or Feammox-generated NO_2^- followed by denitrification or anammox are the only possible sources of $^{30}N_2$ (see Table S1). These soils are rich in poorly crystalline Fe (6.2 ± 0.2 mg Fe g^{-1} soil, Dubinsky et al. 2010), so it is likely that sufficient background Fe(III) was available to drive $^{30}N_2$ production with the addition of $^{15}NH_4^+$ alone. From the $^{15}NH_4^+$ only treatment, we estimated the background Feammox rate to be 0.32 ± 0.13 μg N g^{-1} d^{-1} (± SE) and in the presence of Fe(III), it increased to 1.20 ± 0.28 μg N g^{-1} d^{-1}.

We also measured significant $^{29}N_2$ production following the addition of $^{15}NH_4^+$ alone ($p = 0.03$) as well as the addition of Fe(III) and $^{15}NH_4^+$ together ($p < 0.001$) (Figure 1b). This is the first documented case of anaerobic $^{15}NH_4^+$ oxidation to $^{29}N_2$ in soils. The increase in $^{29}N_2$ was significantly greater following Fe(III) and $^{15}NH_4^+$ addition compared to $^{15}NH_4^+$ addition alone ($p = 0.02$). The production of $^{29}N_2$ could result from anammox, from the use of background $^{14}NH_4^+$ along with added $^{15}NH_4^+$ in Feammox to N_2, or a combination of pathways involving Feammox-generated NO_2^-/NO_3^- (Table 1). Overall, $^{29}N_2$ accounted for approximately 60 % of the ^{15}N-N_2 produced, and Fe(III) addition increased $^{29}N_2$ production by approximately 100 %. Thus, Feammox accounts for some, if not all, of the $^{29}N_2$ production. Considering the production of both $^{30}N_2$ and $^{29}N_2$, anaerobic NH_4^+ oxidation consumed 5 to 14 % of the added $^{15}NH_4^+$ label.

To separate Feammox to N_2 from Feammox to NO_2^- and NO_3^-, we added acetylene (C_2H_2) to block the reduction of N_2O to N_2 (Yoshinari et al. 1977). Previous research had speculated a role of Fe in NO_2^- production in anaerobic sediments (Clement et al. 2005), and in one study recorded the presence of $^{15}NO_2^-$ following $^{15}NH_4^+$ addition (Shrestha et al. 2009). We did not assay for NO_2^- directly because it is very dynamic in low redox soils, and thus unlikely to accumulate (Van Cleemput and Samater 1996). The presence of C_2H_2 decreased $^{30}N_2$ production ($p < 0.08$), indicating that some NO_2^-/NO_3^- was produced via Feammox and then subsequently reduced to N_2O and N_2 via denitrification or reduced to N_2 via anammox, which is also inhibited by C_2H_2 (Jetten et al. 1998; Jensen et al. 2007). From N_2O accumulation in the C_2H_2 treatment, maximum rates of Feammox to NO_2^-/NO_3^- were 0.25 ± 0.06 μg N g^{-1} d^{-1}; thus Feammox to NO_2^-/NO_3^- accounted for approximately 21 % of total $^{15}NH_4^+$ oxidation via Feammox. Feammox-generated NO_2^- has many potential fates: N_2O or N_2 via denitrification, NH_4^+ via DNRA (Silver et al. 2001), and organic N via abiotic reduction (Dail et al. 2001), but see (Colman et al. 2007; Colman et al. 2008; Dail et al. 2001). Thus, our approach may underestimate Feammox to NO_2^-. However, these data suggest that Feammox to N_2 dominates over denitrification of Feammox-generated NO_2^- as an N_2 production pathway.

The presence of C_2H_2 completely inhibited $^{29}N_2$ production with $^{15}NH_4^+$ and Fe(III) addition (Figure 1b). The different responses of $^{29}N_2$ and $^{30}N_2$ production to C_2H_2 may, in part, reflect the occurrence of anammox, which is inhibited by C_2H_2 (Jetten et al. 1998; Jensen et al. 2007). The statistically not significant decrease in $^{30}N_2$ production in the presence of C_2H_2 suggests that Feammox to N_2 is not inhibited by C_2H_2 because it is the only known pathway for

$^{30}N_2$ production under those conditions. We would expect that if Feammox to N_2 is dominantly responsible for $^{30}N_2$ production in the presence of C_2H_2, then some amount of $^{29}N_2$ production from the combination of added $^{15}NH_4^+$ and background $^{14}NH_4^+$ should result from on-going Feammox to N_2. This suggests that Feammox to N_2 may preferentially use the added $^{15}NH_4^+$ to produce $^{30}N_2$. However, when $^{15}NH_4^+$ was added without C_2H_2, $^{29}N_2$ production accounted for approximately 60 % of the ^{15}N-N_2 produced, close to the value (50 %) predicted from random combinations of $^{14}NH_4^+$ and $^{15}NH_4^+$. Thus, our data do not suggest preferential $^{15}NH_4^+$ use by Feammox. At this time, we cannot explain the differing patterns in $^{29}N_2$ and $^{30}N_2$ production. We do not even know if Feammox is an abiotic or biotic process, but given the metabolic diversity of iron-reducing microbes (Weber et al. 2006), it is possible that Feammox is microbially mediated. Further investigation into the nature of Feammox may reveal why $^{29}N_2$ and $^{30}N_2$ production responded differently to C_2H_2.

Feammox is likely to occur naturally in upland soils that experience periods of anoxia or contain anoxic microsites. Frequent low redox events have been measured in upland soils in humid regions or during periods of rainfall, driven by rates of O_2 consumption that exceed diffusive resupply (Schuur and Matson 2001; Silver et al. 1999). Even in well-drained soils, low redox events or reduced microsites can drive high rates of Fe reduction in well-aggregated clay and organic colloids (Liptzin and Silver 2009).

Feammox can result in the significant gaseous loss of N from terrestrial soils under natural conditions. Iron reduction rates in surface soils of these humid tropical forests ranges from 2.7 μg Fe(II) g^{-1} d^- under ambient oxygen conditions (Liptzin and Silver 2009) to 76 μg Fe(II) g^{-1} d^{-1} under anoxic conditions (Chacon et al. 2006). If 1% of the average Fe reduction rate of 39 μg Fe(II) g^{-1} d^{-1} is associated with Feammox, then stoichiometrically, the range in NH_4^+ consumption would be 0.015 – 0.029 μg N g^{-1} d^{-1} depending on which Feammox pathway dominates. This is equivalent to approximately 3-7 kg NH_4^+ oxidized ha^{-1} y^{-1}, an amount similar to estimates of total denitrification for this forest (Chestnut et al. 1999).

Dinitrogen production via Feammox in terrestrial soils could have major implications for ecosystem and global N budgets. At the ecosystem scale, terrestrial N_2 production rates derived from methods that specifically target denitrification, such as acetylene inhibition (e.g., Chestnut et al. 1999), ^{15}N tracer using $^{15}NO_3^-$ (Stevens and Laughlin 1998) and isotope budgets incorporating fractionation from NO_3^--derived gaseous losses only (Houlton et al. 2006), could significantly underestimate total N_2 production. Assuming similar Fe(III) pools and reduction rates, Feammox in humid tropical forests alone could account for 4.2 Tg N yr^{-1} if 1 % of Fe reduction in surface soils (top 0-10 cm) is involved in Feammox to N_2. This amounts to 3-4 % of global soil denitrification estimated by global models and mass balance calculations (Galloway et al. 2004; Seitzinger et al. 2006).

References

Achard F et al. (2002) Determination of deforestation rates of the world's humid tropical forests. Science 297:999-1002

Anschutz P, Sundby B, Lefrancois L, Luther GW, Mucci A (2000) Interactions between metal oxides and species of nitrogen and iodine in bioturbated marine sediments. Geochimica Et Cosmochimica Acta 64:2751-2763

Chacon N, Silver WL, Dubinsky EA, Cusack DF (2006) Iron reduction and soil phosphorus solubilization in humid tropical forests soils: The roles of labile carbon pools and an electron shuttle compound. Biogeochemistry 78:67-84

Chestnut T, Zarin D, McDowell W, Keller M (1999) A nitrogen budget for late-successional hillslope tabonuco forest, Puerto Rico. Biogeochemistry 46:85-108

Clement JC, Shrestha J, Ehrenfeld JG, Jaffe PR (2005) Ammonium oxidation coupled to dissimilatory reduction of iron under anaerobic conditions in wetland soils. Soil Biology & Biochemistry 37:2323-2328

Colman B (2009) Understanding and eliminating iron interference in colorimetric nitrate and nitrite analysis. Environmental Monitoring and Assessment:10.1007/s10661-10009-10974-x

Colman B, Fierer N, Schimel J (2007) Abiotic nitrate incorporation in soil: is it real? Biogeochemistry 84:161-169

Colman B, Fierer N, Schimel J (2008) Abiotic nitrate incorporation, anaerobic microsites, and the ferrous wheel. Biogeochemistry 91:223-227

Dail D, Davidson E, Chorover J (2001) Rapid abiotic transformation of nitrate in an acid forest soil. Biogeochemistry 54:131-146

Dalsgaard T, Thamdrup B (2002) Factors controlling anaerobic ammonium oxidation with nitrite in marine sediments. Applied and Environmental Microbiology 68:3802-3808

Galloway J et al. (2004) Nitrogen cycles: past, present, and future. Biogeochemistry 70:153-226

Houlton BZ, Sigman DM, Hedin LO (2006) Isotopic evidence for large gaseous nitrogen losses from tropical rainforests. Proceedings of the National Academy of Sciences of the United States of America 103:8745-8750

Hulth S, Aller RC, Gilbert F (1999) Coupled anoxic nitrification manganese reduction in marine sediments. Geochimica Et Cosmochimica Acta 63:49-66

Humbert S, Tarnawksi S, Fromin N, Mallet M, Aragno M, Zopfi J (2010) Molecular detection of anammox bacteria in terrestrial ecosystems: distribution and diversity. The ISME Journal 4:450-454

Jensen M, Thamdrup B, Dalsgaard T (2007) Effects of specific inhibitors on anammox and denitrification in marine sediments. Applied and Environmental Microbiology 73:3151-3158

Jetten MSM et al. (1998) The anaerobic oxidation of ammonium. FEMS Microbiology Reviews 22:421-437

Jetten M, van Niftrik L, Strous M, Kartal B, Keltjens J, Op den Camp H (2009) Biochemistry and molecular biology of anammox bacteria. Critical Review in Biochemistry and Molecular Biology 44:65-84

Kuypers M, et al. (2005) Massive nitrogen loss from the Benguela upwelling system through anaerobic ammonium oxidation. Proceedings of the National Academy of Sciences 102:6478-6483

Liptzin D, Silver W (2009) Effects of carbon addition on iron reduction and phosphorus availability in a humid tropical forest soil. Soil Biology & Biochemistry 41:1696-1702
Lovley DR, Phillips EJP (1986) Organic matter mineralization with reduction of ferric iron in anaerobic sediments. Applied and Environmental Microbiology 51:683-689
Luther GW, Sundby B, Lewis BL, Brendel PJ, Silverberg N (1997) Interactions of manganese with the nitrogen cycle: Alternative pathways to dinitrogen. Geochimica Et Cosmochimica Acta 61:4043-4052
Nicholls J, Trimmer M (2009) Widespread occurrence of the anammox reaction in estuarine sediments. Aquatic Microbial Ecology 55:105-113
Penton C, Devol A, Tiedje J (2006) Molecular evidence for the broad distribution of anaerobic ammonium-oxidizing bacteria in freshwater and marine sediments. Applied and Environmental Microbiology 72:6829-6832
Pett-Ridge J, Silver WL, Firestone MK (2006) Redox fluctuations frame microbial community impacts on N-cycling rates in a humid tropical forest soil. Biogeochemistry 81:95-110
Rich J, Dale O, Song B, Ward B (2008) Anaerobic ammonium oxidation (Anammox) in Chesapeake Bay sediments. Microbial Ecology 55:311-320
Sawayama S (2006) Possibility of anoxic ferric ammonium oxidation. Journal of Bioscience and Bioengineering 101:70-72
Schubert CJ, Durisch-Kaiser E, Wehrli B, Thamdrup B, Lam P, Kuypers MMM (2006) Anaerobic ammonium oxidation in a tropical freshwater system (Lake Tanganyika). Environmental Microbiology 8:1857-1863
Schuur EAG, Matson PA (2001) Net primary productivity and nutrient cycling across a mesic to wet precipitation gradient in Hawaiian montane forest. Oecologia 128:431-442
Seitzinger S et al. (2006) Denitrification across landscapes and waterscapes: A synthesis. Ecological Applications 16:2064-2090
Shrestha J, Rich J, Ehrenfeld J, Jaffe P (2009) Oxidation of ammonium to nitrite under iron-reducing conditions in wetland soils: Laboratory, field demonstrations, and push-pull rate determination. Soil Science 174:156-164
Silver W, Scatena F, Johnson A, Siccama T, Sanchez M (1994) Nutrient availability in a montane wet tropical forest - spatial patterns and methodological considerations. Plant and Soil 164:129-145
Silver WL, Herman DJ, Firestone MK (2001) Dissimilatory nitrate reduction to ammonium in upland tropical forest soils. Ecology 82:2410-2416
Silver WL, Lugo AE, Keller M (1999) Soil oxygen availability and biogeochemistry along rainfall and topographic gradients in upland wet tropical forest soils. Biogeochemistry 44:301-328
Stevens R, Laughlin R (1998) Measurement of nitrous oxide and di-nitrogen emissions from agricultural soils. Nutrient Cycling in Agroecosystems 52:131-139
Templer P, Silver W, Pett-Ridge J, DeAngelis K, Firestone MK (2008) Plant and microbial controls on nitrogen retention and loss in a humid tropical forest. Ecology in press
Van Cleemput O, Samater AH (1996) Nitrite in soils: Accumulation and role in the formation of gaseous N compounds. Fertilizer Research 45:81-89
Vitousek PM, Howarth RW (1991) Nitrogen limitation on land and in the sea: How can it occur. Biogeochemistry 13:87-115
Weber KA, Achenbach LA, Coates JD (2006) Microorganisms pumping iron: Anaerobic microbial iron oxidation and reduction. Nature Reviews Microbiology 4:752-764

Yoshinari T, Hynes R, Knowles R (1977) Acetylene inhibition of nitrous oxide reduction and measurement of denitrification and nitrogen fixation in soil. Soil Biology & Biochemistry 9:177-183

Tables

Table 1. Potential pathways for $^{30}N_2$ and $^{29}N_2$ production from $^{15}NH_4^+$ under anoxic conditions.*

Product	Nitrogen Substrate 1**	Nitrogen Substrate 2	Process
$^{30}N_2$	Added $^{15}NH_4^+$	Added $^{15}NH_4^+$	Feammox to N_2
	Added $^{15}NH_4^+$	Feammox-generated $^{15}NO_2^-$/$^{15}NO_3^-$	Anammox
	Feammox-generated $^{15}NO_2^-$/$^{15}NO_3^-$	Feammox-generated $^{15}NO_2^-$/$^{15}NO_3^-$	Denitrification
$^{29}N_2$	Added $^{15}NH_4^+$	Background $^{14}NH_4^+$	Feammox to N_2
	Added $^{15}NH_4^+$	Background $^{14}NO_2^-$/$^{14}NO_3^-$	Anammox
	Feammox-generated $^{15}NO_2^-$/$^{15}NO_3^-$	Background $^{14}NH_4^+$	Anammox
	Feammox-generated $^{15}NO_2^-$/$^{15}NO_3^-$	Background $^{14}NO_2^-$/$^{14}NO_3^-$	Denitrification

* Dissimilatory NO_3^- reduction to NH_4^+ cycles background $^{14}NO_2^-$/$^{14}NO_3^-$ or Feammox-generated $^{15}NO_2^-$/$^{15}NO_3^-$ to $^{14}NH_4^+$ or $^{15}NH_4^+$, respectively. Thus, it does not create additional pathways for $^{30}N_2$ and $^{29}N_2$ production from $^{15}NH_4^+$.
** Feammox can generate $^{15}NO_2^-$ or $^{15}NO_3^-$ from added $^{15}NH_4^+$.

Figure Legends

Figure 1. (a) $^{30}N_2$ mole fraction and (b) $^{29}N_2$ mole fraction following the addition of $^{15}NH_4^+$, $^{15}NH_4^+$ + Fe(III), and $^{15}NH_4^+$ + Fe(III) + C_2H_2. Treatment values greater than the blank (i.e., soil free) values represent significant $^{15}N_2$ production. Letters indicate statistically significant differences among treatments, and error bars represent ± SE (n = 8).

Figures

Figure 1.

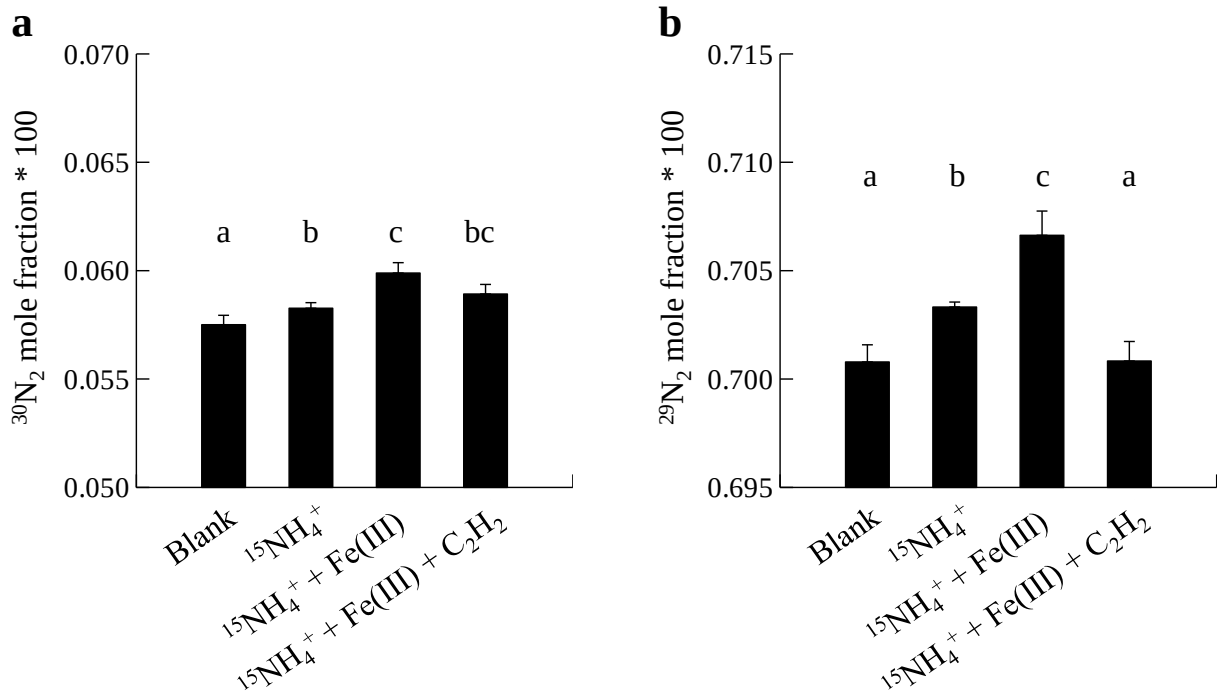

Appendix

Soil collection and pre-incubation

Surface soil (0-10 cm depth) was collected from a wet tropical forest in the Luquillo Mountains, Puerto Rico, USA with a mean annual temperature of 19.1° C and mean annual precipitation of 3500 mm (Brown et al. 1983, Weaver and Murphy 1990). The soil was shipped overnight to the University of California, Berkeley at ambient temperature in gas permeable bags. Large roots, leaves, worms, and rocks were removed by hand. The fresh soil was then slurried in a 3:1 ratio of mL of deionized water (DI) to grams of soil (dry equivalent). Slurry aliquots, 100 g each, were then divided into 240 mL jars covered with perforated plastic wrap to minimize evaporative losses. We also prepared blank jars containing 100 mL deionized water. The slurries and blank jars were pre-incubated in the dark in an anaerobic glove box for 6 days.

The entire experiment ($^{15}NH_4^+$, Fe(III), and C_2H_2 treatments) was performed in the anaerobic glove box (Coy Laboratory Products Inc., Grass Lake, MI) equipped with palladium catalyst packs to remove oxygen and a gas analyzer to monitor oxygen concentrations, which remained at 0 ppm throughout the experiment. The glove box headspace composition was approximately 90% N_2, 8% CO_2, and 2% H_2.

Experimental Design

We used three slurry treatments, $^{15}NH_4^+$ only, $^{15}NH_4^+$ plus Fe(III), and $^{15}NH_4^+$, Fe(III) plus C_2H_2, as well as a soil-free blank jar treatment (n = 8 per treatment). Background NH_4^+ concentration was 5.15 ± 0.13 μg N g^{-1} after the pre-incubation. Ammonium pools typically range from 1-15 μg N g^{-1} in this ecosystem (Pett-Ridge et al. 2006; Silver et al. 2001; Templer et al. 2008). We added 6 μgN-$^{15}NH_4Cl$ g^{-1} (in DI) to each slurry, increasing the ^{15}N enrichment of the NH_4^+ pool to approximately 54 atom %. We added sufficient Fe(III) to drive Feammox to NO_2^- using a stoichiometric molar ratio of 6:1 Fe(III) to $^{15}NH_4^+$. The Fe(III) was added as hydrous ferric oxide (HFO) synthesized from ferric chloride according to Lovley and Phillips (1986). The amount of $^{15}NH_4^+$ added was chosen as a balance between the ability to detect changes in $^{29}N_2$ and $^{30}N_2$ mole fractions and the potential stimulation of anaerobic NH_4^+ oxidation.

Sampling and Analysis

The $^{15}NH_4^+$ and Fe(III) solutions were de-gassed and placed in the glove box overnight before use. To begin the incubations, 1 mL of each treatment solution was stirred into the slurry. For the $^{15}NH_4^+$ only treatment of the first experiment, 1 mL de-gassed DI was added in lieu of the Fe(III) solution. The slurry jar was sealed with a custom-made aluminum lid and viton gasket with an 1/8" Swagelok o-seal fitting and septum for gas sampling. For the C_2H_2 treatment, 50 mL headspace gas was removed and replaced with 50 mL C_2H_2. The C_2H_2 was generated from calcium carbide and de-gassed DI inside of a pre-evacuated vial that had been flushed with helium three times. All jars were shaken vigorously to distribute the treatment solutions and dissolve the C_2H_2.

After 24 hours, each jar was shaken vigorously to equilibrate the N_2 between dissolved and gas phases. Duplicate 100 μL gas samples were taken with gas-tight syringes equipped with zero-volume stopcocks. A third gas sample (50 mL) was then taken with a polypropylene syringe and stored in a pre-evacuated 40 mL serum bottle sealed with a butyl rubber septum and an aluminum crimp.

After the final gas sampling, 50 g of de-gassed 4M KCl was weighed into each slurry. The KCl and slurry mixture was shaken in the glove box for one hour, and then removed for gravity filtration on the bench top. Soil extracts were frozen until colorimetric analysis for ammonium and nitrate analysis on a lachat autoanalyzer. The extracts were filtered to remove Fe that could interfere with colorimetric nitrate analysis (Colman 2009).

Gas samples were immediately analyzed for $^{15}N_2$ on a Europa 20-20 isotope ratio mass spectrometer by direct injection from the gas-tight syringes. The sample was injected upstream of a heated copper reduction tube, Carbosorb trap, and magnesium perchlorate trap to remove oxygen, carbon dioxide, and water vapor online. Room air was used as reference samples that were periodically analyzed throughout the day to account for instrument drift. The standard deviation of the references over the course of one day was 10^{-6} for $^{29}N_2$ mole fraction and 10^{-5} for the $^{30}N_2$ mole fraction. Stored gas samples from the first experiment were analyzed for N_2O concentration on a Shimadzu GC-14A equipped with an ECD.

Nitrogen Transformation Rate Calculations

We calculated $^{15}N\text{-}NH_4^+$ oxidation rates from the difference in jar headspace $^{29}N_2$ and $^{30}N_2$ mole fractions between samples and soil-free blanks (where $^{29}N_2$ mole fraction = moles of $^{29}N_2$ divided by moles of total N_2). We calculated the moles of headspace $^{29}N_2$ and $^{30}N_2$ by multiplying the $^{29}N_2$ and $^{30}N_2$ mole fractions by the moles of total headspace N_2. We determined the moles of total headspace N_2 in the jars by using the ideal gas law. The atmospheric pressure was assumed to be 1 atm, and the air temperature was maintained at 24° C throughout the experiments. The jar headspace volume was calculated from the empty jar volume (240 mL) and the weight of the slurry, which was consistently 75 % water (density, 1 g cm^{-3}) and 25 % dry soil equivalent (bulk density, 0.63 g cm^{-3} from Silver et al. 1994). The background air in the glove box was approximately 90 % N_2; sensitivity analyses show that a 5 % error in the assumed N_2 concentration translates into a 5 % error in the calculated NH_4^+ oxidation rates.

To determine $^{15}N\text{-}NH_4^+$ oxidation rates from $^{15}N_2$ production, we used the stoichiometry of the Feammox to N_2 pathway (equation 1), which states that 2 moles of NH_4^+ are required to produce one mole of N_2. We accounted for the fact that only one N atom in $^{29}N_2$ is ^{15}N-labeled whereas both N atoms in $^{30}N_2$ are ^{15}N-labeled. The NH_4^+ oxidation rates were expressed per gram of dry soil equivalent in each jar. Recognizing that the addition of $^{15}NH_4^+$ and Fe(III) stimulated anaerobic NH_4^+ oxidation, we conservatively report the oxidation of $^{15}NH_4^+$ as Feammox or anaerobic NH_4^+ oxidation rates rather than scaling the rates to the ^{15}N-enrichment of the NH_4^+ pools to obtain total rates including oxidation of both $^{14}NH_4^+$ and $^{15}NH_4^+$.

Statistical Analyses

We performed all statistical analyses using SYSTAT Version 10 (SPSS Inc., Evanston, IL). We log-transformed data as needed to meet the assumptions of analysis of variance (ANOVA). We performed student's t-tests to compare $^{29}N_2$ and $^{30}N_2$ mole fractions between treatments and blanks to determine if NH_4^+ oxidation occurred for a given treatment. We compared NH_4^+ oxidation rates among treatments using one-way ANOVA.

Free Energy Calculations

The conditions for the free energy calculations for Feammox are: $[NH_4^+] = 0.0002$ M; $[Fe(OH)_3] = 0.012$ mol L^{-1}; $[Fe^{2+}] = 10^{-12}$ M; and $[N_2] = 0.001$ M, $[NO_2^-] = 0.00001$ M, or $[NO_3^-$

] = 0.00001 M. The pH used in the calculations was 5, and the temperature used in the calculations was 24 °C.

Calculation of Global N_2 Flux from Feammox

We used the estimated global humid tropical forest cover in 1997, 1116 million ha (Achard et al. 2002). Assuming a bulk density of 0.63 g cm^{-3} (Silver et al. 1994), the mass of the top 10 cm of humid tropical forest soils is 703 Pg. Iron reduction rates in surface soils of humid tropical forests ranges 2.7 µg Fe(II) g^{-1} d^{-} under ambient oxygen conditions (Liptzin and Silver 2009) to 76 µg Fe(II) g^{-1} d^{-1} under anoxic conditions (Chacon et al. 2006). If 1% of the average Fe reduction rate, 39 µg Fe(II) g^{-1} d^{-1} , is associated with Feammox to N_2, then humid tropical forest surface soils could release 4.2 TgN y^{-1} as N_2 directly via Feammox.

Chapter 5. Regional assessment of soil nitrogen cycling in California ecosystems

Abstract

Microbial transformations of nitrogen (N) affect the potential for soil N to be taken up by plants or lost from terrestrial ecosystems via gaseous emissions and leaching. The controls on soil N cycling are often studied within ecosystems so that N cycling can be difficult to predict at larger scales relevant to regional or global biogeochemical models. We measured gross N cycling together with a suite of additional soil biogeochemical characteristics on 33 soils from five biome classifications in California including deserts, forests, grasslands, shrublands, and wetlands. Gravimetric soil moisture, soil N concentrations, soil organic carbon (SOC) concentrations, and pH varied significantly among ecosystem types ($p < 0.05$). Shrublands and grasslands exhibited the highest gross mineralization rates while forests exhibited the lowest gross nitrification rates. Microbial biomass N, SOC content, and soil ammonium (NH_4^+) concentrations together explained 80 % of the variability in gross mineralization rates. Gross nitrification rates were best predicted by the combination of soil NO_3^- concentrations and soil C:N ratios ($R^2 = 0.59$). A negative relationship between gross nitrification and soil C:N ratios was driven by forest soils with high C:N ratios (> 15). Dissimilatory nitrate (NO_3^-) reduction to NH_4^+ (DNRA) occurred in all soils. The positive relationship between DNRA rates and soil NO_3^- concentrations ($R^2 = 0.61$) implies that DNRA rates were limited by NO_3^-. Predictable patterns in gross soil N cycling rates across broad biomes classes suggest that there are universal controls on N cycling that be accounted for in large-scale biogeochemical models.

Introduction

Internal soil nitrogen (N) cycling regulates the loss and retention of N in ecosystems. Changes in soil N cycling in response to anthropogenic N deposition and global change can lead to changes in net primary productivity, soil nitrous oxide (N_2O) emissions, and nitrate (NO_3^-) leaching into groundwater (Vitousek et al. 1997; Galloway et al. 2003). Policymakers recognize the need for stronger regulation of N inputs and monitoring of N exports from ecosystems (UNEP and WHRC 2007). However, policy is made at the regional or national scales, while ecosystem studies are often conducted at the local scale. For example, differences in soil N cycling rates have been demonstrated in cross-site comparisons of single species forest plots (Zak et al. 1986; Lovett et al. 2004), different topographical positions within a landscape (Zak and Grigal 1991), grasslands versus forests (McKinley et al. 2008), and similar ecosystems that experience a range in background N deposition rates (Rao et al. 2009) or climate (Barrett and Burke 2000). Most policies, and the models that inform them, cannot take into account such subtleties.

California presents an exceptional challenge to understanding and modeling ecosystem processes at the regional scale because it includes many bioregions that host a high diversity of ecosystems (Hickman 1993; Lenihan et al. 2003). A meta-analysis of woodlands, grasslands, and agricultural land suggests that controls on N cycling are consistent across broad classes of ecosystems (Booth et al. 2005). However, relatively few studies have been conducted in the semi-arid ecosystems typical of California. These ecosystems experience a Mediterranean climate characterized by cool wet winters and hot dry summers. Furthermore, almost a third of the land area in California is desert (Lenihan et al. 2003). Deserts are often not included in cross-

ecosystem comparisons because it is assumed that limited water availability decreases the importance of these ecosystems in regional biogeochemical assessments.

Here we present a survey of soil properties and gross N cycling rates in ecosystems from a wide geographical range in California. We classified the ecosystems into five broad biome groups: deserts, forests, grasslands, shrublands, and wetlands. Our goals were to determine (1) if there are consistent and predictable patterns in basic soil properties and gross N cycling rates across biomes, and (2) to determine if gross N cycling rates can be predicted based on soil properties across biomes. Soil N pools and net N cycling rates are commonly reported indices of ecosystem N cycling, but they may not elucidate gross N cycling rates that represent a more comprehensive view of N transformations (Davidson et al. 1992). We performed short-term gross N cycling assays in the laboratory to measure rates of soil N mineralization, nitrification, and dissimilatory nitrate (NO_3^-) reduction to ammonium (NH_4^+) (DNRA) among the diverse California ecosystems. While short-term laboratory assays may not reflect field rates of gross N cycling over long times scales (i.e., months to years), especially because of seasonality in field conditions, they provide a comparable index among soils from different ecosystems while maintaining soil moisture and substrate availability similar to native conditions.

Methods

Study Sites

Our study utilized 33 existing research sites at 27 study areas located within 8 out of 10 bioregions in California (Hickman 1993) (Figure 1). We grouped the sites into the following major biomes that represent approximately 97 % of the land cover in California: desert, forest, grassland, and shrubland (Lenihan et al. 2003) (Table 1). Alpine and subalpine forests, which were not included in our study, represent the remaining 3 % of California. We also included a salt marsh and a spring-fed wetland to characterize wetlands and broaden the spectrum of ecosystems sampled. Soils were collected from 27 sites in January 2007 (wet season), and from 6 high elevation sites in the Sierra Nevada in May 2007 after snowmelt. Much of California experiences a Mediterranean climate with dry summers and wet winters, so we timed the soil sampling to avoid the pulses of high microbial activity that occur with the first precipitation events of the wet season (Chou et al. 2008; Xiang et al. 2008).

These sites span a range of background N deposition rates (0.6 to 18.4 kg N ha^{-1} y^{-1}) and include three sites that received experimental fertilizer additions (Table 1). Background total (wet plus dry) atmospheric N deposition rates for the sites were obtained from the 4-km grid resolution Community Multiscale Air Quality model for California in 2002 (Tonnesen et al. 2007). The grassland soil from the University of California-Irvine Arboretum received a total of 76.4 kg N ha^{-1} as NPK (29:3:4) fertilizer in 2006 (Bijoor et al. 2009). The desert soil from Pinto Basin, Joshua Tree National Park received 60 kg N ha^{-1} y^{-1} as NH_4NO_3 during the period 2002-2009 (Allen et al. 2009), and the shrubland soil from Lake Skinner has received 60 kg N ha^{-1} y^{-1} as NH_4NO_3 since 1994 (Sirulnik et al. 2007).

Gross N Cycling Assays

Soil cores were collected from the top 10 cm of mineral soil and stored in gas permeable bags at ambient temperature for no more than one week. One day before the gross N cycling assays were performed each soil core was gently broken up by hand to remove large rocks and roots while maintaining soil aggregation. A 10 g subsample was used for determination of gravimetric soil moisture. A 5 g subsample was extracted in 2 M KCl for colorimetric

determination of ammonium (NH_4^+) and NO_3^- concentrations (Lachat Quik Chem flow injection analyzer, Lachat Instruments, Milwaukee, WI) so that an appropriate amount of ^{15}N label could be added for gross N cycling assays. Subsamples (90 g) were split into separate gas permeable bags for $^{15}NH_4^+$ and $^{15}NO_3^-$ addition to determine gross mineralization and nitrification rates, respectively; a 30 g subsample was split for the determination of initial (t_0) NH_4^+ and NO_3^- concentrations for the gross N cycling assays. The remaining soil was air-dried for determination of pH as well as total soil N and soil organic carbon (SOC) concentration (detailed below)

To accommodate the range in soil NH_4^+ and NO_3^- concentrations among sites, the soils were divided into 4 to 7 groups so that the initial ^{15}N enrichment would be approximately 10 to 20 atom % based on the preliminary measurements of soil NH_4^+ and NO_3^- concentrations. One mL of the appropriate ^{15}N label solution was added to each 90 g bag of soil, and then the soil was gently homogenized by hand to distribute the label. The soil was incubated in a sealed Mason jar with an ambient air headspace for three hours. The incubated soil was split for 2 M KCl extraction, 0.5 M K_2SO_4 extraction, and fumigation in chloroform for 5 days before extraction in 0.5 M K_2SO_4. The initial ^{15}N enrichment was not measured directly, but was calculated based on the ^{15}N label added and the initial NH_4^+ and NO_3^- pools (Silver et al. 2005). We assumed that the background ^{15}N enrichment of the NH_4^+ and NO_3^- pools were at natural abundance, 0.3663 atom %.

The ^{15}N enrichment of NH_4^+ and NO_3^- were determined using the diffusion technique (Herman et al. 1995) and analysis on an isotope ratio mass spectrometer (PDZ Europa, Limited, Crewe, UK). Gross mineralization and nitrification rates were calculated according to Kirkham and Bartholomew (1954), and DNRA rates were calculated according to Silver et al. (2005).

Microbial Biomass N

Alkaline potassium persulfate digestion followed by colorimetric determination of NO_3^- was used to determine total N in the K_2SO_4 extracts (Cabrera and Beare 1993). Microbial biomass N (MBN) was calculated from the difference in total N between fumigated and unfumigated soils, assuming an extraction efficiency of 0.54 (Brookes et al. 1985).

Chemical Analyses

The air-dried soil samples were passed through a 2 mm sieve and then ground by hand using a mortar and pestle. Roots and large pieces of organic matter were picked out by hand. We tested for the presence of carbonates by adding a drop of 1 M HCl to a subsample of each soil to check for effervescence. Inorganic C was removed from 2 g ground air-dried soil by twice-washing with 30 mL 0.1 N HCl (allowing the soil slurry to stand for 1 hour each time), twice-washing with 30 mL DI, and then freeze-drying (unpublished protocol from T. Baisden). After each washing, the soil slurry was centrifuged, and the supernatant was removed via aspiration. The ground soils were analyzed on a CE Elantec elemental analyzer (Lakewood, New Jersey) for concentrations of soil organic C (SOC) and total N, and the C:N ratio. Soil pH was measured in soil slurries with a 2:1 ratio of DI water to air-dried soil.

Data Analyses

Statistical analyses were performed using SYSTAT Version 10 (SPSS Inc., Evanston, IL). All data, except soil C:N ratios, were $\log_{10}$-transformed to achieve normal distributions. We compared soil properties and gross N cycling rates among biomes using ANOVAs and Tukey multiple comparison tests. We also tested for biome differences in gross N cycling rates using

ANCOVAs with soil properties as covariates. We replicated at the biome level using sites from each biome as the replicates for that biome. Because the sample size for wetlands (n = 2) was unbalanced with those for the other biomes (n = 7-9), we did not include wetlands in the comparisons among biomes. We used linear regressions to explore relationships among soil properties and gross N cycling rates across all biomes. SYSTAT identified outliers using the Hadi robust outlier detection. We excluded data points that were consistently identified as statistical outliers (i.e., in most or all analyses involving a given a response variable), although they may not be ecological outliers. Statistical significance was determined at p-values < 0.05.

Results

Patterns in Soil Properties Across Biomes

Most soil properties varied significantly and predictably across biomes (Table 2). pH ranged from 5.1 to 9.9 while gravimetric soil moisture ranged from 0.2 to 50.5 %. Microbial biomass N also spanned a wide range, from 1.0 to 247.0 μg N g^{-1}. Total soil N concentrations ranged from 0.01 to 0.52 %, SOC concentrations ranged from 0.08 to 11.75 %, and soil C:N ratios ranged from 6.6 to 37.6. Desert soils exhibited higher pH ($p < 0.001$) and lower total soil N concentrations ($p < 0.001$, Figure 2a), SOC concentration ($p < 0.001$, Figure 2b), MBN ($p < 0.001$), and gravimetric soil moisture ($p < 0.001$) compared to soils from all other biomes. Forest soils had the highest C:N ratios ($p < 0.001$) and SOC concentrations ($p < 0.001$), but they also had the lowest soil NO_3^- concentrations ($p < 0.001$, Figure 2c). Oak woodlands with a grass understory are a common ecosystem type found in California. The oak woodland soils followed the same patterns as the grassland soils for this suite of soil properties (data not shown), so we classified them as grasslands.

Total soil N concentration was strongly correlated to many soil variables. The strongest relationship was with SOC concentration (Figure 3a), which explained 88 % of the variability in soil N concentration. The strong correlation between total soil N and SOC concentrations resulted in similar relationships for both C and N with additional soil properties. Total soil N concentration showed a negative correlation with soil moisture ($R^2 = 0.59$) for desert soils whereas it showed a positive correlation for all other biomes together ($R^2 = 0.41$, Figure 3b). Total soil N concentration was also correlated to pH across all biomes ($R^2 = 0.32$, Figure 3c). This relationship may reflect multicollinearity because pH was negatively correlated with soil moisture ($R^2 = 0.30$). Microbial biomass N exhibited a strong positive relationship with total N concentration ($R^2 = 0.65$, Figure 3d). Forward stepwise multiple linear regressions showed that SOC concentration and soil moisture together were positively correlated with total N concentration, explaining 90 % of the variability in total N concentration (Table 3).

When all biomes were considered together, pH explained 23% of the variability in MBN ($\log(y) = [-3.80 * \log(x)] + 4.59$, $n = 33$, $p < 0.001$). In desert soils, MBN was negatively correlated to soil moisture ($\log(y) = [-0.90 * \log(x)] + 0.80$, $n = 7$, $R^2 = 0.68$, $p = 0.02$) whereas across all other biomes, it was positively correlated to soil moisture ($\log(y) = [0.48 * \log(x)] + 1.20$, $n = 26$, $R^2 = 0.37$, $p = 0.001$).

Soil NH_4^+ concentrations were best predicted by the combination of gross nitrification rates and DNRA rates ($R^2 = 0.80$, Table 3). The same predictors explained 70 % of the variability in soil NO_3^- concentrations (Table 3). For both of these analyses, we excluded a grassland soil that was consistently identified as an outlier in analyses involving gross nitrification rates (discussed later).

Patterns in Gross N Cycling Rates

There were statistically significant differences in gross N transformations among biomes despite high variability within biomes (Figure 2d). When soil from a botanical garden was excluded, gross mineralization rates were higher in grasslands and shrublands compared to deserts and forests ($p = 0.02$, $n = 26$). The botanical garden soil was not fertilized, but it may be an outlier because it was irrigated. Forest soils exhibited lower gross nitrification rates than soils from other biomes ($p = 0.02$, $n = 22$). Rates of DNRA did not differ significantly among biomes.

Across biomes, gross mineralization rates ranged from 2.36 to 81.4 μg N g^{-1} d^{-1}, with the highest rate from a spring-fed wetland soil and the lowest rate from the botanical garden soil. Gross mineralization rates were correlated to many soil variables. Microbial biomass N explained 27 % of the variability in gross mineralization rates; this relationship was improved to $R^2 = 0.48$ by excluding two outliers, the botanical garden soil as well as soil from a giant Sequoia forest (Figure 4a). Gravimetric soil moisture also exhibited a positive relationship with gross mineralization rates ($R^2 = 0.25$, $p = 0.005$) that was improved to $R^2 = 0.43$ ($p < 0.001$) by excluding the same two outliers (Figure 4b). The exclusion of the outliers did not significantly change the regression equations in either case. However, soil NH_4^+ concentrations ($R^2 = 0.42$, $p < 0.001$) and soil N concentration ($R^2 = 0.23$, $p = 0.01$) were positively correlated to gross mineralization rates only when three outliers, the aforementioned two soils as well as a desert soil from Wide Canyon in Joshua Tree National Park, were excluded (Figures 4c-d). Microbial biomass N, SOC concentration, and soil NH_4^+ concentrations together explained 80 % of the variability in gross mineralization rates when the three outliers were excluded (Table 3). The three consistent outlier sites exhibited the lowest gross mineralization rates (< 6 μg N g^{-1} d^{-1}), suggesting unknown factors that may be limiting mineralization at these sites.

Gross nitrification rates were greatest in a chaparral shrubland soil from the Irvine Ranch Land Reserve (71.1 μg N g^{-1} d^{-1}) and lowest in a mixed conifer forest soil from the Blodgett Forest Research Station (0.26 μg N g^{-1} d^{-1}). Gross nitrification rates were positively correlated to soil NO_3^- concentrations ($R^2 = 0.34$, $p = 0.003$). The relationship was strengthened ($R^2 = 0.48$, $p < 0.001$) when one outlier, an annual grassland soil from the Irvine Ranch Land Reserve, was excluded (Figure 5a). This soil exhibited a low gross nitrification rate (0.46 μg N g^{-1} d^{-1}) as well as high pH (7.0) compared to soils from other sites, but there were no other indications that this soil would be an outlier. However, it was consistently identified as a statistical outlier in all regression analyses predicting gross nitrification rates and thus was excluded. Soil C:N ratios ($R^2 = 0.48$, $p < 0.001$) exhibited negative relationships with gross nitrification rates (Figure 5b). Gross nitrification rates were best predicted by the combination of soil NO_3^- concentration and soil C:N ratios ($R^2 = 0.59$, Table 3).

Dissimilatory NO_3^- reduction to NH_4^+ occurred in all soils. When considering soils with detectable NO_3^- concentrations, NO_3^- concentrations alone explained 61 % of the variability in DNRA rates (Figure 6a). Soil NH_4^+ concentrations were also positively correlated to DNRA rates ($R^2 = 0.75$, Figure 6b). Soil NH_4^+ concentrations and gross nitrification rates together explained 83 % of the variability in DNRA rates (Table 3). The Durbin-Watson statistic for this relationship was 1.603, suggesting that the variables were not auto-correlated.

Background atmospheric wet and dry N deposition ranged from 0.6 to 18.4 kg N ha^{-1} y^{-1} but did not differ significantly among biomes. Only 4 sites located in the urban areas of Irvine and Riverside, California received greater than 10 kg N ha^{-1} y^{-1}. Atmospheric N deposition rates were not correlated with any soil properties or gross N cycling rates across all sites. Soils from sites that received experimental fertilization did not appear as outliers in any of the analyses.

Discussion

Biome Level Differences in Soil Properties

Clear biome level differences in soil properties emerged from our analysis of California soils. Compared to soils from the other ecosystem types, desert soils had lower soil moisture, SOC concentration, soil N concentration, and MBN as well as the highest pH. We collected soils from the locations typically sampled by the investigators at each research site, and thus our study included desert and shrubland soils from both interspaces and beneath plants. Plants act as "islands of fertility" in deserts so that soil N content, inorganic N concentrations, and N cycling rates are often elevated beneath plants relative to interspaces (Schlesinger and Pilmanis 1998; Billings et al. 2004; Schade and Hobbie 2005). However, differences among biomes were large and generally exceeded variability within biomes so that sampling location was not a factor.

Relationships among Soil Properties

The strong positive correlations between total soil N concentration and SOC concentration as well as between total soil N concentration and MBN were consistent with those reported in the literature for grasslands and forests (Wardle 1992; Cleveland and Liptzin 2007). While these relationships were expected, they have rarely been experimentally demonstrated in one study.

Desert soils exhibited a negative relationship between total soil N concentration and soil moisture whereas soils from all other ecosystems together exhibited a positive relationship between the two variables. A positive relationship between total soil N concentration and precipitation has long been recognized (Jenny and Leonard 1934). Net primary productivity increases with mean annual precipitation (MAP), which leads to increased litter inputs to the soil and can result in higher total soil N concentrations (Post et al. 1985). A negative relationship between soil N concentration and MAP was observed in the transition from the arid to extreme hyperarid soils of the Atacama desert (Ewing et al. 2007). This was attributed to the accumulation of NO_3^- from atmospheric deposition due to minimal biological activity. In the arid desert soils we sampled, minimal plant uptake of N as well as low leaching losses at very low soil moisture (< 1 g H_2O g^{-1}) may have caused N accumulation in the soil.

We also observed a negative relationship between MBN and soil moisture in desert soils that departed from the positive relationship observed across all other ecosystems. This may reflect the strong relationship of MBN with total soil N concentration, which showed the same pattern with soil moisture. However, a negative correlation between MBN and soil moisture has been previously been reported and could be due to the growth of drought tolerant microbes (Wardle 1992).

Biome Level Differences in Gross N Cycling Rates

We found remarkably predictable patterns in gross N cycling rates among biomes despite high variability within biomes. The gross N cycling rates we reported are for short term laboratory assays, and thus reflect rates that may not be sustainable over longer time periods. Moreover, soils from each site were collected only once, during the wet season. Ecosystems that experience Mediterranean climates exhibit dramatic temporal dynamics in microbial activity due to seasonal changes in water availability as well as temperature (Austin et al. 2004). Regardless, these data indicate that distinct patterns exist in instantaneous N pools and fluxes at the scale of biomes in California.

Soil C:N ratios may largely drive the biome level differences in gross mineralization and nitrification rates that we observed. Gross mineralization rates were highest in grasslands and shrublands, which had lower soil C:N ratios than forests. Higher quality of litter inputs (e.g., lower C:N and less woody, lignaceous material) incorporated into grassland and shrubland soils may drive the higher gross mineralization rates. Despite similar soil C:N ratios, deserts likely exhibited lower gross mineralization rates than grasslands and shrublands due to significantly lower microbial biomass. The high soil C:N ratios in forests likely explain the lower gross nitrification rates measured in that biome. Heterotrophs can outcompete autotrophic nitrifiers for NH_4^+ at high soil C:N ratios (Riha et al. 1985; Verhagen et al. 1995). Thus, at high soil C:N ratios, NH_4^+ assimilation may limit nitrification.

Surprisingly, desert soils, with an average soil moisture of 1.9 ± 0.8 %, exhibited similar short-term gross N cycling rates to the other biomes. A concern with performing gross N cycling assays on dry soils is that the ^{15}N label is typically delivered in deionized water so that gross N cycling rates can be stimulated (Willison et al. 1998). This methodological artifact is more of a concern when using intact soil cores because a large volume of ^{15}N label solution is required to distribute the ^{15}N label throughout the soil (Sparling et al. 1995). We mixed 1 mL ^{15}N label solution into 90 g field moist soil by hand; thus, we increased soil moisture by less than 1 g H_2O g^{-1} soil while evenly distributing the ^{15}N label. All of the desert soils as well as three shrubland soils and one grassland soil had soil moisture less than 6 %, and these soils generally did not appear as outliers in any of the analyses. Only one of the soils, from a grassland in a botanical garden, was an outlier for regression analyses predicting gross mineralization rates. This suggests that the addition of ^{15}N label in a small volume of water relative to the mass of soil assayed may not stimulate microbial N cycling. Thus, our data show that short-term gross N cycling rates in deserts can be comparable to those in other biomes despite much lower soil moisture content. It is possible that N cycling in desert soils is sustained by the activity of fungi, which are more drought tolerant than bacteria (Wilson and Griffith 1975; Adebayo and Harris 1971) and can be more abundant than bacteria in desert soils (Clark et al. 2009).

Our study documents the occurrence of DNRA in unsaturated soils from a range of ecosystems. It is possible that re-mineralization of $^{15}NO_3$ assimilated by microbes could account for the movement of $^{15}NO_3^-$ into the NH_4^+ pool. However, we think this is highly unlikely given the short time period of the incubation and the general preference for NH_4^+ uptake over NO_3^- (Vitousek and Matson 1988).The DNRA assays were performed under ambient oxygen (O_2) conditions and at field soil moisture. We did not expect to detect DNRA in all of the soils because DNRA is generally thought to require anaerobic conditions. Silver et al. (2001) observed the occurrence of DNRA in humid tropical forest soils incubated under ambient O_2 conditions, and rates were comparable to those reported here. It is thought that, in unsaturated soils, DNRA occurs in anaerobic micro-sites within soil aggregates (Sexstone et al. 1985) or in micro-sites of high biological O_2 consumption (Parkin 1987). However, we measured the occurrence of DNRA in dry desert soils that likely did not contain many anaerobic microsites. Aerobes as well as facultative anaerobes have been demonstrated to perform DNRA in pure cultures (Tiedje 1988), but DNRA via aerobic metabolism has not been demonstrated in soil. Pett-Ridge et al. (2006) found that DNRA rates were highest in tropical forest soils incubated under oxic conditions compared to anoxic conditions. Our data provide additional evidence that DNRA can occur in unsaturated soils and may be performed by aerobes. The widespread occurrence of DNRA in unsaturated soils suggests that DNRA may play a more important role in terrestrial N cycling than previously thought.

Controls on Gross N Cycling Rates

Gross mineralization rates were most strongly correlated with MBN. This relationship has been previously documented (Zak and Grigal 1991; Booth et al. 2005) and simply reflects the limitation of gross mineralization by microbial biomass. When MBN was taken into account, SOC concentration exhibited a negative relationship with gross mineralization rates. Booth et al. (2005) hypothesized that the negative relationship between gross mineralization rates and soil C:N ratios observed in that study could be explained by lower yields of N per C mineralized at high soil C:N ratios and/or high concentrations of recalcitrant compounds in soils with high C:N ratios or SOC concentrations. We found a negative relationship of gross mineralization with SOC concentration but not C:N ratios, providing support for their latter hypothesis.

Net nitrification rates are more commonly measured than gross nitrification rates, and a negative relationship with soil C:N ratios has been widely reported for forests (e.g. Venterea et al. 2003; Lovett et al. 2004). Soil C:N ratios could exert a negative control on NH_4^+ supply to nitrifiers or a positive control on NO_3^- consumption to limit net nitrification rates. We observed a negative relationship between gross nitrification rates and soil C:N ratios that has previously been reported in cross-site comparisons of forests (Christenson et al. 2009; Bengtsson et al. 2003). The relationship in our data set was driven by the forest soils. However, this may be due to the paucity of soils from other ecosystem types with C:N ratios greater than 20. The similar negative correlation of soil C:N ratios with net and gross nitrification rates suggests that decreased availability of NH_4^+ for nitrifiers at high C:N ratios is more likely limiting nitrification.

Dissimilatory NO_3^- reduction to NH_4^+ may play an important role in N retention where NO_3^- availability is high. In a humid tropical forest soil the supply of NO_3^- likely limited DNRA rates (Silver et al. 2001). We observed a strong positive relationship between DNRA and soil NO_3^- concentrations, suggesting that DNRA is limited by NO_3^- availability in this study as well. Impressively, 80 % of the variability in soil NH_4^+ concentrations was explained by gross nitrification and DNRA rates together. Gross nitrification, which consumes NH_4^+, exerted a negative control on soil NH_4^+ concentrations whereas DNRA, which produces NH_4^+, exerted a positive control. This implies that the balance between gross nitrification and DNRA rates can strongly influence soil NH_4^+ concentrations. Despite the potential importance of DNRA in terrestrial N cycling, little is known about the mechanisms regulating DNRA as well as the organisms that perform it (Tiedje 1988).

Conclusions

This study has implications for environmental policy at the regional level in California. Despite differences in vegetation type, atmospheric N deposition rates, and local climate among other factors, ecosystems across the diverse bioregions in California group into broad biomes that exhibit predictable patterns in soil properties and N cycling. This can simplify policy prescriptions for a large region with complex landscapes. The consistent relationships between soil properties and N cycling rates across all biomes that we report can help improve biogeochemical models that operate on a regional scale. Moreover, they add to the growing body of evidence that suggests that the fundamental controls on biogeochemical cycling are broadly applicable across bioclimatic, soil, and vegetation classifications (Fierer et al. 2006; Parton et al. 2007; Cleveland and Liptzin 2007; Manzoni et al. 2008; Fierer et al. 2009; Jones et al. 2009). Regional to global scale experimental studies can increase our confidence in understanding terrestrial N cycling at the scale relevant to policymakers.

References

Adebayo AA, Harris RF (1971) Fungal growth responses to osmotic as compared to matric water potential. Soil Society of America Proceedings 35:465-469

Austin AT et al. (2004) Water pulses and biogeochemical cycles in arid and semiarid ecosystems. Oecologia 141:221-235

Barrett JE, Burke IC (2000) Potential nitrogen immobilization in grassland soils across a soil organic matter gradient. Soil Biology & Biochemistry 32:1707-1716

Bengtsson G, Bengtson P, Mansson KF (2003) Gross nitrogen mineralization, immobilization, and nitrification rates as a function of soil C/N ratio and microbial activity. Soil Biology & Biochemistry 35:143-154

Bijoor NS, Czimczik CI, Pataki DE, Billings SA (2008) Effects of temperature and fertilization on nitrogen cycling and community composition of an urban lawn. Global Change Biology 14:2119-2131

Billings SA, Schaeffer SM, Evans RD (2004) Soil microbial activity and N availability with elevated CO_2 in Mojave desert soils. Global Biogeochemical Cycles 18:GB1011, doi:10.1029/2003GB002137

Booth MS, Stark JM, Rastetter E (2005) Controls on nitrogen cycling in terrestrial ecosystems: A synthetic analysis of literature data. Ecological Monographs 75:139-157

Brookes PC, Landman A, Pruden G, Jenkinson DS (1985) Chloroform fumigation and the release of soil nitrogen: A rapid direct extraction method to measure microbial biomass nitrogen in soil. Soil Biology & Biochemistry 17:837-842

Cabrera ML, Beare MH (1993) Alkaline persulfate oxidation for determining total nitrogen in microbial biomass extracts. Soil Science Society of America Journal 57:1007-1012

Chou WW, Silver WL, Jackson RD, Thompson AW, Allen-Diaz B (2008) The sensitivity of annual grassland carbon cycling to the quantity and timing of rainfall. Global Change Biology 14:1382-1394

Christenson LM, Lovett GM, Weathers KC, Arthur MA (2009) The influence of tree species, nitrogen fertilization, and soil C to N ratio on gross soil nitrogen transformations. Soil Science Society of America Journal 73:638-646

Clark JS, Campbell JH, Grizzle H, Acosta-Martinez V, and Zak JC (2009) Soil microbial community response to drought and precipitation variability in the Chihuahuan Desert. Microbial Ecology 57:248-260

Cleveland CC, Liptzin D (2007) C:N:P stoichiometry in soil: Is there a "Redfield ratio" for the microbial biomass? Biogeochemistry 85:235-252

Davidson EA, Hart SC, Firestone MK (1992) Internal cycling of nitrate in soils of a mature coniferous forest. Ecology 73:1148-1156

Ewing SA et al. (2007) Rainfall limit of the N cycle on Earth. Global Biogeochemical Cycles 21:GB2009, doi:10.1029/2006GB002838

Fierer N, Jackson RB (2006) The diversity and biogeography of soil bacterial communities. Proceedings of the National Academy of Sciences of the United States of America 103:626-631

Fierer N, Strickland MS, Liptzin D, Bradford MA, Cleveland CC (2009) Global patterns in belowground communities. Ecology Letters 12:1238-1249

Galloway JN et al. (2003) The nitrogen cascade. Bioscience 53:341-356

Herman D, Brooks P, Ashraf M, Azam F, Mulvaney R (1995) Evaluation of methods for nitrogen-15 analysis of inorganic nitrogen in soil extracts. II Diffusion methods. Communications in Soil Science and Plant Analysis 26:1675-1685
Hickman J (1993) The Jepson manual: higher plants of California. University of California Press, Berkeley, CA
Jenny H, Leonard CD (1934) Functional relationships between soil properties and rainfall. Soil Science 38:363-381
Jones DL et al. (2009) Soil organic nitrogen mineralization across a global latitudinal gradient. Global Biogeochemical Cycles 23:GB1016, doi:10.1029/2008GB003250
Kirkham D, Bartholomew W (1954) Equations for following nutrient transformations in soil, utilizing tracer data. Soil Science Society of America Journal 18:33-34
Lenihan JM, Drapek R, Bachelet D, Neilson RP (2003) Climate change effects on vegetation distribution, carbon, and fire in California. Ecological Applications 13:1667-1681
Lovett GM, Weathers KC, Arthur MA, Schultz JC (2004) Nitrogen cycling in a northern hardwood forest: Do species matter? Biogeochemistry 67:289-308
Manzoni S, Jackson RB, Trofymow JA, Porporato A (2008) The global stoichiometry of litter nitrogen mineralization. Science 321:684-686
McKinley DC, Rice CW, Blair JM (2008) Conversion of grassland to coniferous woodland has limited effects on soil nitrogen cycle processes. Soil Biology & Biochemistry 40:2627-2633
Parkin TB (1987) Soil microsites as a source of denitrification variability. Soil Science Society of America Journal 51:1194-1199.
Parton W et al. (2007) Global-scale similarities in nitrogen release patterns during long-term decomposition. Science 315:361-364
Pett-Ridge J, Silver WL, Firestone MK (2006) Redox fluctuations frame microbial community impacts on N-cycling rates in a humid tropical forest soil. Biogeochemistry 81:95-110
Post WM, Pastor J, Zinke PJ, Stangenberger AG (1985) Global patterns of soil nitrogen storage. Nature 317:613-616
Rao LE, Parker DR, Bytnerowicz A, Allen EB (2009) Nitrogen mineralization across an atmospheric nitrogen deposition gradient in Southern California deserts. Journal of Arid Environments 73:920-930
Riha SJ, Campbell GS, and Wolfe J (1986) A model of competition for ammonium among heterotrophs, nitrifiers, and roots. Soil Science Society of America Journal 50:1463-1466.
Schade JD, Hobbie SE (2005) Spatial and temporal variation in islands of fertility in the Sonoran Desert. Biogeochemistry 73:541-553
Schlesinger WH, Pilmanis AM (1998) Plant-soil interactions in deserts. Biogeochemistry 42:169-187
Sexstone AJ, Revsbech NP, Parkin TB, Tiedje JM (1985) Direct measurement of oxygen profiles anddenitrification rates in soil aggregates. Soil Science Society of America Journal 49:645-651
Silver WL, Herman DJ, Firestone MK (2001) Dissimilatory nitrate reduction to ammonium in upland tropical forest soils. Ecology 82:2410-2416
Silver WL, Thompson AW, Reich A, Ewel JJ, Firestone MK (2005) Nitrogen cycling in tropical plantation forests: Potential controls on nitrogen retention. Ecological Applications 15:1604-1614

Sirulnik AG, Allen EB, Meixner T, Allen MF (2007) Impacts of anthropogenic N additions on nitrogen mineralization from plant litter in exotic annual grasslands. Soil Biology & Biochemistry 39:24-32

Sparling GP, Murphy DV, Thompson RB, Fillery IRP (1995) Short-term net N mineralization from plant residues and gross and net N mineralization from soil organic-matter after rewetting of a seasonally dry soil. Australian Journal of Soil Research 33:961-973

Tiedje JM (1988) Ecology of denitrification and dissimilatory nitrate reduction to ammonium. In: Zehdner AJB (eds) Biology of Anaerobic Microorganisms. John Wiley and Sons, New York, NY, Pages 179-244

Tonnesen G, Wang Z, M O, Chien C (2007) Assessment of nitrogen deposition: Modeling and habitat assessment. In. California Energy Commission PIER Energy-Related Environmental Research CEC-500-2005-032

UNEP and WHRC. 2007. Reactive Nitrogen in the Environment: Too Much or Too Little of a Good Thing. United Nations Environment Programme, Paris, France.

Venterea RT, Lovett GM, Groffman PM, Schwarz PA (2003) Landscape patterns of net nitrification in a northern hardwood-conifer forest. Soil Science Society of America Journal 67:527-539

Verhagen FJM, Laanbroek HJ, Woldendorp JW (1995) Competition for ammonium between plant roots and nitrifying and heterotrophic bacteria and the effects of protozoan grazing. Plant and Soil 170:241-250

Vitousek PM and Matson PA (1988) Nitrogen transformations in a range of tropical forest soils. Soil Biology and Biochemistry 20:361-367

Vitousek PM et al. (1997) Human alteration of the global nitrogen cycle: Sources and consequences. Ecological Applications 7:737-750

Wardle DA (1992) A comparative assessment of factors which influence microbial biomass carbon and nitrogen levels in soil. Biological Reviews of the Cambridge Philosophical Society 67:321-358

Willison TW, Baker JC, Murphy DV, and Goulding KWT (1988) Comparison of a wet and dry ^{15}N isotopic dilution technique as a short-term nitrification assay. Soil Biology and Biochemistry 30:661-663

Wilson JM and Griffin DM (1975) Water potential and the respiration of microorganisms in the soil. Soil Biology and Biochemistry 7:199-204

Xiang SR, Doyle A, Holden PA, and Schimel JP (2008) Drying and rewetting effects on C and N mineralization and microbial activity in surface and subsurface California grassland soils. Soil Biology and Biochemistry 40:2281-2289

Zak DR, Pregitzer KS, Host GE (1986) Landscape variation in nitrogen mineralization and nitrification. Canadian Journal of Forest Research 16:1258-1263

Zak DR and Girgal DF (1991) Nitrogen mineralization, nitrification and denitrification in upland and wetland ecosystems. Oecologia 88:189-196

Tables

Table S1. Study site locations and characteristics.

Site	Biome	Ecosystem	Study Site	Location (latitude-longitude)	Background atmospheric wet + dry N deposition (kg N ha^{-1} y^{-1})
1	Desert	Cold desert*	Mono Basin Ecosystem Research Site	38.083333 N -118.933330 W	0.6
2		Creosote bush scrub	Wide Canyon, Joshua Tree National Park, control plot	33.831353 N -115.757072 W	2.4
3		Cold desert*	Mammoth Mountain	37.636944 N -188.978890 W	2.5
4		Pinyon-juniper woodland	Burn Reserve, Mojave Desert	34.137472 N -116.436582 W	3.9
5		Creosote bush scrub	Deep Canyon Desert Research Center, Sonoran Desert	33.610649 N -116.452827 W	5.8
6		Creosote bush scrub	Pinto Basin, Joshua Tree National Park, control plot	33.942964 N -116.394257 W	7.8
7		Creosote bush scrub	Pinto Basin, Joshua Tree National Park, fertilized plot	33.942964 N -116.394257 W	7.8
8	Forest	Mixed conifer	Sequoia National Park	36.596184 N -118.734956 W	3.3
9		Mixed conifer	El Dorado National Forest	38.966667 N -120.316667 W	4.6
10		Giant Sequoia	Whitaker Forest	36.702989 N -118.933010 W	5.3
11		Mixed conifer dominated by ponderosa pine	Blodgett Forest Research Station	38.900000 N -120.630000 W	5.9
12		Redwood-Douglas fir	Casper Creek Experimental Watershed, Jackson Demonstration State Forest	37.407897 N -122.004146 W	7.3
13		Yellow pine forest	James Reserve, San Bernadino Mountains	33.808056 N -116.771667 W	8.7
14		Mixed conifer and hardwood	James Reserve, San Bernadino Mountains	33.808056 N -116.771667 W	8.7
15	Grassland	Oak woodland	Hopland Research and Extension Center	39.000000 N -123.533899 W	2.8
16		Oak woodland (sparse canopy)	Sierra Foothills Research and Extension Center	39.250000 N -121.283330 W	6.7
17		Oak woodland (dense canopy) **	Sierra Foothills Research and Extension Center	39.250000 N -121.283330 W	6.7

18		Oak woodland	San Joaquin Experimental Range, California State University-Fresno	37.095833 N -199.729167 W	7.3
19		Annual grassland	Modesto	37.659790 N -120.459020 W	7.5
20		Oak woodland	Tonzi Ranch	38.440000 N -120.950440 W	8.2
21		Oak woodland	Vyra Ranch	38.440000 N -120.950440 W	8.2
22		Urban turfgrass	University of California-Irvine Arboretum, low fertilization plot	33.669464 N -117.823110 W	12. 7
23		*Bromus* dominated garden	University of California-Riverside Botanic Gardens	33.967560 N -117.316630 W	13.4
24		Annual grassland	Irvine Ranch Land Reserve	33.736580 N -117.694580 W	18.4
25	Shrubland	Coastal steppe-mixed * Forest	Mattole Beach	40.270000 N -124.350000 W	1.5
26		Chaparral shrubland*	Montana de Oro State Park	35.290000 N -120.880000 W	3.7
27		Chaparral shrubland	Burn Pinon Ridge Reserve, Mojave Desert	34.137472 N -116.436582 W	3.9
28		Coastal shrubland*	Tennessee Valley, Golden Gate National Recreational Area	37.851389 N -122.533899 W	5.6
29		Chaparral shrubland	Lake Skinner, control plots	33.609438 N -117.032003 W	8.7
30		Chaparral shrubland	Lake Skinner, fertilized plots	33.609438 N -117.032003 W	8.7
31		Chaparral shrubland	Irvine Ranch Land Reserve	33.734295 N -117.695938 W	18.4
32	Wetland	Salt marsh	Giacomini wetland, Point Reyes National Seashore	38.100010 N -122.850010 W	3.3
33		Spring-fed wetland	Sierra Foothills Research and Extension Center	39.250000 N -121.283330 W	6.7

*Sampled from under a plants rather than from interspaces. Other shrublands and deserts were sampled from interspaces.

**Sampled from under tree canopy rather than in open grassland area. Other oak woodlands were sampled from open grassland areas.

Table 2. Soil properties and gross nitrogen cycling rates by biome (mean ± SE). Different letters within a row indicate statistically significant differences among ecosystems ($p < 0.05$). The absence of letters in a row indicates no significant differences among ecosystems.

	Desert	Forest	Grassland	Shrubland	Wetland*
n**	7	7	10	7	2
Gravimetric soil moisture (%)	1.9 ± 0.8 a	18.3 ± 2.7 b	15.7 ± 1.8 b	8.1 ± 2.5 c	47.9 ± 2.6
pH	8.1 ± 0.4 a	6.1 ± 0.3 b	6.1 ± 0.2 b	6.1 ± 0.2 b	6.3 ± 0.2
Soil C:N	14.6 ± 4.0 a	23.2 ± 0.8 b	10.7 ± 0.7 a	12.6 ± 0.6 a	13.9 ± 0.3
Soil organic C concentration (%)	0.53 ± 0.21 a	5.52 ± 1.52 c	1.93 ± 0.36 b	2.00 ± 0.64 b	3.38 ± 0.49
Soil N concentration (%)	0.03 ± 0.01 a	0.23 ± 0.06 b	0.18 ± 0.03 b	0.17 ± 0.06 b	0.25 ± 0.04
Microbial biomass N ($\mu g\ N\ g^{-1}$)	6.9 ± 2.5 a	80.1 ± 29.3 b	52.3 ± 7.0 b	14.6 ± 2.3 b	48.9 ± 13.1
Soil NO_3^- concentration ($\mu g\ N\ g^{-1}$)	6.1 ± 4.0 b	0.15 ± 0.09 a	3.3 ± 0.8 b	8.4 ± 3.6 b	0.01 ± 0.00
Soil NH_4^+ concentration ($\mu g\ N\ g^{-1}$)	1.3 ± 0.5	1.0 ± 0.4	4.5 ± 2.8	2.1 ± 1.2	1.1 ± 0.4
Gross mineralization rate ($\mu g\ N\ g^{-1}\ d^{-1}$)	17.8 ± 6.1, n = 5 b	23.6 ± 7.4, n = 6 b	42.2 ± 7.1, n = 9 a	39.0 ± 7.4, n = 6 a	75.4 ± 6.0
Gross nitrification rate ($\mu g\ N\ g^{-1}\ d^{-1}$)	15.2 ± 3.9, n = 4 a	3.7 ± 1.5, n = 6 b	19.7 ± 6.2 a	33.7 ± 18.9, n = 3 a	8.9, n = 1
DNRA rate ($\mu g\ N\ g^{-1}\ d^{-1}$)	0.16 ± 0.11, n = 5	0.018 ± 0.007, n = 2	0.65 ± 0.47	0.33 ± 0.18	0.04, n =1

* Wetlands were not included in comparisons among biomes because of the small sample size.

**Sample size unless otherwise noted.

Table 3. Multiple regression equations that best predict soil N cycling variables. All variables were $\log_{10}$-transformed except for soil C:N ratios.

Dependent variable	Independent variable	Regression coefficient	P-value	n	R^2	P-value	Outliers removed
Soil N concentration	Constant	-1.19 ± 0.05	< 0.001	33	0.90	< 0.001	
	Soil organic C (SOC) concentration	0.72 ± 0.06	< 0.001				
	Gravimetric soil moisture	0.12 ± 0.05	0.03				
Soil NH_4^+ concentration	Constant	1.06 ± 0.18	< 0.001	19	0.80	< 0.001	Site 24
	Gross nitrification rate	-0.26 ± 0.12	0.04				
	Dissimilatory NO_3^- reduction to NH_4^+ (DNRA) rate	0.65 ± 0.08	< 0.001				
Soil NO_3^- concentration	Constant	-1.02 ± 0.57	0.09	19	0.70	< 0.001	Site 24
	Gross nitrification rate	1.47 ± 0.38	0.001				
	DNRA rate	0.72 ± 0.22	0.005				
Gross mineralization rate	Constant	0.71 ± 0.16	< 0.001	23	0.80	< 0.001	Sites 2, 10, 23
	Microbial biomass N	0.48 ± 0.10	0.002				
	SOC concentration	-0.30 ± 0.12	0.02				
	Soil NH_4^+ concentration	0.25 ± 0.07	< 0.001				
Gross nitrification rate	Constant	1.62 ± 0.26	< 0.001	22	0.59	< 0.001	Site 24
	Soil NO_3^- concentration	0.22 ± 0.10	0.04				
	Soil C:N ratio	-0.04 ± 0.02	0.04				
DNRA rate	Constant	-1.64 ± 0.16	< 0.001	20	0.83	< 0.001	
	Soil NH_4^+ concentration	1.22 ± 0.15	< 0.001				
	Gross nitrification	0.44 ± 0.14	0.005				

Figure Legends

Figure 1. Map depicting study site locations (black dots) and atmospheric wet plus dry N deposition rates (color transitions from dark blue to dark red indicate low to high rates). The N deposition rates are shown with 36 km grid resolution and were obtained from Tonneson et al. (2007). The lines represent boundaries between California counties.

Figure 2. (a) Total soil N concentrations, (b) soil organic C concentrations, (c) soil NH_4^+ (black bar) and NO_3^- (gray bar) concentrations, and (d) gross N mineralization (black bars) and nitrification (gray bar) rates by biome, where D = desert, F = forest, G = grassland, and S = shrubland. Significant differences among biomes are indicated by different lowercase letters for variables shown in black bars and by different uppercase letters for variables shown in gray bars ($p < 0.05$). Error bars represent standard errors using sites within biomes as replicates.

Figure 3. Total soil N concentration versus (a) soil organic C concentration with the solid line representing the regression equation, $\log(y) = [0.81 * \log(x)] - 1.10$, $n = 33$, $p < 0.001$ (b) gravimetric soil moisture with a dashed regression line for deserts, $\log(y) = [-0.39 * \log(x)] - 1.54$, $n = 7$, $p < 0.001$, and a solid regression line for all other biomes, $\log(y) = [0.47 * \log(x)] - 1.32$, $n = 26$, $p < 0.001$, (c) pH with a regression line, $\log(y) = [-3.46 * \log(x)] + 1.84$, $n = 33$, $p = 0.001$, and (d) microbial biomass N (MBN) with a regression line, $\log(y) = [0.63* \log(x)] - 1.92$, $n = 33$, $p < 0.001$. Symbols represent ecosystem types: desert (•), forest (x), grassland (filled Δ), shrubland (+), and wetland (filled square). All axes are on $\log_{10}$ scales.

Figure 4. Gross mineralization rates versus (a) microbial biomass N (MBN) with the regression line, $\log(y) = [0.33 * \log(x)] + 1.02$, $n = 26$, $p < 0.001$, (b) gravimetric soil moisture with the regression line, $\log(y) = [0.41 * \log(x)] + 1.09$, $n = 27$, $p < 0.001$, (c) soil NH_4^+ concentration with regression line, $\log(y) = [0.41 * \log(x)] + 1.53$, $n = 26$, $p < 0.001$, (d) total soil N concentration with regression line, $\log(y) = [0.32 * \log(x)] + 1.82$, $n = 26$, $p = 0.01$. The solid lines represent the regression lines for data sets excluding the circled outliers. Symbols representing ecosystem types are same as in Figure 3. All axes are on $\log_{10}$ scales.

Figure 5. Gross nitrification rates versus (a) soil NO_3^- concentrations with the regression line, $\log(y) = [0.36 * \log(x)] + 1.07$, $n = 22$, $p < 0.001$, (b) soil C:N ratios with the regression line, $\log(y) = [-0.06 * \log(x)] + 1.77$, $n = 23$, $p = 0.005$. The solid lines represent the regression lines for data sets excluding the circled outliers. Symbols representing ecosystem types are same as in Figure 3. All axes are on $\log_{10}$ scales.

Figure 6. Dissimilatory NO_3^- reduction to NH_4^+ (DNRA) rates versus (a) soil NO_3^- concentrations with the regression line, $\log(y) = [0.99 * \log(x)] - 1.44$, $n = 20$, $p < 0.001$, (b) soil NH_4^+ concentrations with the regression line, $\log(y) = [1.28 * \log(x)] - 1.14$, $n = 25$, $p < 0.001$. The solid lines represent the regression lines. Symbols representing ecosystem types are same as in Figure 3. All axes are on $\log_{10}$ scales.

Figures

Figure 1.

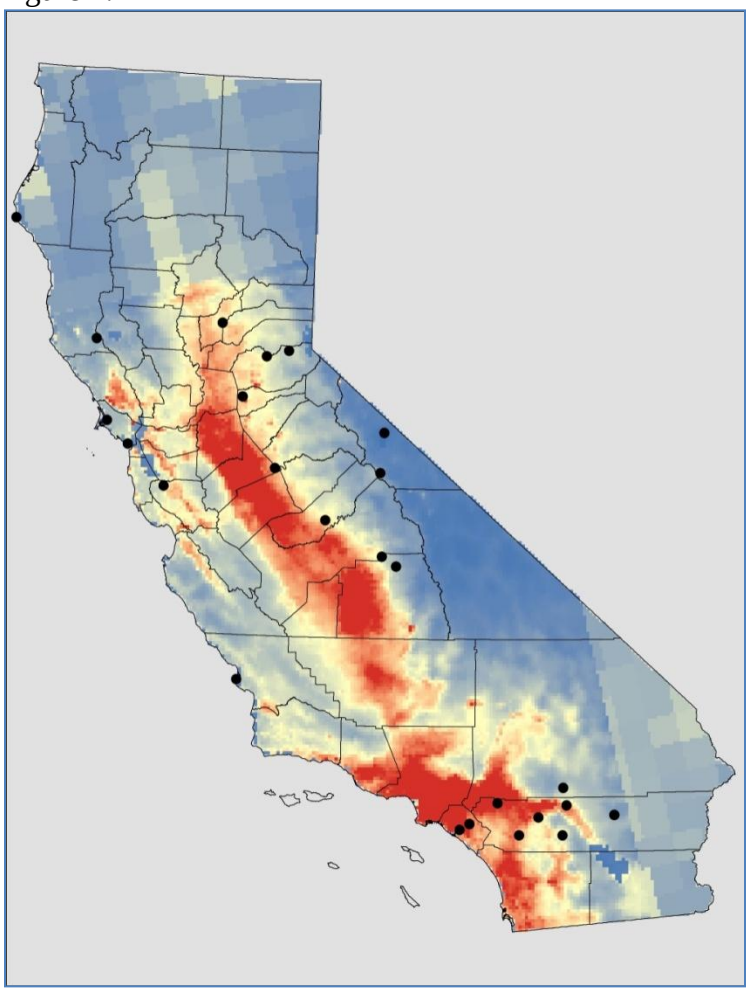

Figure 2.

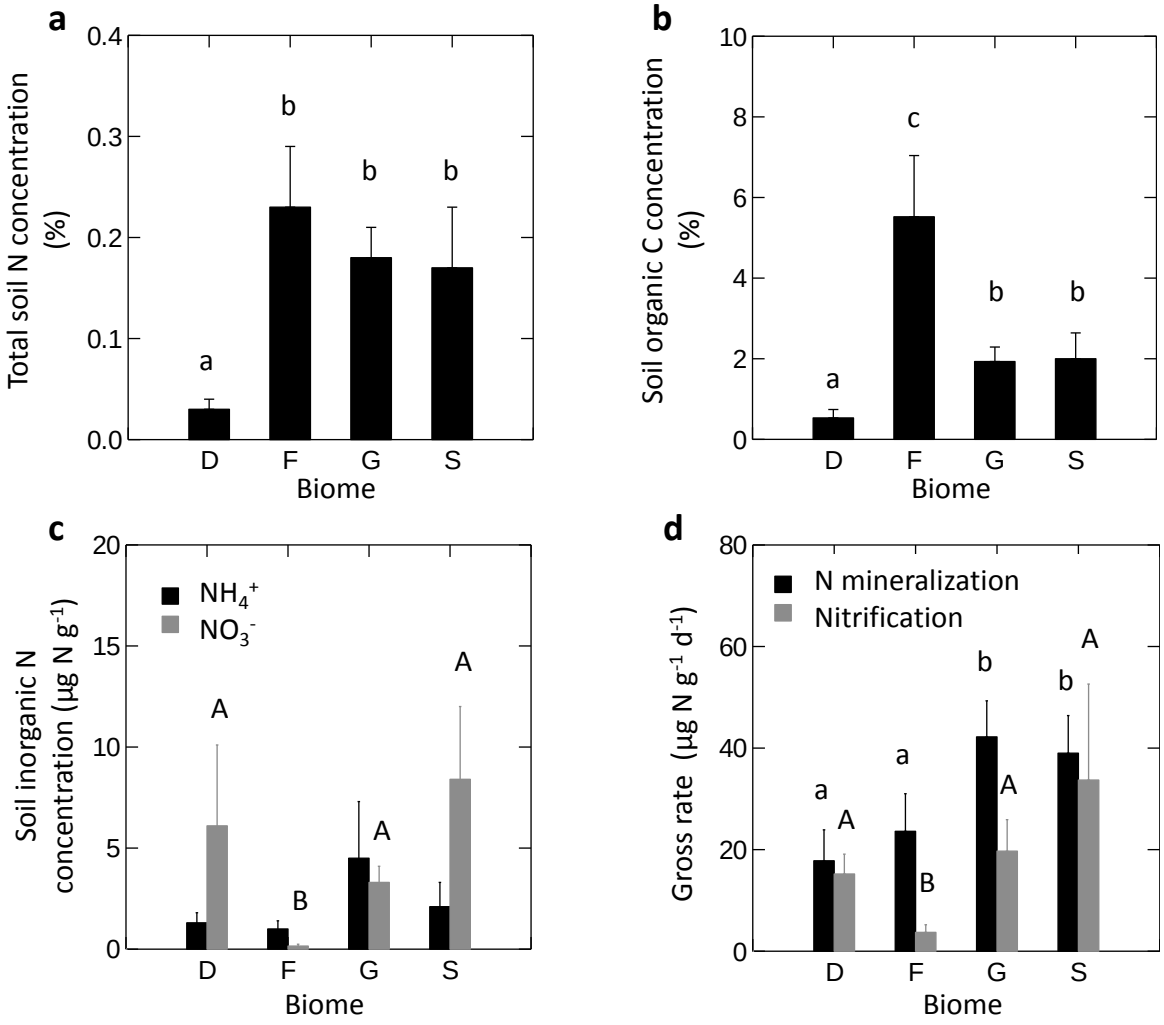
a
Total soil N concentration (%)
0.0
0.1
0.2
0.3
0.4
a
b
b
b
D
F
G
S
Biome
b
Soil organic C concentration (%)
0
2
4
6
8
10
a
c
b
b
D
F
G
S
Biome
c
Soil inorganic N concentration (µg N g-1)
0
5
10
15
20
NH4+
NO3-
A
B
A
A
D
F
G
S
Biome
d
Gross rate (µg N g-1 d-1)
0
20
40
60
80
N mineralization
Nitrification
a
A
a
B
b
A
b
A
D
F
G
S
Biome

Figure 3.

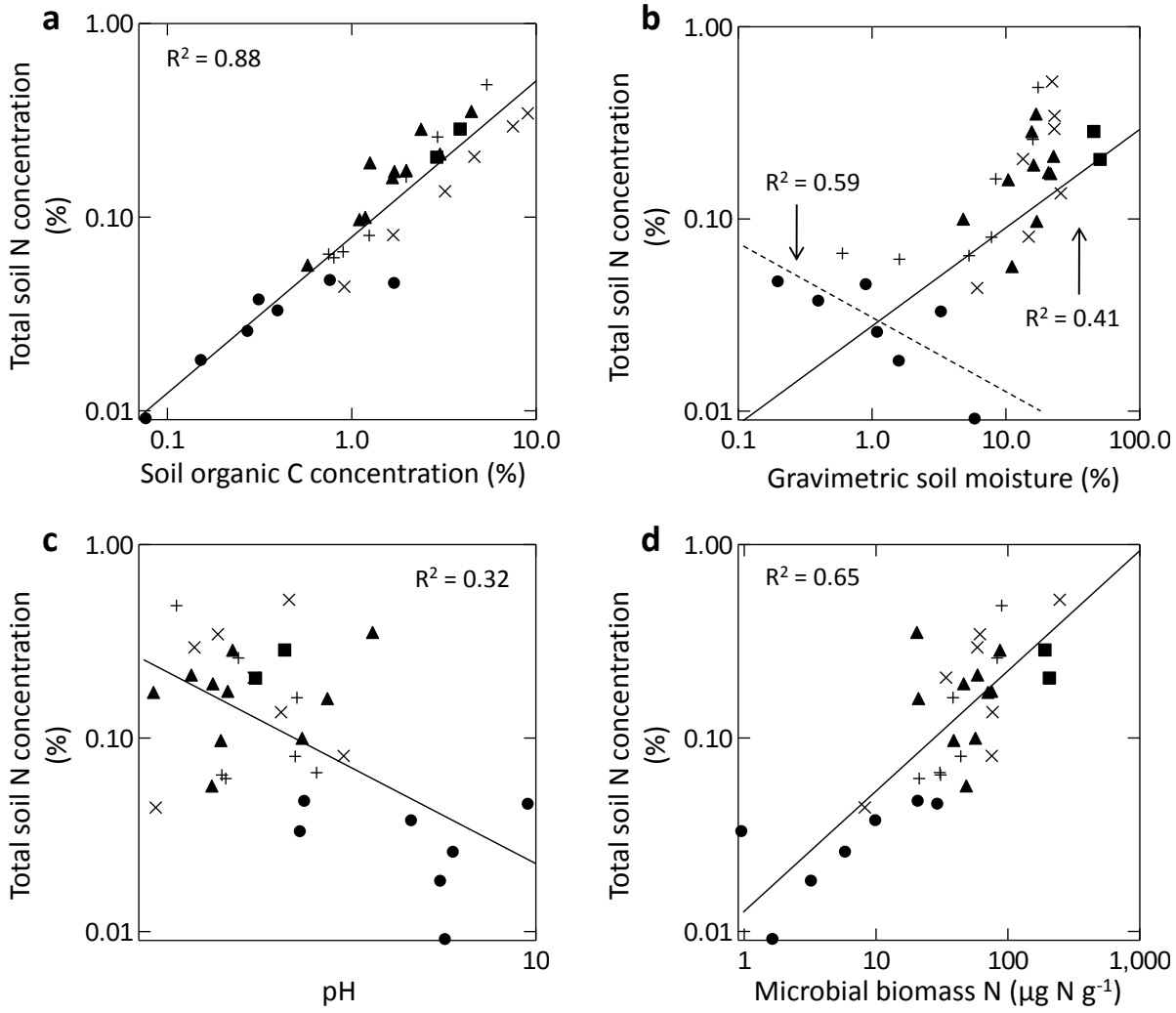
a
1.00
0.10
0.01
R² = 0.88
Total soil N concentration (%)
0.1
1.0
10.0
Soil organic C concentration (%)
b
1.00
0.10
0.01
R² = 0.59
R² = 0.41
Total soil N concentration (%)
0.1
1.0
10.0
100.0
Gravimetric soil moisture (%)
c
1.00
0.10
0.01
R² = 0.32
Total soil N concentration (%)
10
pH
d
1.00
0.10
0.01
R² = 0.65
Total soil N concentration (%)
1
10
100
1,000
Microbial biomass N (µg N g-1)

Figure 4.

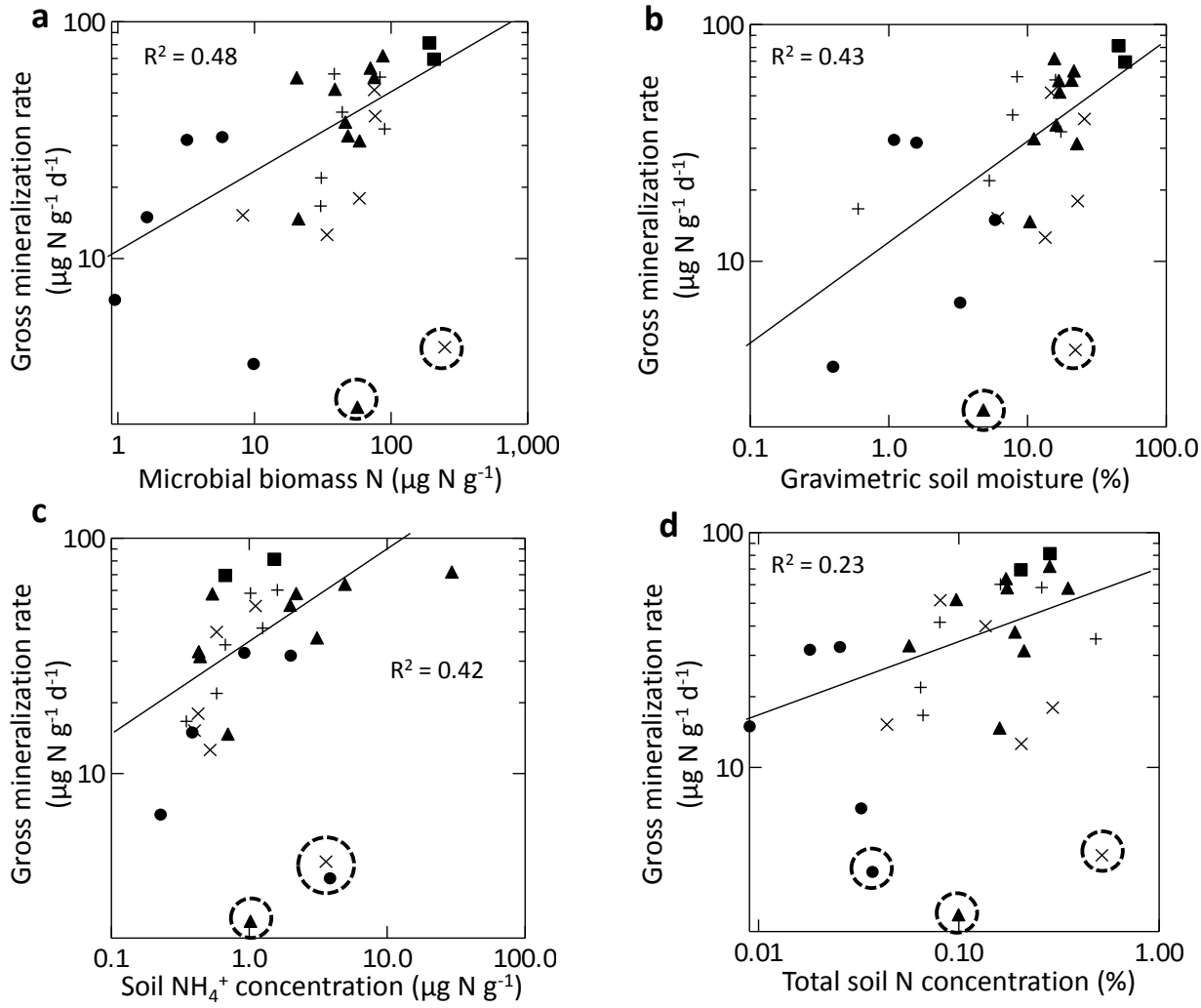
a
b
c
d
Gross mineralization rate (µg N g-1 d-1)
R2 = 0.48
R2 = 0.43
R2 = 0.42
R2 = 0.23
Microbial biomass N (µg N g-1)
Gravimetric soil moisture (%)
Soil NH4+ concentration (µg N g-1)
Total soil N concentration (%)
100
10
1
10
100
1,000
0.1
1.0
10.0
100.0
0.01
0.10
1.00

Figure 5.

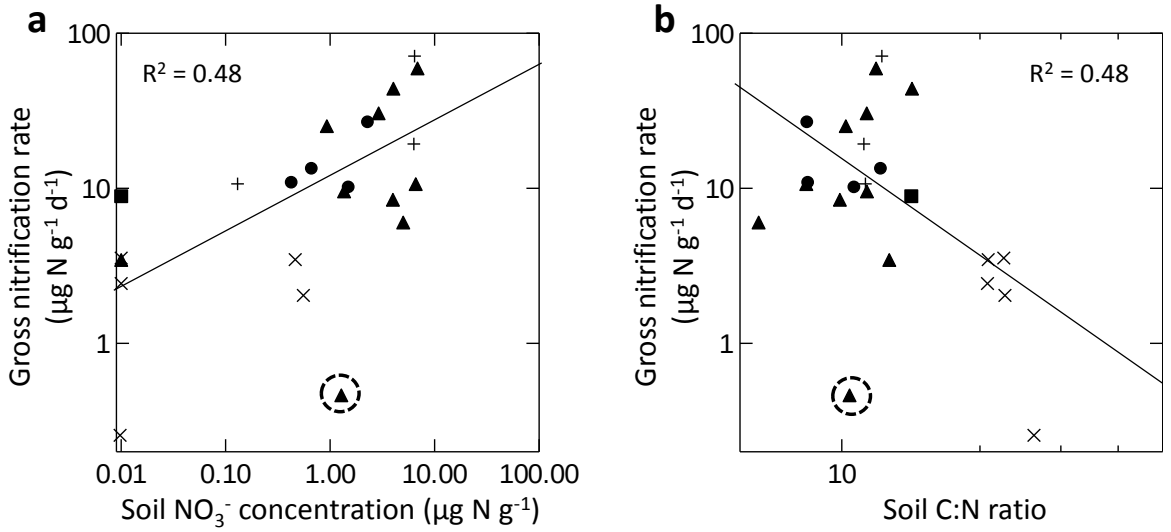

Figure 6.

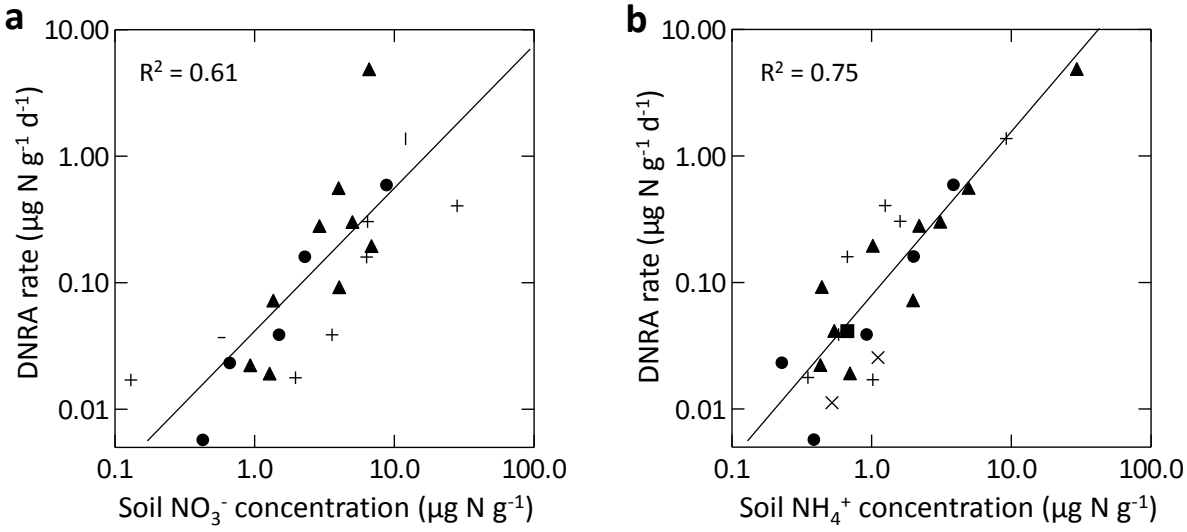

Chapter 6. Conclusion and Synthesis

Soil dinitrogen (N_2) emissions are the most poorly understood portion of the global nitrogen (N) cycle because they are difficult to measure against the high background N_2 concentration in the atmosphere. I have presented two new methods that have the potential to be use widely to measure field rates of N_2 production: the N_2/Ar technique, which is used to measure net N_2 fluxes (Chapter 2), and the ^{15}N-nitrous oxide (N_2O) pool dilution technique, which is used to measure N_2O consumption to N_2 as well as gross N_2O production (Chapter 3). In terrestrial ecosystems, N_2 was thought to be produced only via reduction of N_2O by denitrification. Anaerobic ammonium (NH_4^+) oxidation coupled to nitrite (NO_2^-) reduction (termed anammox) or coupled to iron (Fe) reduction (termed Feammox) theoretically can also produce N_2, but these pathways had not previously been demonstrated to occur in upland soils. In a laboratory experiment conducted in an anoxic glove box, I tested the potential for anammox and Feammox to occur in a humid tropical forest soil rich in poorly crystalline Fe oxides (Chapter 4). The N cycle is becoming increasingly complicated as we discover new N transformation pathways, but recent studies showing globally consistent patterns in N release during litter decomposition (Parton et al. 2007; Manzoni et al. 2008), microbial biomass and community composition (Fierer et al. 2006; Cleveland and Liptzin 2007; Fierer et al. 2009), and soil microbial mineralization of amino acids (Jones et al. 2009) suggest that the controls on internal soil N transformations may also be consistent across ecosystem types. Biogeochemical models and policy decisions are performed at the regional scale, so I explored controls on soil N cycling in deserts, forests, grasslands, shrublands, and wetlands across California (Chapter 5). In this chapter, I review the findings of my dissertation research and discuss their implications for future research.

I demonstrated in laboratory experiments that surface soil N_2 fluxes can be measured accurately using the N_2/Ar technique when the solubility and water vapor flux fractionation effects are accounted for (Chapter 2). Corrections for thermal fractionation did not improve N_2 flux estimates, likely because non-steady state temperature conditions did not allow thermal diffusion to be manifested. Critical components of accurately modeling the solubility and water vapor flux fractionation effects included measuring changes in soil temperature and chamber headspace humidity and temperature, as well as measuring soil moisture. The high detection limit and low sample throughput of the N_2/Ar method limits its utility to the validation of soil N_2 flux measurements in terrestrial ecosystems with high N_2 fluxes. However, there are modifications to the sampling protocol, such as increasing the sampling time period and increasing the surface flux chamber basal area relative to the height, which can easily lower the detection limit. Moreover, using online gas preparation with a continuous flow isotope ratio mass spectrometer will increase throughput and may also improve measurement precision to further lower the detection limit. These modifications could potentially allow the N_2/Ar technique to be used widely to measure surface soil N_2 fluxes.

I used the $^{15}N_2O$ pool dilution technique to measure gross N_2O production and consumption in a peatland pasture (Chapter 3). I found that the $^{15}N_2O$ pool dilution method provides accurate field estimates of gross N_2O production and consumption rates. However, diffusion modeling incorporating lateral diffusion may better elucidate how deep the $^{15}N_2O$ tracer is able to diffuse during the sampling period and improve the accuracy of the measurements. I found that gross N_2O consumption was a small proportion of gross N_2O production across a micro-topographical gradient in the pasture. Gross N_2O production rates

were best predicted by the combination of mineral N concentrations and denitrifying enzyme activity. Gross N_2O consumption rates were most strongly correlated to soil oxygen concentrations when the pasture was divided by soil moisture. This study demonstrates that surface soil N_2O dynamics measured in the field can be related to soil properties that may act as controls on N_2O production and consumption.

Previously, denitrification was assumed to be the only pathway for N_2 production in terrestrial soils, but I have shown that Feammox can also lead to N_2 production, both directly and via denitrification of Feammox-generated NO_2^- (Chapter 4). The production of $^{29}N_2$ from $^{15}NH_4^+$ addition that was inhibited by the presence of acetylene suggests that anammox could also have occurred in the humid tropical forest soil that I studied. If we attribute just 1 % of Fe reduction in the top 10 cm of soil to Feammox, Feammox rates could be comparable to total denitrification rates in the wet tropical forests of the Luquillo Mountains, Puerto Rico.

The production of N_2 in soils by Feammox suggests a major distinction between methods that measure N_2 fluxes directly versus indirectly (i.e., measure N_2O reduction by denitrification). Methods that measure net N_2 fluxes, such as the N_2/Ar technique, would be useful for constructing ecosystem N budgets whereas methods that measure denitrification to N_2, such as the $^{15}N_2O$ pool dilution technique, would be useful for understanding the controls on denitrification and the N_2O:N_2 ratio of denitrification end-products. These methods could even potentially be used together to quantify field rates of N_2 production via anaerobic NH_4^+ oxidation.

In chapter 5, I showed that the a relatively small suite of soil characteristics can be used to predict gross N cycling processes in a wide range of bioregions and cover types in California. Gross mineralization rates were most strongly correlated to microbial biomass N as a single variable. Gross nitrification rates were best predicted by the combination of soil nitrate (NO_3^-) concentration and soil C:N ratios. Dissimilatory NO_3^- reduction to NH_4^+ (DNRA) occurred in all soils and had strong positive relationship with both soil NO_3^- and NH_4^+ concentrations. This was surprising because DNRA is thought to be a strictly anaerobic process, and I performed the gross N cycling assays under ambient oxygen conditions and field soil moisture. Other studies have suggested the potential for DNRA to occur under aerobic conditions (Pett-Ridge et al. 2006; Tiedje 1988). This warrants further investigation because the strong positive relationship between DNRA rates and soil NH_4^+ concentrations suggests that DNRA could be an important N retention process across ecosystem types. Overall, this work suggests that the controls on N cycling processes are similar across the broad range of ecosystem types found in California. This implies that policymakers can address N pollution and greenhouse gas emissions at the regional scale.

My dissertation research has contributed new tools and evidence to improve our understanding of the controls on N_2O and N_2 fluxes as well as the internal N transformations that provide the substrates for N_2O and N_2 production. However, the novel demonstration of Feammox in upland soils also complicates our current understanding of terrestrial N cycling. For example, gaseous N losses from the soil NH_4^+ pool under anoxic conditions challenges the perception of DNRA as a N retention process. Investigations of the increasingly intricate and complex web of soil N transformations together with more broad-scale studies that explore universal, fundamental mechanisms controlling N processes will ultimately lead to a greater understanding of terrestrial N cycling.

References

Cleveland CC, Liptzin D (2007) C:N:P stoichiometry in soil: Is there a "Redfield ratio" for the microbial biomass? Biogeochemistry 85:235-252

Fierer N, Jackson RB (2006) The diversity and biogeography of soil bacterial communities. Proceedings of the National Academy of Sciences of the United States of America 103:626-631

Fierer N, Strickland MS, Liptzin D, Bradford MA, Cleveland CC (2009) Global patterns in belowground communities. Ecology Letters 12:1238-1249

Jones DL et al. (2009) Soil organic nitrogen mineralization across a global latitudinal gradient. Global Biogeochemical Cycles 23:GB1016, doi:10.1029/2008GB003250

Manzoni S, Jackson RB, Trofymow JA, Porporato A (2008) The global stoichiometry of litter nitrogen mineralization. Science 321:684-686

Parton W et al. (2007) Global-scale similarities in nitrogen release patterns during long-term decomposition. Science 315:361-364

Pett-Ridge J, Silver WL, Firestone MK (2006) Redox fluctuations frame microbial community impacts on N-cycling rates in a humid tropical forest soil. Biogeochemistry 81:95-110

Tiedje JM (1988) Ecology of denitrification and dissimilatory nitrate reduction to ammonium. In: Zehdner AJB (eds) Biology of Anaerobic Microorganisms. John Wiley and Sons, New York, NY, Pages 179-244